

Sintering kinetics and properties of highly pure lead zirconate titanate ceramics

Von der Fakultät für Biologie, Chemie und Geowissenschaften der
Universität Bayreuth

Zur Erlangung der Würde eines Doktors der Naturwissenschaften

– Dr. rer. nat. –

Genehmigte Dissertation

Vorgelegt von

Xianliang Huang (黄贤良)
aus AnQing, China

Würzburg 2009

Erklärung

Hiermit erkläre ich ehrenwörtlich, daß ich die Dissertation „Sintering kinetics and properties of highly pure lead zirconate titanate ceramics“ selbständig angefertigt und keine anderen als die von mir angegebenen Quellen und Hilfsmittel benutzt habe.

Ich erkläre außerdem, daß diese Dissertation weder in gleicher oder anderer Form bereits in einem anderen Prüfungsverfahren vorgelegen hat.

Ich habe früher außer den mit dem Zulassungsgesuch urkundlich vorgelegten Graden keine weiteren akademischen Grade erworben oder zu erwerben versucht.

Würzburg, den 27. 07. 2009

Xianliang Huang

To those who have supported me through this endeavor

In memory of a dear friend Patrick Fiedler

Table of Contents

Abstract	i
Zusammenfassung	iii
Chapter 1 Introduction	1
1.1 Piezoelectricity	1
1.2 Ferroelectricity	2
1.3 Lead zirconate titanate.....	6
1.3.1 Phase diagram and morphotropic phase boundary (MPB)	6
1.3.2 Synthesis and reaction sequences of PZT	7
1.3.3 Studies on sintering	8
1.3.4 Major variables affecting the properties of PZT ceramics	11
1.3.5 Dopant effects on PZT ceramics.....	14
1.4 Purpose of present research.....	17
Chapter 2 Experimental procedure	19
2.1 Characterizing Methods	19
2.1.1 Powder characterization	19
2.1.2 Characterization of sintered PZT ceramics	20
2.2 Specimen Preparation.....	22
2.2.1 Raw materials	22
2.2.2 Synthesis of PZT powders	22
2.2.3 Green sample preparation and sintering.....	25
2.3 In situ measurement of sintering behavior	25
2.3.1 General procedure	25
2.3.2 Sintering in closed crucible.....	26
Chapter 3 Data evaluation	28
3.1 Rietveld refinement.....	28
3.2 Image analysis.....	29
3.2.1 Grain size measurement.....	29
3.2.2 Homogeneity evaluation	29
3.3 Sintering behavior of PZT ceramics in TOMMI.....	30
3.3.1 Temperature calibration.....	30

3.3.2	Correction of thermal expansion	30
3.3.3	Calculation of sintering temperatures.....	31
3.3.4	Kinetic field and activation energy for sintering of PZT	31
Chapter 4 Lead zirconate titanate ceramics from different raw materials and with lead nonstoichiometry..... 33		
4.1	Introduction.....	33
4.2	Comparison of PZT ceramics prepared from industrial-used and highly pure raw materials.....	33
4.2.1	Differential Thermal Analysis.....	33
4.2.2	X-ray Diffraction Analysis	33
4.2.3	<i>In situ</i> sintering behavior	34
4.2.4	Sintering behavior with uniaxial load.....	36
4.2.5	Dielectric and piezoelectric properties.....	36
4.2.6	Ferroelectric properties	37
4.3	Effect of lead nonstoichiometry on highly pure PZT	38
4.3.1	Phase determination.....	38
4.3.2	Sintering behavior.....	40
4.3.3	Microstructure properties.....	42
4.3.4	Dielectric and Ferroelectric properties.....	44
4.4	Summary	47
Chapter 5 Systematic study of the impurity effect on lead zirconate titanate ceramics.....49		
5.1	Introduction.....	49
5.2	Impurities originating from customary raw materials.....	50
5.2.1	Sintering behavior of PZT prepared with mixed raw materials.....	50
5.2.2	Sintering behavior of highly pure PZT doped with impurities.....	52
5.2.3	Microstructural and electrical properties of PZT doped with impurities.....	55
5.3	Individual impurities, Na, Y or Si in highly pure PZT ceramics	58
5.3.1	Microstructure properties.....	58
5.3.2	Sintering behavior of PZT ceramics with Na, Y and Si modification	62
5.3.3	Impurity level dependent piezoelectric and dielectric properties	64
5.3.4	Ferroelectric properties	69
5.4	Summary	71
Chapter 6 Studies on sintering kinetics of PZT by the kinetic field method73		
6.1	Introduction.....	73
6.2	Sintering behavior at different heating rate.....	73

6.3	Kinetic field and apparent activation energy for sintering of PZT	74
6.4	The fitting of iso-strain lines	76
6.5	Microstructure analysis	78
6.6	Summary	80
Chapter 7 Conclusions.....		81
References.....		83
List of Figures.....		91
List of Tables.....		94
List of symbols.....		95
Acknowledgments		97
Curriculum Vitae.....		99

Abstract

Lead zirconate titanate (PZT) has been widely applied in actuators and sensors due to its excellent piezoelectric and ferroelectric properties. However, impurities, one of the major problems involved in the mass production of PZT ceramics, have not attracted enough attention. In this thesis, investigations on the effects of impurities from the raw materials on the sintering and properties of lead zirconate titanate with a composition of $\text{PbZr}_{0.53}\text{Ti}_{0.47}\text{O}_3$ were conducted. The impact of starting materials, lead nonstoichiometry, and dopants was examined. The sintering behavior was monitored in a thermo-optical dilatometer and a kinetic-field approach was employed to obtain the activation energy for sintering of PZT ceramics with different compositions. The bulk ceramics were characterized in terms of microstructure, dielectric, piezoelectric and ferroelectric properties.

At first, a comparison in sintering between the PZT samples prepared from industrially used (IM) and highly pure raw materials (HM) was made. Reduced sintering temperatures and higher densification rate were observed on the IM sample owing to the secondary phase on the grain boundary. Different electric properties of these two samples were also evidenced. To evaluate their contributions to the observed difference of IM and HM samples, various impurities, which were identified in the IM raw materials, were added in the highly pure samples. It was shown that the sintering was changed through the formation of charged vacancies (impurity Na, Fe, Al, Y) or melt phase (Si) with low melting point.

The most important impurity species was identified as Na, Y and Si and their effect on the ceramics properties was investigated as a function of dopant concentration. They showed grain growth inhibition effect on PZT ceramics. The strongest effect was achieved by doping with Na. The grain size was reduced from 13 μm of undoped PZT to 2 μm at a doping level of 1mol%. The dielectric constant was increased with Na doping, which was attributed to the decreasing grain size. In addition, because of the oxygen vacancies caused by the Na doping, "hard" piezoelectric behavior and ferroelectric properties were observed. Rare earth impurity, such as Y, with a valence and ion radius between A site and B site elements in PZT lattice, results in a combination of "soft" and "hard" characteristics. Melt phase formed from Si showed deteriorated effect on the properties of PZT ceramics.

Deviations from the stoichiometric composition could result when the impurities were not considered in the weight fractions of the raw materials. The lead content in the system was affected

by the crystalline phase of starting components as well. PbO concentration was changed during calcination depending on the formation kinetics of intermediate lead titanate. Sintering temperatures were dramatically reduced and densification rates were strongly enhanced by the introduction of lead oxide excess. The reason was believed to be associated with the liquid phase formed by PbO during sintering because of its low melting point. Rapid densification was observed at low level of PbO excess. However, a sluggish rearrangement process with low densification rate occurred in the PZT with 3.0% PbO excess at a temperature below the melting point of PbO. A small force (as small as 0.1MPa) on the sample could result in rapid densification and an additional densification maximum was evidenced. The tetragonal lattice distortion in the lead deficient samples was verified by Rietveld refinement, from which internal stress was introduced and attributed to the high dielectric constant. Moreover, the increasing amount of lead deficiency could result in the segregation of ZrO_2 . It shifts the Zr/Ti ratio to the Ti-rich side, which may be attributed to a higher dielectric constant as well. The lead excess is favorable in improving both the microstructure and electrical properties of PZT ceramics. However, deteriorated properties were found in the samples in which the lead oxide excess is beyond a certain level (1.5 mol% PbO).

The kinetic field diagram was constructed using the shrinkage data from the optical dilatometry. Different dependence of activation energy on the fractional density was observed. It is attributed to the variation in the activation energies in densification and grain growth. By fitting the iso-strain lines, activation energy between 350-360 kJ/mol was obtained for densification of pure HM PZT sample and samples doped with 0.5% Na or Si. Smaller values were acquired for grain growth. Although liquid phase was present in Si-doped samples and the ones with PbO excess, a better match can be achieved using a solid state sintering model. The enhanced inhomogeneity and the rapid densification were suggested to explain the difficulty in fitting the sintering curves of 1.5wt%PbO added sample.

Sinterkinetik und Eigenschaften von hochreinen Blei-Zirkonat-Titanat-Keramiken

Zusammenfassung

Blei-Zirkonat-Titanat (PZT) ist weit verbreitet in Aktoren und Sensoren aufgrund seiner hervorragenden piezoelektrischen und ferroelektrischen Eigenschaften. Allerdings wurde Verunreinigungen, die eines der Hauptprobleme in der industriellen Massenfertigung von PZT-Keramiken darstellen nicht genügend Aufmerksamkeit gewidmet. In der vorliegenden Arbeit wurde der Einfluss von Verunreinigungen aus den Rohstoffen auf das Sinterverhalten und die Eigenschaften von PZT ($\text{PbZr}_{0.53}\text{Ti}_{0.47}\text{O}_3$) untersucht. Der Einfluss der Ausgangsstoffe, Abweichungen von der stöchiometrischen Bleikonzentration sowie von Dotierungen wurde gemessen. Das Sinterverhalten wurde in einem thermo-optischen Dilatometer aufgezeichnet. Ein Kinetic Field-Ansatz wurde verwendet, um die Aktivierungsenergie zum Sintern von PZT-Keramiken mit unterschiedlichen Zusammensetzungen zu ermitteln.

Zunächst wurde ein Vergleich von PZT-Proben, die aus industriell verwendeten (IM) bzw. hochreinen (HM) Rohstoffen hergestellt worden waren, durchgeführt. Eine verringerte Sinter Temperatur und eine höhere Verdichtungsrate wurden für IM-Proben festgestellt und einer Sekundärphase auf den Korngrenzflächen zugeschrieben. Unterschiedliche elektrische Eigenschaften dieser beiden Probentypen wurden ebenfalls nachgewiesen. Um den Beitrag verschiedener Verunreinigungen auf die beobachteten Unterschiede zwischen IM und HM-Proben zu bewerten, wurden Verunreinigungen, die in den IM Rohstoffen identifiziert worden waren, zu den hochreinen Proben zugefügt. Es wurde gezeigt, dass das Sinterverhalten durch die Bildung geladener Leerstellen im PZT-Gitter (Dotierung mit: Na, Fe, Al, Y) oder Schmelzphasen (Dotierung mit: Si) mit niedrigem Schmelzpunkt beeinflusst wurde.

Als wichtigste Verunreinigungen wurden Na, Y und Si identifiziert. Ihr Einfluss auf die Eigenschaften der Keramiken wurde als Funktion der Dotierungskonzentration untersucht. Alle drei zeigten eine Unterdrückung des Kornwachstums in PZT-Keramiken. Der stärkste Effekt wurde durch Dotierung mit Na erreicht. Die Korngröße wurde von 13 μm bei undotiertem PZT auf 2 μm bei Dotierung mit 1mol% Na verringert. Die Permittivitätszahl stieg durch Na-Dotierung an, was auf die abnehmende Korngröße zurückgeführt wurde. Zusätzlich wurden 'hartes' piezoelektrisches und ferroelektrisches Verhalten festgestellt, was auf Sauerstoffleerstellen -

aufgrund der Na-Dotierung - zurückgeführt wurde. Selten-Erd-Verunreinigungen wie Y mit Wertigkeit und Ionenradius zwischen denen der A und B-Atome im PZT-Gitter zeigten eine Kombination von harten und weichen Eigenschaften. Schmelzphase, die mit Si gebildet wurde, zeigte einen nachteiligen Effekt auf die Eigenschaften von PZT-Keramiken.

Abweichungen von der stöchiometrischen Zusammensetzung können auftreten, wenn Verunreinigungen bei der Einwaage der Rohstoffe nicht berücksichtigt werden. Der Bleioxidanteil im PZT-System wurde auch durch die Kristallphase der Ausgangsverbindungen beeinflusst. Während der Kalzinierung änderte sich der PbO-Gehalt abhängig von der Bildungskinetik intermediärer Blei-Titanate. Durch Überschüsse an Bleioxid wurden die Sintertemperatur drastisch abgesenkt und die Verdichtungsrate erhöht. Dies wurde auf Bildung einer bleioxidhaltigen Schmelzphase mit niedrigem Schmelzpunkt zurückgeführt. Eine schnelle Verdichtung wurde bei niedrigem PbO-Überschuss beobachtet. Allerdings trat eine niedrige Verdichtungsrate - entsprechend einer verzögerten Teilchenumordnung - in PZT mit 3% PbO Überschuss im Temperaturbereich unterhalb des PbO-Schmelzpunktes auf. Ein kleiner Druck von nur 0.1 MPa auf die Proben bewirkte eine schnelle Verdichtung und ein zusätzliches Maximum der Verdichtungsrate wurde beobachtet. Eine tetragonale Gitterverzerrung in Proben mit unterstöchiometrischem Bleigehalt wurde durch Rietveld-Verfeinerung bestätigt. Sie verursacht innere Spannungen, auf die die hohe Permittivitätszahl dieser Proben zurückgeführt wurde. Außerdem kann ein wachsendes Defizit an PbO eine Ausscheidung von ZrO_2 bewirken. Es verschiebt das Zr/Ti-Verhältnis zur Ti-reichen Seite, was ebenfalls zu einer höheren Permittivitätszahl führt. Ein Bleioxidüberschuss ist vorteilhaft, weil er die Mikrostruktur und die elektrischen Eigenschaften von PZT-Keramiken verbessert. Allerdings wurden schlechtere Eigenschaften in Proben gemessen, bei denen der Bleioxidüberschuss über einem Grenzwert lag ($> 1.5 \text{ mol\% PbO}$).

Mithilfe der Schwindungsdaten aus der optischen Dilatometrie wurden Kinetic Field-Diagramme konstruiert. Eine unterschiedliche Abhängigkeit der Gesamtaktivierungsenergie von der fraktionellen Dichte wurde beobachtet. Dies wurde auf das Zusammenspiel von Verdichtungsmechanismen und Kornwachstum zurückgeführt. Aus den Iso-Schwindungslinien wurde eine Aktivierungsenergie von 350-360 kJ/mol für die Verdichtung von reinen HM PZT-Proben und Proben, die mit 0.5% Na oder Si dotiert waren ermittelt. Die Aktivierungsenergie für das Kornwachstum war geringer. Obwohl Flüssigphase in den mit Si-dotierten Proben und den Proben mit PbO-Überschuss vorhanden war, wurde eine bessere Übereinstimmung zwischen Modellrechnungen und experimentellen Daten bei Verwendung eines Festphasensintermodells

gefunden. Die Schwierigkeit in der theoretischen Beschreibung von Sinterkurven mit hohem PbO-Überschuss (1.5wt%) wurde durch die stärkere Inhomogenität und die schnelle Verdichtung erklärt.

Chapter 1 Introduction

1.1 Piezoelectricity

Piezoelectricity, a property possessed by a select group of materials, was first discovered in Quartz, Rochelle salt and some minerals in 1880 by Jacques and Pierre Curie (Haertling 1999). The name “piezo” is derived from the Greek, meaning “to press”; hence, piezoelectricity is the ability to generate electric charge when subjected to mechanical stress. Various types of ceramics with different compositions have been discovered and improved since 1940s. The early commercial piezoelectric products were made of barium titanate. An advance of great practical importance was the discovery of strong and stable piezoelectric effects in lead zirconate titanate (PZT) solid solutions (Jaffe, Roth et al. 1954). Since then, piezoelectric materials have become the common electromechanical transducers which can transfer energy between electrical and mechanical states.

In piezoelectric crystals two effects are operative. The direct effect (designated as a generator) is identified with the phenomenon whereby electrical charge (polarization) is generated from a mechanical stress, whereas the converse effect (designated as a motor) is associated with the mechanical movement generated by the application of an electrical field (Haertling 1999). The basic equations that describe these two effects in regard to electric and elastic properties are (Jaffe, Cook et al. 1971)

$$D = d \cdot X \text{ (generator)} \quad (1.1)$$

$$S = d \cdot E \text{ (motor)} \quad (1.2)$$

where D is the dielectric displacement (consider it equal to polarization), X -the stress, E -the electric field, S -the strain, d -a piezoelectric coefficient. Furthermore, these properties have directional quantities, and, hence, they are usually specified with subscripts to identify the conditions under which they are determined. Conventionally, the first subscript of the d coefficient gives the “electrical” direction while the second gives the component of mechanical deformation or stress (Jaffe, Cook et al. 1971). For example, d_{33} implies the polarization generated in the third or vertical direction when the stress is applied in the third direction; d_{31} indicates that this piezoelectric coefficient is related to the generation of polarization in the electrodes along the third direction and perpendicular to the stress mechanically applied in the first or lateral direction (Haertling 1999). Equations in matrix form that specify these properties along different orientations of the materials

are available (Jaffe, Cook et al. 1971; Xu 1991). The d coefficients for the direct and converse effects have the identical value and are usually expressed as $\times 10^{-12}$ C/N for the direct effect and $\times 10^{-12}$ m/V for the converse effect. High d coefficients are desirable for those materials that are utilized in motional or vibrational devices, such as sonar and speakers.

The piezoelectric coupling factor (e.g., k_{33} , k_{31} , and k_p) is a convenient and direct measurement of the overall strength of the electromechanical effect, i.e., the ability of the ceramic transducer to convert one form of energy to another. The actual relationship is in terms of k^2 :

$$k^2 = \frac{\text{mechanical energy converted to electrical energy}}{\text{input mechanical energy}} \quad (1.3)$$

or

$$k^2 = \frac{\text{electrical energy converted to mechanical energy}}{\text{input electrical energy}} \quad (1.4)$$

Because the conversion of electrical to mechanical energy is always incomplete, k is always less than unity.

1.2 Ferroelectricity

Ferroelectrics are subgroups of piezoelectric crystals. All noncentro-symmetric point groups, except 432 point group, exhibit piezoelectric effect. However, only 10 polar crystals in which the direction of the electric dipole is reversible by means of electric field can be ferroelectrics (Xu 1991). Most ferroelectrics undergo a structural phase transition from a high-temperature nonferroelectric or paraelectric phase into a low-temperature ferroelectric phase. The temperature of the phase transition is called Curie point. Taken lead titanate as an example, it is a perovskite crystal which transforms from a nonferroelectric cubic to a ferroelectric tetragonal phase at 490°C (Nelmes and Kuhs 1985). As shown Figure 1.1, the non-polar cubic structure shows paraelectric phase, with Pb^{2+} ions at the cube corners, O^{2-} ions at the face centers and Ti^{4+} ion at the body center. As it is cooled from high temperature paraelectric phase to low temperature ferroelectric tetragonal phase, the unit cell slightly deforms, with Pb and Ti ions displaced relative to the O^{2-} ions, thereby creating a dipole (Nelmes and Kuhs 1985). The spontaneous polarization (P_s) is defined by the value of the dipole moment per unit volume. In general, uniform alignment of electric dipoles only occurs in certain region of a crystal. Such regions with uniform polarization are called domains, in which the polarizations have a common direction of spontaneous polarization. Domains form to minimize

the electrostatic energy associated with mechanical constraints as the ferroelectric material is cooled through paraelectric-ferroelectric phase transition (Arlt 1990). The intersection of two domains with different orientations results in the formation of a domain wall. Across these walls, the direction of polarization change. The walls which separate domains with oppositely orientated polarization are called 180° walls and those which separate regions with mutually perpendicular polarization are called 90° walls, as illustrated in Figure 1.2 (Damjanovic 1998). Taken PbTiO_3 as an example, the domain walls may therefore separate regions in which polarization orientation is antiparallel (180° walls) or perpendicular (90° walls) to each other. The types of domain walls, which can occur in a ferroelectric crystal, depend on the symmetry of both the nonferroelectric and ferroelectric phases of the crystal. In the rhombohedral phase of PZT, the direction of polarization develops along the body diagonals (direction $\langle 111 \rangle$) of the paraelectric cubic unit cell, which gives eight possible directions of the spontaneous polarization with 180° , 71° and 109° domain walls (Jaffe, Cook et al. 1971). Several mathematical treatments have been proposed to derive possible types of domain walls in a ferroelectric material (Fousek and Janovec 1969; Li, Fang et al. 2006).

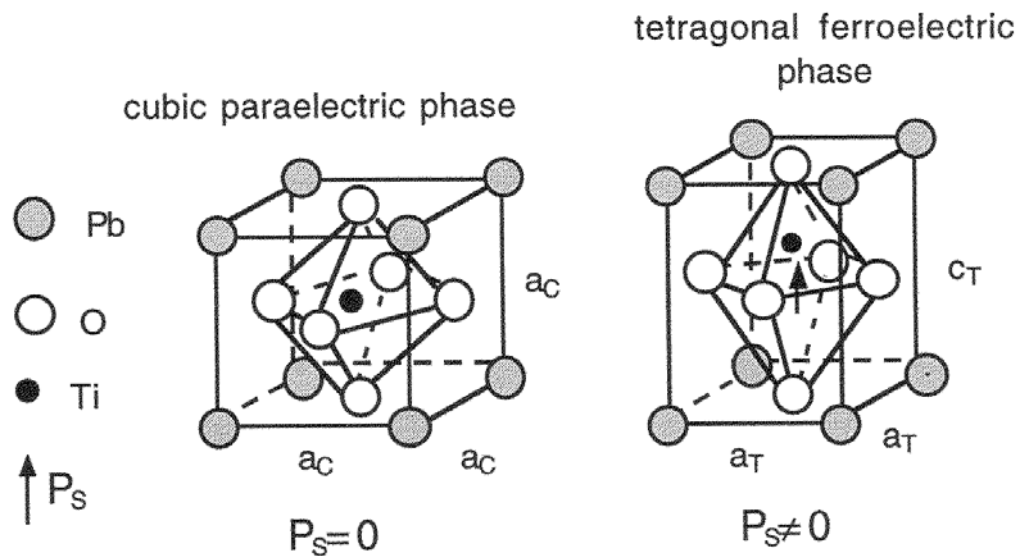


Figure 1.1 The perovskite structure ABO_3 , shown here for PbTiO_3 which has a cubic structure in the paraelectric phase and tetragonal structure in the ferroelectric phase (Nelmes and Kuhs 1985)

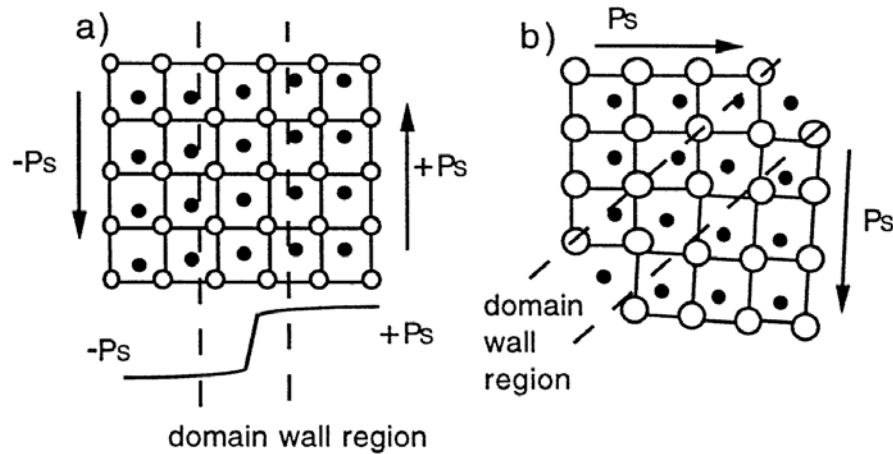


Figure 1.2 Illustration of (a) 180° and (b) 90° ferroelectric domains and domain-wall regions in a tetragonal perovskite ferroelectric. The schematic change of polarization across the domain wall is shown for a 180° wall in (a). Tetragonal distortion in (b) is exaggerated. (Damjanovic 1998)

Owing to the random orientations of the domains, the piezoelectric effects of individual domains will cancel and such samples do not possess any piezoelectric property. However, a strong electric field may reverse the spontaneous polarization of domains. Polycrystalline ferroelectric materials may be brought into a polar state by applying an electric field usually ranging from 10 to 100 kV/cm at high temperatures. This process, called poling, cannot orient grains, but can reorient domains within individual grains along the direction of the field. The dynamic process of domain reversal is called “domain switching”. The poling process is illustrated in Figure 1.3. Ideally the 180° domain switching would cause no stress and strain. It was proposed that after poling all of the 180° domains switched to the closest possible direction whereas only 12% of 90° domains for a well poled BaTiO_3 and 44–51% of 90° domains in tetragonal PZT switched to the direction which was close to the field direction (Subbarao, McQuarrie et al. 1957; Berlincourt and Krueger 1959).

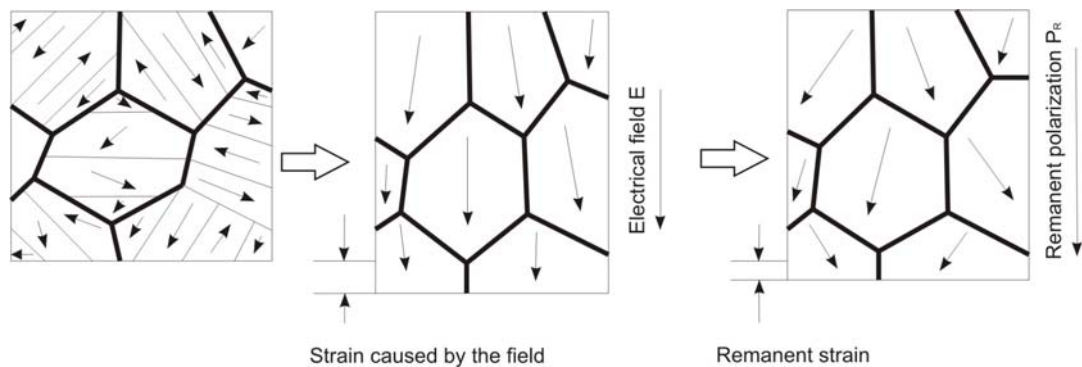


Figure 1.3 A polycrystalline ferroelectric with random orientation of grains before, during and after poling. Many domain walls are present in the poled material; however, the net remnant polarization is nonzero. (Xu 1991).

One consequence of the domain wall switching is the occurrence of the ferroelectric hysteresis loop which is the most important characteristic of ferroelectric material. Figure 1.4 displays a schematic diagram for polarization reversal with an electric field (P-E) for PZT. Saturation polarization P_{sat} is defined as the polarization induced by the maximum field, whereas spontaneous polarization P_s is the y -axis intercept of the linear extrapolation from the tangent of P_{sat} . Ideally, the entire value of P_s would be maintained as remnant polarization P_R after the coercive field is removed. However, some re-randomization does occur at room temperature and P_R is often less than P_s . The coercive field E_c is the field at which polarization reversal occurs. An ideal hysteresis loop is symmetrical so that $+E_c = -E_c$ and $+P_R = -P_R$. For non-ferroelectric materials a straight line is generated while for ferroelectric materials a hysteresis loop should be observed. Double loop like hysteresis was first observed in lead zirconate by Shirane, which was associated with antiferroelectricity (Shirane, Sawaguchi et al. 1951). Merz observed a similar shape of loop in $BaTiO_3$ just above the Curie temperature (Merz 1953). The double loop shape in this case showed a paraelectric to ferroelectric phase transition. Double loop hysteresis was also reported in aged ferroelectric ceramics. It was assumed that the intergranular and interdomain stress was strong enough to switch domains back to their original orientations when the external field decreased down to zero. In addition, it was believed that the double loop like P-E hysteresis in aged ferroelectrics was associated with acceptor type defects (Tan, Li et al. 1999).

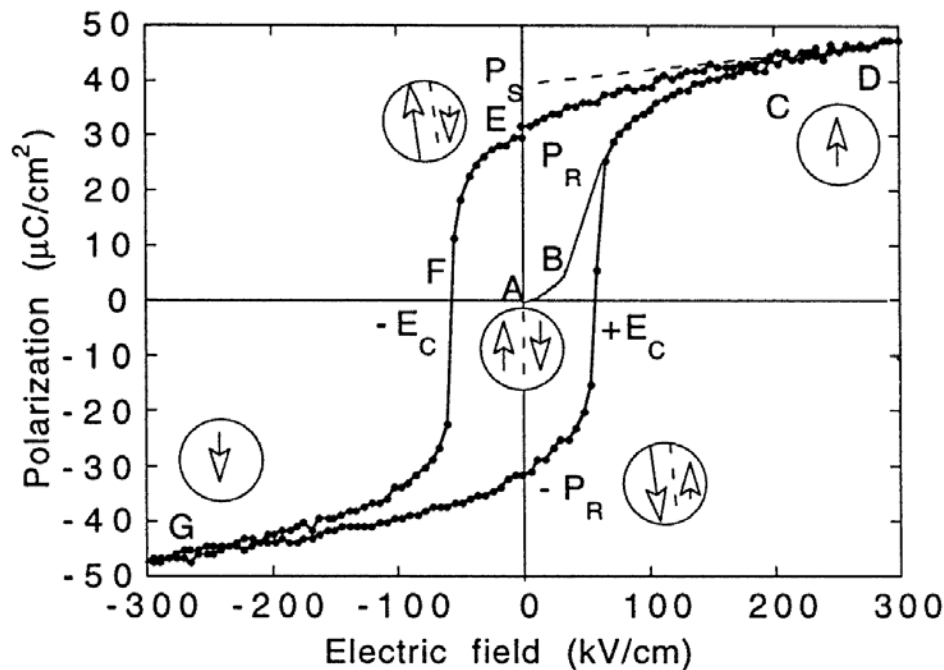


Figure 1.4 Schematic of Polarization-Electric (P-E) field hysteresis loop. Circles with arrows represent the polarization state of the materials at the indicated fields. The symbols are explained in the text. (Damjanovic 1998)

It is known that any process that inhibits nucleation of new oppositely oriented domains or reduces the movements of domain walls will affect the polarization and strain hysteresis loop characteristics (Damjanovic 1998). It is said that domain walls become pinned or clamped by the defects and imperfections. Some common domain wall pinning defects include oxygen vacancies and electrons trapped in the domain-wall area. An oxygen vacancy–acceptor dipole pair, on the other hand, may interact with polarization within a domain and make the domain switching more difficult, effectively clamping the domain wall. Displacement of domain walls also contributes to the dielectric and mechanical losses of ferroelectric materials. Four types of contribution to losses were proposed by Härdtl (Härdtl 1982). In addition to domain wall motion, the others are 1) a fundamental lattice contribution which should also happen in domain free monocrystals 2) a microstructural contribution which typically occurs in polycrystalline samples, and 3) a conductivity contribution in highly-ohmic samples. However, in most ceramics, the loss due to domain wall motion was believed to significantly exceed the other three types.

1.3 Lead zirconate titanate

Since the discovery of ferroelectric ceramics, lead zirconate titanate (PZT) has emerged as one of the most widely studied and technologically important ferroelectric oxides because of its excellent piezoelectric properties and high Curie temperature above 300°C. It has been extensively applied in piezoelectric micromotors, microrobots, actuators, transducers, positioning devices for fine control of motion, and so on (Jaffe, Cook et al. 1971).

1.3.1 Phase diagram and morphotropic phase boundary (MPB)

Lead zirconate titanate (PZT) is a solid solution phase of the $x\text{PbZrO}_3-(1-x)\text{PbTiO}_3$ ($0 < x < 1$) binary system. Its chemical formula is $\text{Pb}(\text{Zr}_x\text{Ti}_{1-x})\text{O}_3$. PZT ceramics exhibit three different phases (tetragonal, rhombohedral or orthorhombic) at room temperature depending on the composition. PZT has the perovskite ABO_3 structure with Pb occupying A-sites and Zr and Ti ions occupying B-sites at random. The temperature-composition phase diagram of PZT solid solutions, proposed by Jaffe et al (Jaffe, Cook et al. 1971), is shown in Figure 1.5. Above Curie temperature, the material is paraelectric or non-ferroelectric within all material compositions. At lower temperatures, a transition to either the tetragonal (F_T) or rhombohedral (F_R) ferroelectric phases occurs. Compositions rich in PbTiO_3 can not be successfully poled, but a significant piezoelectric effect exists throughout the rhombohedral range (Jaffe, Cook et al. 1971). In the region where the Zr/Ti ratio lies between 100/0 and 94/6, the solid solution is an antiferroelectric orthorhombic phase exhibiting no observable piezoelectric effect. A morphotropic phase boundary (MPB) exists

between the tetragonal phase region (on the Ti-rich side) and the rhombohedral phase region (on the Zr-rich side) close to the point $Zr/Ti = 53/47$. According to Uta Lange (Lange 2003), the position of the MPB was shifted to Ti-rich compositions by reducing the grain size. Near this MPB, PZT materials exhibit enhanced dielectric constant, remnant polarization, and piezoelectric coefficient. It has been suggested that compositions near the MPB do not clearly differentiate between the tetragonal and rhombohedral symmetries, and thus possess both of their characteristics. Because of these phases coexisting, a total of fourteen possible polarization directions (six tetragonal $\langle 001 \rangle$ and eight rhombohedral $\langle 111 \rangle$) with reference to the cubic prototype cell axes exist. The large number of polarization directions enables optimized crystallographic orientations to be established from grain to grain in the poling process and, in turn, results in anomalously high piezoelectric properties (Randall, Kim et al. 1998). It has been recently reported that a stable monoclinic phase has been discovered close to the MPB (Noheda, Cox et al. 1999; Noheda, Gonzalo et al. 2000). The high piezoelectric response in PZT close to the MPB is caused by the piezoelectric strain that is not along the polar directions but along those directions associated with the monoclinic distortion (Guo, Cross et al. 2000). The width of the MPB has been investigated by many researchers as well and has found to be related to the compositional homogeneity and the sample processing (Cao and Cross 1993).

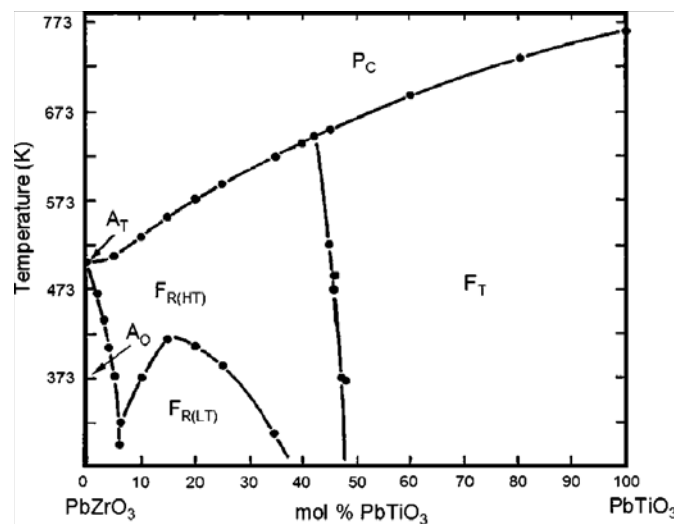


Figure 1.5 Phase diagram of lead zirconate titanate $Pb(Zr_xTi_{1-x})O_3$ (Jaffe, Cook et al. 1971)

1.3.2 Synthesis and reaction sequences of PZT

The fabrication of PZT ceramics is usually achieved via the conventional mixed oxide route. In general, it involves the following steps: weighing the raw materials in appropriate proportions; ball milling; calcining; grinding; pressing; sintering; electroding and poling (Haertling 1999). Calcining

and sintering will be introduced in details due to their importance in the manufacture process of PZT ceramics.

During the calcination, the raw materials PbO, ZrO₂ and TiO₂ react with each other to form PZT solid solution. The reaction mechanisms and sequences of these oxides have been investigated by many scientists. Table 1.1 compares the reaction sequences of PZT formation suggested by these scientists. No agreement among the results of various workers regarding reaction sequences and the formation of intermediate products has been achieved. There is, however, general agreement that the first step of the mixed oxide reaction route for compositions near the MPB is the reaction of PbO with TiO₂ to form PbTiO₃. The contradictory findings were related to the presence or absence of intermediate products like PrZrO₃ and PbO solid solution. These differences have been ascribed to the processing, raw materials as well as coexistence of tetragonal and rhombohedral phases at and near the MPB. Venkataramani and Biggers reported that a different reaction sequence occurred, depending on the ZrO₂ source. Ultrafine ZrO₂ powder resulted in formation of an intermediate PbZrO₃ phase, while a commercial ZrO₂ powder caused the formation of intermediate PbTiO₃ (Venkataramani 1980). However, the reaction sequence remained unchanged when chemically prepared submicron TiO₂ was used (Kington, Terblanché et al. 1982).

Table 1.1 Comparison of reaction sequences in formation of PZT

(Matsuo and Sasaki 1965)	(Hankey and Diggers 1981)	(Hiremath, Kington et al. 1983)	(Chandratreya, Fulrath et al. 1981)
P+Z+T	P+Z+T	P+Z+T	PZT
PT+P+T+Z	PT+P+T+Z	PT+P+T+Z	PT+P+T+Z
PT+PZ _x T _{1-x}	PT+P (ss)	PT+PZ+Z+T	PZT
PZT	PZT	PZT	

P=PbO; Z=ZrO₂; T=TiO₂; PT=PbTiO₃; PZ=PbZrO₃; PZ_xT_{1-x}= intermediate PZT composition; P(ss)= solid solution of PbO, PbTiO₃ and ZrO₂.

1.3.3 Studies on sintering

1.3.3.1 Basic theoretical background of sintering

After being formed into a desired shape, the compact of PZT powder is fired at high temperature to get dense structure. This process is called "sintering". The driving force for all sintering process is the reduction of surface free energy. Differences in sintering behavior for different materials are the result of different mechanisms of material transport, which in crystalline solid occurs by a process of diffusion involving atoms, ions or molecules. Four primary mechanisms for solid state

sintering are recognized: evaporation-condensification, surface diffusion, grain boundary and volume diffusion. Crystalline solids are not ideal in structure and contain various imperfections, "defects". It is the presence of these defects that enhance diffusional mass transport. Because they control the rate at which matter is transported, the slowest diffusing species control the rates of sintering and other mass transport processes (Rahaman 2003). Defects in PZT could be introduced by the impurities in the raw materials, dopants, lead oxide evaporation and oxygen loss or uptake during the sintering process and so on.

Sintering may be assisted by a liquid phase. Comparing to solid state sintering, the presence of the liquid phase leads to improved densification through enhanced rearrangement of the solid particles and enhanced matter transport through the liquid. It is generally agreed that liquid phase sintering proceeds in a sequence of three dominant stages: 1) redistribution of the liquid and rearrangement of the solid particles; 2) densification and grain shape accommodation by solution-precipitation; 3) final stage of sintering driven by the residual porosity in the liquid (German 1985). The wetting behavior of the solid by the liquid, the dihedral angle between the solid-liquid interfaces, and the solubility of solid in the liquid are the main kinetic and thermodynamic factors controlling the sintering process. Detailed information regarding the solid state sintering and liquid phase sintering can be found elsewhere (German 1985; German 1996; Rahaman 2003).

1.3.3.2 Solutions for the reduction of lead loss during sintering of PZT

Because the sintering temperature of PZT ceramics is usually between 1200-1350°C and the melting point of PbO is about 890°C, the volatility of the PbO component of PZT ceramics during sintering has been an obstruct to produce high-quality PZT ferroelectric ceramics (Kington and Clark 1983). At sintering temperature, the PbO vapour pressure of PZT is rather high, so that a weight loss of the order of 1 percent occurs. When the weight loss is above a certain limit, segregation of ZrO₂ will start, which will result in a troublesome second phase (Webster, Weston et al. 1967). To solve this problem, Atkin and Fulrath (Atkin and Fulrath 1971) and Holman and Fulrath (Holman and Fulrath 1973) investigated the use of powders of particular compositions (usually PbZrO₃+ZrO₂, PbZrO₃+PbO, and so on) to maintain a PbO-rich atmosphere in sintering enclosures, and the vapor-phase equilibration of PbO between sintering compact and powders. This method was demonstrated to be useful for minimize the fluctuations in compositions, while it was suggested that direct contact between PZT compact and powders used for controlling PbO partial pressure should be avoided (Kington and Clark 1983). As an alternative method, excess PbO was added into the system to compensate the weigh loss, and in this way, a stoichiometric composition could be achieved, too.

Low temperature sintering has also been studied to reduce the evaporation of PbO. Moreover, low-temperature sintering of PZT ceramics offers the advantages of reducing energy consumption and fabrication cost. Therefore, special attention has been paid to lowering the sintering temperature, which has been reported by many researchers using different techniques. Firstly, low temperature sintering was achieved by adding liquid phase into the system. Liquid phase was introduced by low melting additives and glasses, such as PbO-Cu₂O (Corker, Whatmore et al. 2000), BiFeO₃-Ba(Cu_{0.5}W_{0.5})O₃ (Kaneko, Dong et al. 1998), V₂O₅ (Wittmer and Buchanan 1981), with which the samples can be sintered at 900-1150°C. Secondly, the sintering temperature can be reduced to about 900°C by using ultrafine powders prepared by chemical processing (Mal and Choudhary 1997) or high energy ball milling (Kong, Zhu et al. 2000). Last but not least, Li and Park managed to lower the sintering temperature by using a hot isostatic process (Li, Wang et al. 2000) and spark plasma sintering (Park, Chung et al. 2001). However, low temperature sintered samples usually show poor dielectric and piezoelectric properties (Zhu, Li et al. 2005).

1.3.3.3 Investigations on the sintering kinetics

In spite of the variety and number of investigated PZT systems, there have been few attempts to study the sintering behavior of the pure PZT system and systems with liquid phase. In early 1960s, Atkin (Atkin and Fulrath 1971) studied PZT systems doped with Al and Nb by sintering the samples at different temperatures using isothermal methods. The shrinkage and density were measured after cooling down as function of sintering temperature as well as sintering time. The grain size of the samples was also determined. The sintering kinetic of these samples was suggested to follow the Coble model. In doped samples, oxygen vacancies were believed to be the rate-controlling species. A. Kingon (Kingon and Clark 1983) reported the sintering behavior of PZT within a wide range of PbO content (from -1.6% to 19%) using a similar sintering method as Atkin. It was concluded that a liquid phase mechanism dominated the sintering of PZT with excess PbO and the presence of excess PbO substantially enhanced the densification rate during the initial and intermediate stages of sintering, though not the final stage. The results on sintering of PZT samples with PbO deficiency were in agreement with Atkin's postulate of oxygen vacancy-limited diffusion in the final stage. It was, on the other hand, suggested that a more sophisticated sintering model than simple model, such as the Coble model, should be employed to describe the sintering kinetics of PZT system.

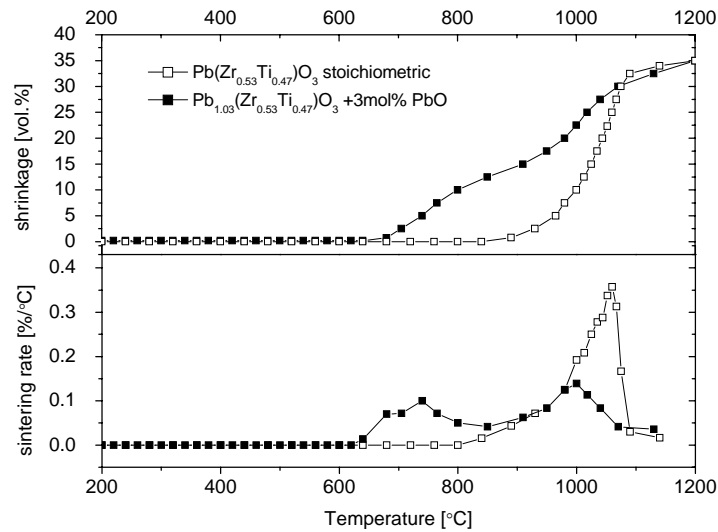


Figure 1.6 Shrinkage and densification rate curves of stoichiometric PZT and the sample with 3mol% PbO excess (Hammer and Hoffmann 1998)

Dilatometry was also employed to study the sintering behavior as it provides the possibility to study the sintering behavior *in situ*. Hammer and Hofmann (Hammer and Hoffmann 1998) reported the densification behavior and chemical homogeneity of stoichiometric PZT ceramic and PZT samples with 3 mol% PbO excess containing different La concentrations. Sintering curves are presented in Figure 1.6. For the stoichiometric composition, densification was attributed to the volume diffusion and considered to be solid state sintering as proposed by Atkin and Fulrath. Particle rearrangement due to liquid phase formed from PbO was believed to explain the maximum of the densification curve at lower temperatures for the samples containing excess PbO, whereas solid state sintering was suggested as the main densification mechanism at high temperatures.

1.3.4 Major variables affecting the properties of PZT ceramics

In a complex system as PZT, properties depend on a number of factors. Variations in many aspects, such as processing conditions (Lal, Gokhale et al. 1989; Ryu, Choi et al. 2001), porosity, homogeneity, stress (Yimnirun, Laosiritaworn et al. 2006), chemical composition (Chen, Long et al. 2003), phase content (Zhu, Li et al. 2005), grain size (Jin, Kim et al. 1997), could alter the dielectric and electromechanical properties of sintered PZT ceramics. Published findings for several variables will be briefly reviewed.

In the preceding section, the composition of PZT ceramic has been noted to significantly affect measured dielectric, ferroelectric and piezoelectric properties. These variations are attributed to a

change in crystal symmetry through chemical composition. As the crystal structure of TiO₂-rich PZT is tetragonal, the rhombohedral structure is found in ZrO₂-rich samples. Du et al. studied the composition dependence of dielectric and piezoelectric properties in ceramics (Pb_{0.95}Sr_{0.05})[(Ni_{1/2}W_{1/2})_{0.02}(Mn_{1/3}Sb_{2/3})_{0.06}(Zr_xTi_y)_{0.92}]O₃, as shown in Figure 1.7 (Du, Qu et al. 2007). The ceramics with different compositions exhibit different behaviors and ceramics with compositions near the morphotropic phase boundary have anomalous dielectric and piezoelectric properties. Based on this phenomenon, various compositions of the PZT system may be chosen to meet the specific requirements in different applications of piezoelectric ceramics (Xu 1991). For example, if a material with a high value of the planar coupling factor (k_p) and a high value of dielectric constant (ϵ_r) is desired, a composition near the MPB should be chosen. On the other hand, if a material with a high mechanical quality factor (Q_m , represents the amount of energy consumed or dissipated per oscillation cycle) and a low dielectric constant (ϵ_r) is desired, a composition far away from MPB should be chosen. Thus, properties of PZT ceramics may be tailored by changing the ratio of Zr/Ti.

For the majority of applications, the perovskite phase is desired because of its high dielectric constant, piezoelectric and ferroelectric properties. However, research has shown that other phases can also develop in the PZT system. As mentioned earlier, lead loss is a major concern for PZT ceramics due to the high sintering temperature. It is known that a pyrochlore phase usually forms in the PZT samples because of the lead deficiency (Fan and Kim 2001). To overcome the problem, adding excess lead oxide in the starting materials is a common approach to compensate the lead loss. However, when the amount of lead excess is above the lead loss in the system, it could lead to another pyrochlore secondary phase. Garg and Agrawal investigated samples with different lead content (Garg and Agrawal 1999). The secondary phases, ZrO₂ and PbO were observed in lead deficient and lead excess samples respectively and attributed to the diminishing properties. A pyrochlore phase was detected in doped PZT as well. Huang (Huang, Chen et al. 2004) reported that Nb doped PZT gave rise to the pyrochlore phase after calcination at 850°C, it was, however, transformed to perovskite after subsequently sintering at 1100°C. The secondary phase was also accounted for the poor properties of samples sintered with low temperature melting additives (Zhilun, Longtu et al. 1989). The reason that the pyrochlore phase is a detrimental phase in ferroelectric materials is associated with its crystal structure. A defect pyrochlore or fluorite phase is cubic, non-ferroelectric and exhibits significantly lower dielectric properties than perovskite PZT. The presence of an uncontrolled pyrochlore-type phase may unintentionally diminish properties. Therefore, it is very important to carefully control the stoichiometry and suppress the formation of secondary phases.

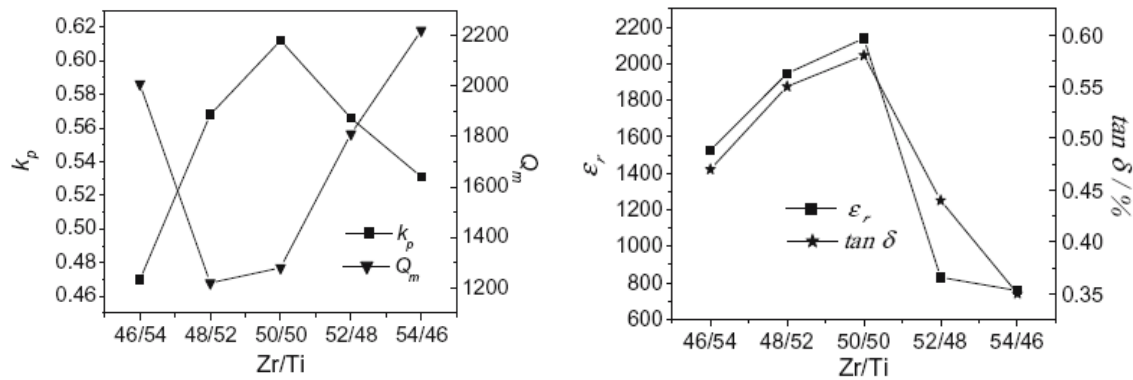


Figure 1.7 (a) Planar coupling factor k_p , mechanical quality factor Q_m and (b) dielectric constant ϵ_r , dielectric loss $\tan \delta$ (1kHz) of $(\text{Pb}_{0.95}\text{Sr}_{0.05})[(\text{Ni}_{1/2}\text{W}_{1/2})_{0.02}(\text{Mn}_{1/3}\text{Sb}_{2/3})_{0.06}(\text{Zr}_x\text{Ti}_{1-y})_{0.92}]\text{O}_3$ ceramics with different Zr/Ti ratio

Grain growth is always an important topic in sintering processes. It can be affected by sintering time, temperature, dopants or even liquid phase. Many attempts have been made to investigate the grain size effect on the piezoelectric properties in PZT ceramics. Some of them are summarized in Table 1.2. In general, the piezoelectric and dielectric properties, such as k_p , d_{33} decreased with the reduction of grain size. These observations were interpreted by the restricted domain motion and reduced domain sizes in fine-grained samples. As the grain size reduced, the grain boundaries would contribute more pinning sites to the domain walls. With less mobility, the contribution of the domain walls to the polarization decreased. It was also argued that larger domain sizes gives more effective poling and, therefore, increases the magnitude of the piezoelectric coefficients. The difficulty in poling of fine grain sized samples is demonstrated in Table 1.2. With the reduction of grain size, the coercive field increased and remnant polarization decreased. However, an opposite behavior of dielectric constant at room temperature was noticed. Although no definite consistence was achieved in all the investigations, most of the studies observed that high dielectric constant was achieved in fine-grained samples. Several models, such as the presence of internal stresses and increased domain wall contributions to the dielectric response in fine-grained ceramics were also proposed to understand the phenomenon. Internal stresses were proposed by Buessem (Buessem, Cross et al. 1966) to explain the high values of dielectric constant for small grain sizes in BaTiO_3 . It is assumed that a certain pattern of internal stresses exist in the small grains, which cannot be released by the formation of 90° domains.

Table 1.2 Grain size effect on the PZT ceramics (as the grain size decreases)

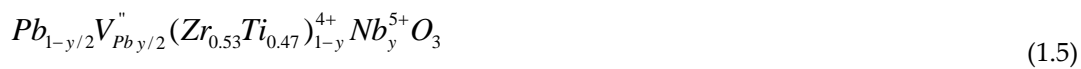
Reference	Grain size (μm)	ϵ_r at room temperature	Piezoelectric properties	Comments
(Haertling 1964)	2-5	Increases	As E_c increases, P_R decreases	Hot pressed PZT containing 2% Bi
†Webster and Weston 1968	1.7-6	Increases	As k_p decreases, P_R decreases	Clamping of domain motion
*Okazaki and Nagata 1971	1.7-6	Increases	k_p, d_{31} decreases	PbZr _{0.51} Ti _{0.49} O ₃ +0.1wt%MnO ₂
(Martirena and Burfoot 1974)	1.8,2.6, 4.6	Decreases	d_{ij} decreases	Hot presses Nb doped PZT
†Yamamoto 1992	0.6-10		E_c increases, P_R decreases	Processing dependence
(Sundar, Kim et al. 1996)	2.4-14	Increases	d_{33} decreases	PbZr _{0.52} Ti _{0.48} O ₃
(Jin, Kim et al. 1997)	1,8,15		E_c increases, P_R increases	PbZr _{0.52} Ti _{0.48} O ₃
(Randall, Kim et al. 1998)	0.9-14.3	Increases	d_{33}, k_p decrease	Nb doped PZT

* from (Xu 1991); †from (Randall, Kim et al. 1998)

1.3.5 Dopant effects on PZT ceramics

Small amount of dopants can considerably change the dielectric and electromechanical properties of PZT ceramics. The effects of dopants have been investigated extensively to improve its piezoelectric properties for various applications in actuators, piezoelectric resonators, transducers, microposition systems, etc. According to the rules of Goldschmidt, the dopant cation enters into the site (A or B) in the ABO₃ perovskite structure if the ion and the substituted ion radii do not differ by more than 15% (Jaffe 1971). A wide variety of cations can be substituted in the perovskite structure. Generally, the dopants can be classified as isovalent substitute, acceptor and donor. The Kroger-Vink notation will be used in the following discussion, i.e. oxygen vacancies are symbolized by $\text{V}_{\text{O}}^{\bullet\bullet}$, lead vacancies by $\text{V}_{\text{Pb}}^{\prime\prime}$. In this notation, the subscript indicates the lattice site occupied by the ion or defect, V is a vacancy and the superscript indicate the local charge difference from that of the perfect lattice, a dot for an extra positive charge and a slash for an extra negative charge.

For isovalent doping, the substituting ions have the same valency and nearly same ionic size as the replaced ions. For example, Sn^{4+} and Hf^{4+} substitute $\text{Zr}^{4+}/\text{Ti}^{4+}$, or Ca^{2+} and Sr^{2+} substitute Pb^{2+} . The isovalent substitution usually causes a little influence in PZT ceramic owing to the fluxing effect of doping ions during the period of sintering which facilitated the densifications [26]. For donor doping, the substituting ions have higher valence than the replaced ions, such as, La^{3+} substituting Pb^{2+} or Nb^{5+} substituting $(\text{Zr}, \text{Ti})^{4+}$, which can be compensated by cation vacancies [27,28]. Lower Q_m and coercive field result from donor doping, together with higher k_p and d_{33} (as illustrated in Figure 1.8a), which is also referred as “soft” piezoelectric behavior.



On the other hand, acceptors having a lower valence than the substituted ions, such as Li^+ for Pb^{2+} , Nd^{3+} for $(\text{Zr}, \text{Ti})^{4+}$, are compensated by oxygen vacancies [29, 30]. Acceptor doping often results in higher Q_m and coercive field, but lower k_p and d_{33} (as displayed in Figure 1.8b). This effect is called “hardening” effect and respective sample is called “hard” PZT. Different behavior from different dopant is usually explained by the introduction of oxygen (acceptor doping) or lead vacancies (donor doping) in the lattice, forming mobile or immobile quenched charged defects, such as dipoles and local stress fields.

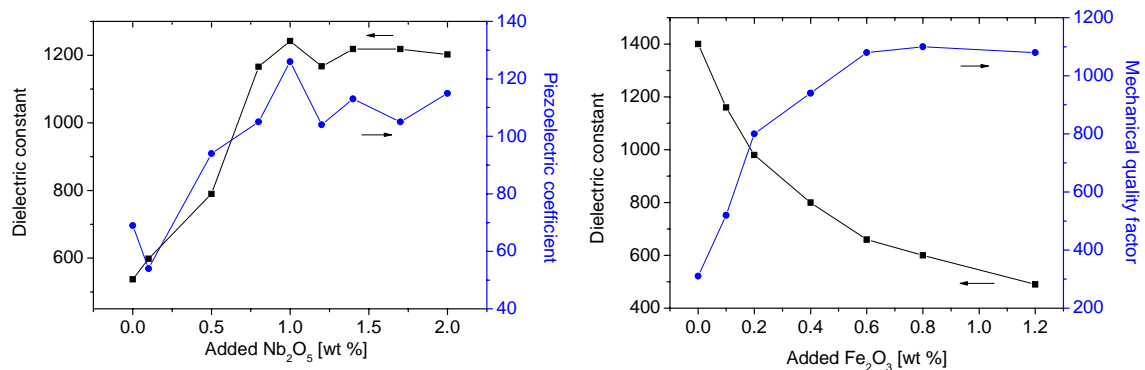


Figure 1.8 Effect of Nb_2O_3 (Kulcsar 1959) and Fe_2O_3 (Weston, Webster et al. 1969) addition on the electrical properties of lead zirconate-lead titanate ceramics

The difference in mobility of the two general types of modifications is believed to account for the difference in the relationship between donor and acceptor doping. Figure 1.9 illustrates the crystal defects in a perovskite structure caused by acceptor or donor elements. Acceptor ions cause the

formation of a dipole which is composed of an acceptor defect and an oxygen vacancy. The defects are generated at high temperature during sintering; however, the oxygen vacancies are still mobile below the Curie temperature, even at room temperature, since the oxygen ions and vacancies are close to each other. The distance is only about 2.9 Å (Figure 1.9a). In contrast, for donor modified PZT, the lead ions and A-site vacancies are separated by the oxygen atoms (Figure 1.9b). A Pb ion cannot easily hop to an adjacent A-site vacancy, therefore it is not effective for donor doping to generate movable dipoles. Tan investigated K and La doped PZT ceramics (Tan, Li et al. 1997). The mobile oxygen-acceptor complex migrated to the domain boundary to pin the domain walls, which made the switching of domain more difficult. Consequently, the coercive field was increased and the energy dissipated during switching was reduced, which then resulted in increased Q_m and increased dissipation factor. Although the A site vacancies were capable to restrain the domain motion as well, they had no sufficient mobility to migrate to the domain walls, which made the domain switching much easier. Tan studied K and La doped PZT as well (Tan, Li et al. 1999). Polarization investigations of lower valence K^+ -modified PZT specimens quenched from various temperatures revealed the evidence of polarization pinning by $K^+ - V_{O^{\bullet\bullet}}$ defect complexes. Studies of higher valent La^{3+} -modified PZT containing excess oxygen vacancies induced by vacuum annealing demonstrated that oxygen vacancies, by themselves, were not capable of polarization and domain boundary pinning. Rather, pinning only occurred in the presence of both lower valent substituents and oxygen vacancies, demonstrating the importance of defect complexes in the pinning mechanism.

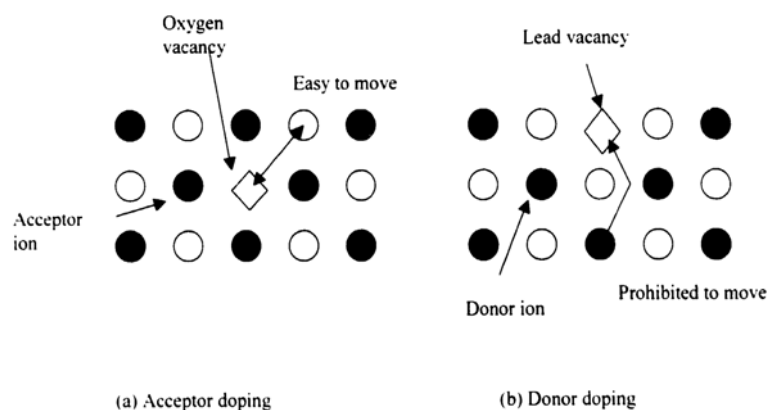


Figure 1.9 Crystalline deficiencies in PZT ceramics (Uchino 2000)

The behavior of polarization may be related to the resistivity of the modified PZT ceramics. Wu reported the DC resistivity of modified PZT ceramics and stated that donors such as La^{3+} , Nb^{5+} , V^{5+} , Sb^{5+} , Ta^{5+} , Mo^{6+} and W^{6+} contributed electrons to the conduction process and increased the

resistivity (Wu, Wu et al. 1983). When acceptors such as Mn^{2+} , Co^{2+} , Cr^{3+} , Fe^{3+} , Co^{3+} , In^{3+} and Er^{3+} were added, they contributed holes to the conduction process and decreased the resistivity. Similar results were obtained by Dih and Fulrath as well (Dih and Fulrath 1978). As shown in Figure 1.10, the bulk resistivity was significantly increased by donor doping (doped with Nb^{5+}) and reduced by acceptor doping (doped with Sc^{3+}).

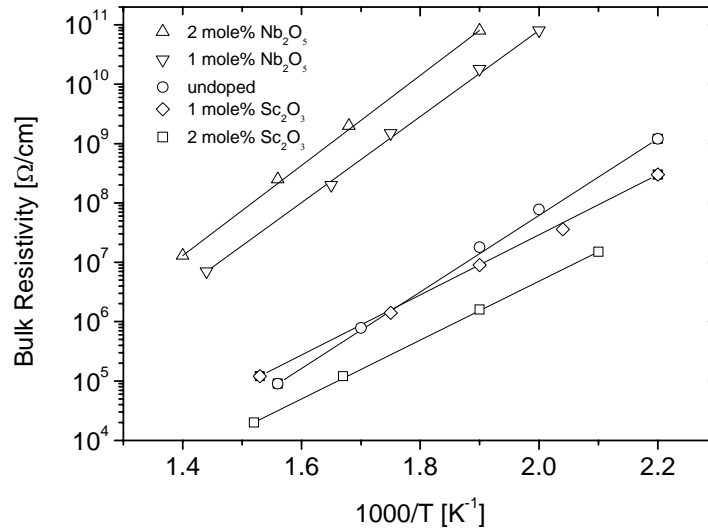


Figure 1.10 DC resistivity of PZT doped with Nb^{5+} and Sc^{3+} as function of temperature (Dih and Fulrath 1978)

1.4 Purpose of present research

The lead zirconate titanate (PZT) system has drawn a considerable amount of attention over the past few decades since Jaffe et al (Jaffe, Roth et al. 1954) reported that it exhibited excellent piezoelectric and dielectric properties. An enormous amount of work has been done on PZT ceramics. Studies have indicated that minor compositional variations in PZT have substantial effect upon densification and electrical properties of the material. However, impurities, one of the major problems involved in the mass production of PZT, have not attracted enough attention. They are inevitable species and usually come from two sources. Firstly, due to the relative higher cost of highly pure materials, the raw materials chosen for production unavoidably contain a certain quantity of impurities. Secondly, although new techniques have been developed (Mal and Choudhary 1997; Li, Wang et al. 2000; Park, Chung et al. 2001), there is a continuing interest in the mixed oxide technique to prepare lead zirconate titanate ceramics because of the convenience and suitability for mass production. During this preparation process, e.g. from the milling components, a small amount of impurities is introduced. It is evident that the dopants may significantly contribute to the sintering of PZT and definitely have an effect on the final electrical properties of

the material. It still, however, remains an open question how the impurities behave and interact with PZT ceramics regarding the small quantities and varieties of elements as well as what kind of impurity would have more profound influence on the material. Moreover, the impurities may interact with PbO during sintering when impurities such as SiO₂, B₂O₃, and BiO₂ are involved. Therefore, it is worthwhile to study their role in sintering and electrical performance in order to improve the properties of PZT ceramics.

In addition, researches often focus on improving the properties by introducing dopants or changing fabrication variables. Few have investigated the sintering kinetics of PZT. Furthermore, it is also difficult to study the densification due to the limitations of measuring tools. This is especially true for the system with liquid phase, because rapid densification often occurs in liquid phase sintering. When a customary dilatometer is used, the pushrod of the dilatometer applies a force on the sample and may change the sintering behavior and cause additional grain sliding.

The objective of this project is to investigate the effect of impurities on sintering and properties of PZT ceramics. To achieve the goal, an optical dilatometer was employed to gain an insight view of sintering *in situ* and avoid the impact that the pushrod of customary dilatometer may apply on the sintering sample. Raw materials used in our study are of purities as high as 99.99% to prevent interactions introduced by contaminants. Industrially used raw materials were also utilized in our study. Comparison of PZT ceramics prepared from different sources of raw materials were made in terms of sintering behavior and properties. The contribution of individual components of the raw materials was discussed. The impurities, characteristic of industrially used materials, were doped into the highly pure raw materials to study their effects. In addition, the effect of lead deficiency and lead excess was investigated as well. The sintering kinetics of PZT ceramics with impurities and lead oxide excess were discussed using kinetic field method.

Chapter 2 Experimental procedure

2.1 Characterizing Methods

2.1.1 Powder characterization

2.1.1.1 Particle size measurement

Particle size has a significant effect on the consolidation and sintering of the powder. In order to compare different samples, similar particle size is required. The particle size distribution of the powders was analyzed using laser light scattering (Malvern Mastersizer S, Herrenberg, Germany). The device uses light scattering to measure the equivalent spherical diameter of particles. The powder was firstly dispersed in Isopropanol under ultrasonic treatment for 2 mins to break down soft agglomerates. The results showed a Gaussian distribution. D_{50} stands for the volume median diameter. D_{50} values were calculated and used to characterize the powders.

2.1.1.2 Optical Emission Spectrometry with Inductively Coupled Plasma

Since the impurity elements had a very low concentration, a technique with high precision and low detection limit is desirable. In the present work, the compositions of the raw materials were analyzed by Optical Emission Spectrometry with Inductively Coupled Plasma (ICP-OES) using a Varian spectrometer (Varian Vista PRO, Springvale, Australia).

2.1.1.3 X-ray diffraction and Rietveld refinement

X-ray diffractometry (XRD) was employed to determine the phases present in the raw materials, and in calcined and sintered samples. The XRD experiments were performed in a Philips PW1710 X-ray diffractometer with a step scan of 0.02° and a count time of 1s. Profiles were collected using filtered $\text{Cu K}\alpha$ radiation with a wavelength of 1.5406 \AA . Qualitative phase analysis was accomplished by comparison with JCPDS database (published by ICDD in 2004) for a matching pattern. Some of the XRD data were processed with the software "Topas" (Bruker AXS, Karlsruhe) based on Rietveld method that will be introduced in the Chapter 3.

2.1.1.4 DTA TG

Simultaneous differential thermal analysis (DTA) and thermo-gravimetric analysis (TG) were carried out by a Netzsch STA 449C equipment. The measurement was performed in air with a heat

rate of 10K/min to 850°C. The weight of each sample was approximately 0.2g, within small variations.

2.1.2 Characterization of sintered PZT ceramics

2.1.2.1 SEM, EDS and Grain size measurement

Scanning electron microscopy (Supra 25, Zeiss, Oberkochen, Germany) was used to observe the microstructure in combination with energy dispersive X-ray spectrometry (EDS) to determine the local composition. To examine the polished surfaces of green samples or porous samples, they were specially prepared to prevent damaging of microstructure from polishing. They were first fixed by a holder and placed in a plastic bottle. After the bottle was evacuated for 15 mins, a mixture of EpoHeat resin and EpoHeat hardener (Buehler GmbH, Düsseldorf, Germany) were poured into it and infiltrated into pores in the samples. After curing at 60°C for 2 hours, the resin cylinders with samples inside were polished with sand paper of 600 grades till the surface of the samples appeared. The section was subsequently polished with sand paper 1200, 2500, 3 μ m diamond suspension and 1 μ m diamond suspension. Then, the resin body was softened at 200°C on a hot plate and the polished samples were taken out and thermally-etched at 800°C for 1 hour.

2.1.2.2 TEM and FIB

Transmission electron microscopy (TEM, JEM-2010, JEOL) was employed to analyze the thin film on the grain boundaries of quenched samples as well as the crystalline nature of these phases. EDS experiments were carried out with the EDAX instrument attached on the TEM column analysed with Genesis Spectrum software (EDAX Inc., Mahwah, NJ 07430, USA). The sample was prepared by the Focused Ion Beam (FIB) technique (Quanta 200 3D, FEI Company, Eindhoven, The Netherlands). The instrument uses gallium ion source. The 30 kV Ga⁺ ions and beam current of 10 pA-7nA were used to prepare the specimen. The working process was observed through an electron microscope.

2.1.2.3 XPS measurements

X-ray Photoelectron Spectroscopy (XPS) were performed on the fracture surfaces of sintered samples. Monochromatic Al K α x-rays are used for the excitation of the sample. After the direct measurement, the fractured surfaces were sputtered for different time and measured once more to gain the information from near surface or bulk regions as well. Sputtering was done by a VG EX05 scanning ion gun with Ar⁺ ions. The erosion rate measured on SiO₂/TiO₂ multilayer material was 10nm per 100s sputtering time. In present study, a sputtering time of 20 s and 4020s were used.

2.1.2.4 Density measurement

The density of samples was measured by Archimedes's method with distilled water as liquid medium. The temperature of each measurement was recorded, to use the respective density of water. For each composition, three runs on three different samples were carried out. The average and standard error were calculated.

2.1.2.5 Dielectric properties and piezoelectric properties

Silver paste with a diameter of 7.5 mm was printed on both sides of the discs and fired at 600°C to form the electrodes. For dielectric and piezoelectric characterization, the specimens with electrodes were polarized in silicon oil at 120°C for 5 min by applying an electric field of 2.1kV/mm. The dielectric constants and electromechanical coupling factors were measured by the series resonance and parallel resonance method using a precision impedance analyzer Agilent 4294. The piezoelectric coefficient d_{33} was determined by a Berlincourt measurement device. All dielectric and piezoelectric quantities reported are averages over at least 3 samples.

$$Q_m = \frac{f_p^2}{2 \cdot \pi \cdot f_s \cdot Z_s \cdot C \cdot (f_p^2 - f_s^2)} \quad (2.1)$$

$$k_p \approx \sqrt{2.5 \frac{f_p - f_s}{f_s} - \left(\frac{f_p - f_s}{f_p} \right)^2} \quad (2.2)$$

$$\varepsilon_r = \frac{C \cdot t_D}{\varepsilon_0 \cdot A} \quad (2.3)$$

f_p : parallel resonance frequency; f_s : series resonance frequency; C : capacitance; Z_s : impedance at resonance; A : electrode area; t_D : thickness of the discs; ε_0 : the permittivity of free space, 8.85×10^{-12} F/m

2.1.2.6 Ferroelectric properties

The P-E (polarization vs. field) measurements were made by using a computer controlled Sawyer-Tower circuit with a four channel oscilloscope TDS460 (Tektronix Inc., USA). Investigations of the P-E hysteresis loop were performed as a function of AC drive excitation under a frequency of 5 Hz (Frequency generator PM5138A, Fluke Corporation, USA) at room temperature. The AC electric fields ranging from 5kV/cm to 30kV/cm were achieved by a high voltage amplifier (P0610, Trek Inc., USA). The measurement was performed in air at room temperature.

2.2 Specimen Preparation

2.2.1 Raw materials

Table 2.1 List of materials used in the present study (wt%)

Materials	Purity*	Supplier	Country
PbO	99.99%	Alfa Aesar	Karlsruhe, Germany
TiO ₂	99.99%	Alfa Aesar	Karlsruhe, Germany
ZrO ₂	99.978%	Alfa Aesar	Karlsruhe, Germany
PbZrO ₃	99%	Sigma Aldrich	Taufkirchen, Germany
Silica sol Levasil®200N	31%‡	H.C. Starck	Goslar, Germany
HfO ₂	98%	Sigma Aldrich	Taufkirchen, Germany
NaNO ₃	>99.5%	Fluka Chemie AG	Buchs, Switzerland
Y(NO ₃) ₃	>99%	Fluka Chemie AG	Buchs, Switzerland
Ba(NO ₃) ₂	>99%	Merck, E.Merck	Darmstadt, Germany
Ca(NO ₃) ₂ ·4H ₂ O	>99%	Fluka Chemie AG	Buchs, Switzerland
Fe(NO ₃) ₃ ·9H ₂ O	>99%	Merck, E.Merck,	Darmstadt, Germany
Al(NO ₃) ₃ ·9H ₂ O	>99%	Fluka Chemie AG,	Buchs Switzerland

* specified by supplier

‡ solid concentration, stabilized with ammonia

2.2.2 Synthesis of PZT powders

The compositions chosen for this study had a Zr/Ti ratio of 53/47 (PbZr_{0.53}Ti_{0.47}O₃) to be close to the morphotropic phase boundary (MPB). Two sources of raw materials were used. Highly pure raw materials (HM) were purchased from Alfa Aesar, Germany (as listed in Table 2.1), while industrially used materials (IM) were obtained directly from ceramic industry. Detailed specifications of these raw materials are given in Table 2.2. The preparation of the samples was conducted according to the industrial process. PbO, ZrO₂ and TiO₂ were weighed in the proper proportions and put into a jar to make a 100-gram batch. The oxides were mixed thoroughly with distilled water. Three methods of mixing were employed, which were wet, dry ball mixing (plastic balls and jars were used to minimize the impurities which might be introduced) and planetary ball milling (stabilized ZrO₂ balls and jars were used). The slurry was then dried overnight and the powder was used in the calcination steps. The calcination was carried out in a resistance-heated furnace with the powder in an alumina crucible with alumina lid at different temperatures. The change in weight during calcination was less than 0.2%. Considering the water content absorbed

by the powder, lead loss during the calcinations process was negligible. Some calcined powder was used for X-ray diffraction measurement. The rest of it was ball-milled again to break down agglomerates and control the particle size. Table 2.3 gives the phases in these calcined powders from different mixing methods analyzed by X-ray diffraction. It was found that single perovskite PZT phase formed above 800°C, while other phases (such as lead zirconate, lead titanate) were also detected in the mixtures using dry mixing and wet mixing technique. The reaction sequence through which PZT solid solutions are formed by solid state reactions in a mixture of PbO-TiO₂-ZrO₂ has been investigated by many groups who have achieved different conclusions. For instance, the appearance of PbZrO₃ as an intermediate phase was discussed controversially.

Powder after wet or dry mixing for 24 hours was slightly compacted and analyzed using back-scattered electron imaging facility of SEM as shown in Figure 2.1. Both wet and dry mixing have little effect on size reduction of the components. The different components in the mixture from wet mixing can be clearly distinguished while less contrast was obtained in the dry-mixed powder.

Table 2.2 Main impurities for industrially used (IM) and highly pure (HM) PbO, ZrO₂ and TiO₂ raw materials (wt %)

	PbO		ZrO ₂		TiO ₂	
	IM	HM	IM	HM	IM	HM
Al ₂ O ₃	<0.001	0.002	0.014	0.004	0.027	<0.001
BaO	<0.001	<0.001	0.011	<0.001	0.002	<0.001
CaO	0.006	0.008	0.025	0.015	0.017	0.002
Fe ₂ O ₃	<0.001	0.002	0.017	0.004	0.002	<0.001
HfO ₂	<0.001	<0.001	2.344	<0.001	0.001	<0.001
Na ₂ O	<0.001	0.018	0.033	0.019	0.030	0.018
SiO ₂	0.009	0.010	0.064	0.011	0.032	0.006
Y ₂ O ₃	<0.001	<0.001	0.112	0.004	<0.001	<0.001
Phase	Massicot	Massicot	Monoclinic	Monoclinic	Anatase	Rutile

Table 2.3 X-ray diffraction results of samples from different mixing methods calcined at different temperatures for 2h (lead zirconate titanate, PZT; lead zirconate, PZ; lead titanate, PT)

Temp(°C)	Dry mixing	Wet mixing	Ball milling
900	PZT+PT+PZ	PZT+PT	PZT
850	PZT+PT+PZ	PZT+PT	PZT
800	PZT+PT+PZ	PZT+PT+PZ	PZT+ PT(few)

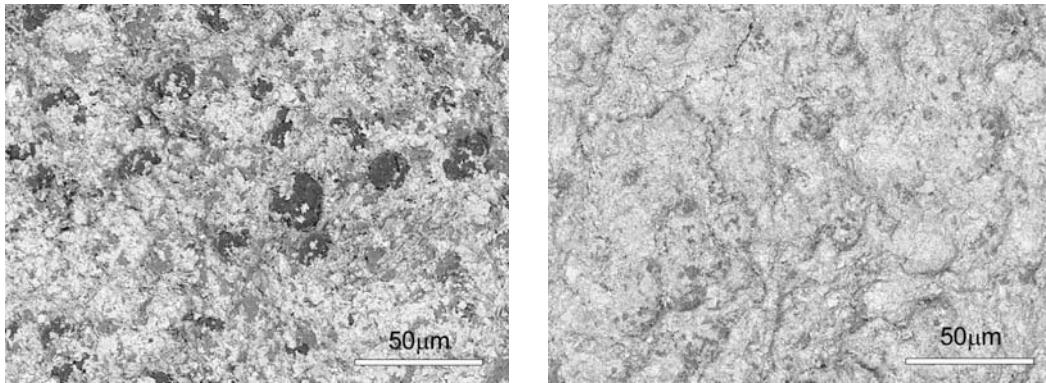


Figure 2.1 Back scattering electron images of reactants after wet mixing (a) and dry mixing (b) for 24 hours (PbO, ZrO₂ and TiO₂ are light grey, dark grey and black, respectively.)

Particle size was measured for a mixture from planetary ball milling (18 hours) and the results revealed a mean particle size of 0.6-1 μm, which is responsible for enhanced activities of raw materials and easy formation of single PZT phase above 800 °C. Table 2.4 presents chemical analysis of mixtures before calcination and PZT powder before sintering using Inductively Coupled Plasma – Atomic Emission Spectrometer (ICP-AES). Impurity concentrations in PZT powder for sintering were slightly higher than in the mixture before calcination. The concentrations of Al₂O₃, Fe₂O₃ and SiO₂ in IM powders are much higher (refer to Table 2.2) and therefore the preparation process was considered sufficiently clean. Therefore, the planetary ball milling method was used to prepare all the samples. Table 2.5 lists the mean particle size of PZT powder with different compositions after calcination and ball-milling. It evidenced that the particle size are in a narrow range, which assured the legality of comparing and discussing the sintering behavior of different systems without consideration of the particle size effect.

Table 2.4 Chemical analysis of mixtures used for calcinations and PZT powder for sintering after ball milling process (wt %)

	Al ₂ O ₃	BaO	CaO	Fe ₂ O ₃	HfO ₂	Na ₂ O	SiO ₂	Y ₂ O ₃
Mixture before calcination	0.001	<0.001	0.026	0.003	<0.001	0.027	0.021	0.001
Calcined PZT powder	0.004	<0.001	0.034	0.011	<0.001	0.035	0.011	0.001

Table 2.5 Mean particle size (D₅₀) of PZT powder with different compositions after calcination and ball-milling

Composition	HM PZT	IM PZT	HM PZT+0.5%Si	HM PZT+0.5%Na
D ₅₀ (μm)	0.77±0.16	0.61±0.12	0.86	0.65

2.2.3 Green sample preparation and sintering

After calcination, the powder was ball-milled again and dried in air overnight in order to obtain the final mixture for green sample preparation. Because the isoelectric point of PZT is close to pH 7 and it was milled with distilled water, some agglomerates must have been formed during the drying process. Therefore, the calcined powders were dissolved in distilled water with ammonia hydroxide to adjust the pH value to 11 and were left under ultrasonic treatment for 10 min. They were then freeze-dried for 18 hrs (Christ Alpha 2-4 freeze dryer, Martin Christ, Osterode, Germany). Cylindrical green samples with a diameter of approximately 10 mm and a height of 20 mm were formed by cold isostatic pressing (CIP) at 160 MPa. Green density was between 58 and 60 % of the theoretical density. For each composition, two cylindrical green samples were prepared. One of them was cut to disks with thickness of 4 mm by a silicon carbide saw to be sintered in Thermal Optical Measurement (TOM) device to study its sintering behavior. The other cylinder was sintered in a MoSi₂-heated furnace at 1280°C for 1h with a heating rate of 5K/min. After sintering, the cylindrical sample was cut into disks with a thickness of 1mm. These discs were subsequently ground and polished with a final thickness of approximately 0.6 mm for the measurement of electrical properties.

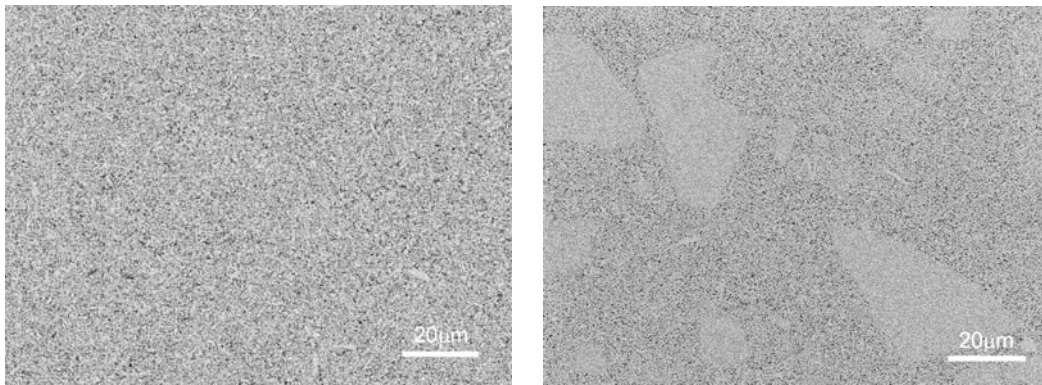


Figure 2.2 SEM images of green compacts from the PZT powder with (a) and without (b) freeze drying process

2.3 *In situ* measurement of sintering behavior

2.3.1 General procedure

In situ measurement of dimensional changes during sintering was achieved using a thermo-optical measuring device (TOMMI), which has been developed by Fraunhofer ISC (Raether, Springer et al. 2001; Raether 2009). TOMMI is the combination of a high temperature furnace (1750 °C) with an optical dilatometer. The contour of samples is imaged by a CMOS camera. Unlike customary push-

rod dilatometers, TOMMI measures dimensional changes via the optical method without a mechanical impact by the measuring device on the samples. Previous measurements by the authors in a push-rod dilatometer (Netzsch Type 402 E/7) have shown anisotropic shrinkage of PZT samples which was attributed to the small force required for the contact between push-rod and sample. The partial pressure of lead oxide vapour in the furnace atmosphere during PZT sintering has to be sufficiently high to avoid evaporation from the sample. Otherwise the shrinkage rate will be significantly reduced. Therefore, either a large volume fraction of the furnace has to be charged with PZT components or closed crucibles have to be applied. With TOMMI, an alumina crucible (70 mm×40 mm×25 mm) with two windows at opposite sides was used (Figure 2.3a). PbZrO_3 powder with a weight of 12g was deposited in the crucible to maintain PbO partial pressure and minimize lead loss from the sample. The PZT sample was placed on a bulk Al_2O_3 ceramic support to prevent direct contact between the sample and the loose PbZrO_3 powder. Sintering with a uniaxial load could be conducted in the TOMMI device as well (as shown in Figure 2.3b). The punch was inserted in the crucible through a small hole in the cover. The size of the hole was slightly bigger than the diameter of the punch so that the punch could move smoothly. The green samples had a diameter of 10mm and a thickness of 4 mm.

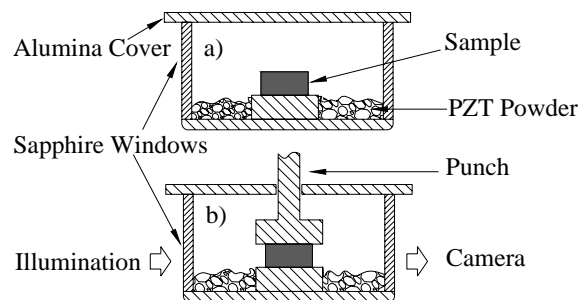


Figure 2.3 Schematic of closed crucible with two sapphire windows in opposite sides either in free sintering (a) or loading dilatometry (b)

2.3.2 Sintering in closed crucible

When PZT samples were sintered in a closed crucible with silica windows, layers were formed because of the condensation of PbO on the surfaces of the two windows which made the windows opaque. Consequently, it was impossible for TOMMI to record the contour of sample and shrinkage data. To study what had happened on the surface, SEM and EDS measurements were employed. It turned out that the composition of the deposited layer was totally different from silica from the contrast in back scattering image (as shown in Figure 2.4). EDS measurements indicated the ratio of Si/Pb was about 0.637, close to that of $\text{Pb}_5\text{Si}_8\text{O}_{21}$ which can be found in SiO_2 -rich part of the SiO_2 - PbO binary phase diagram (Smart and Glasser 1974).

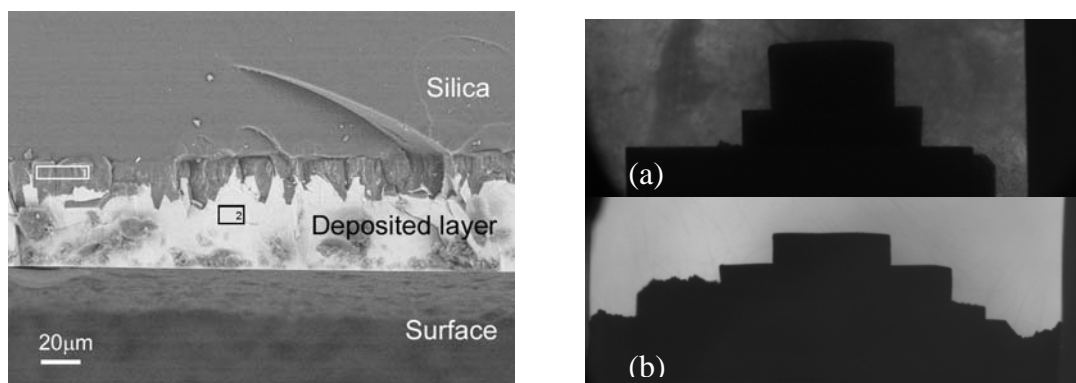


Figure 2.4 Back scattering image of contaminated silica window

Figure 2.5 Images recorded by TOMMI using two different window materials, silica (a), sapphire (b).

Tungsten and platinum layers were deposited on the silica surface to prevent reaction with lead oxide, but this was proven to be inefficient. Finally, it was found out that sapphire was well suited for these windows. Only slight contamination was found on the surface after sintering. Figure 2.5 shows the comparison of the two different windows at 1000°C during sintering in TOMMI.

Chapter 3 Data evaluation

3.1 Rietveld refinement

In order to refine the crystal structure and obtain the lattice parameters, the XRD data was processed with the software “Topas” (Bruker AXS, Karlsruhe) based on Rietveld method. In the Rietveld method the least-square refinements are carried out until the best fit is obtained between the entire observed powder diffraction pattern and the entire calculated pattern based on the simultaneously refined model for crystal structures, instrumental factors and other characteristics (such as lattice parameters, grain sizes) (Young 1995). The instrumental profile was obtained by the refinement of standard material LaB₆ (National Institute of Standards and Technology, USA), with which the instrumental factor was excluded from the further refinement of the samples. The data corresponding to all the compositions was modeled for both tetragonal phase F_T and low temperature rhombohedral phase F_{R (LT)}. The structures of F_T and F_{R (LT)} are P4mm and R3c, respectively, as given in Table 3.1. An example of a fitted profile is showed in Figure 3.1.

Table 3.1 Structure parameters of Pb(Zr_{0.53}Ti_{0.47})O₃ for tetragonal (F_T) and rhombohedral (F_{R (LT)}) phase coexistence model

Tetragonal phase with space group P4mm a=b=4.0353 Å, c=4.1312 Å,				Rhombohedral phase with space group R3c a=b=5.7551 Å, c=14.1782 Å			
Ions	x _T	y _T	z _T	Ions	x _R	y _R	z _R
Pb ²⁺	0.0	0.0	0.0	Pb ²⁺	0.0	0.0	0.286
Zr ⁴⁺ /Ti ⁴⁺	0.5	0.5	0.5518	Zr ⁴⁺ /Ti ⁴⁺	0.0	0	0.020
O _I ²⁻	0.5	0.0	0.5940	O ²⁻	0.172	0.344	0.0833
O _{II} ²⁻	0.5	0.5	0.0891				

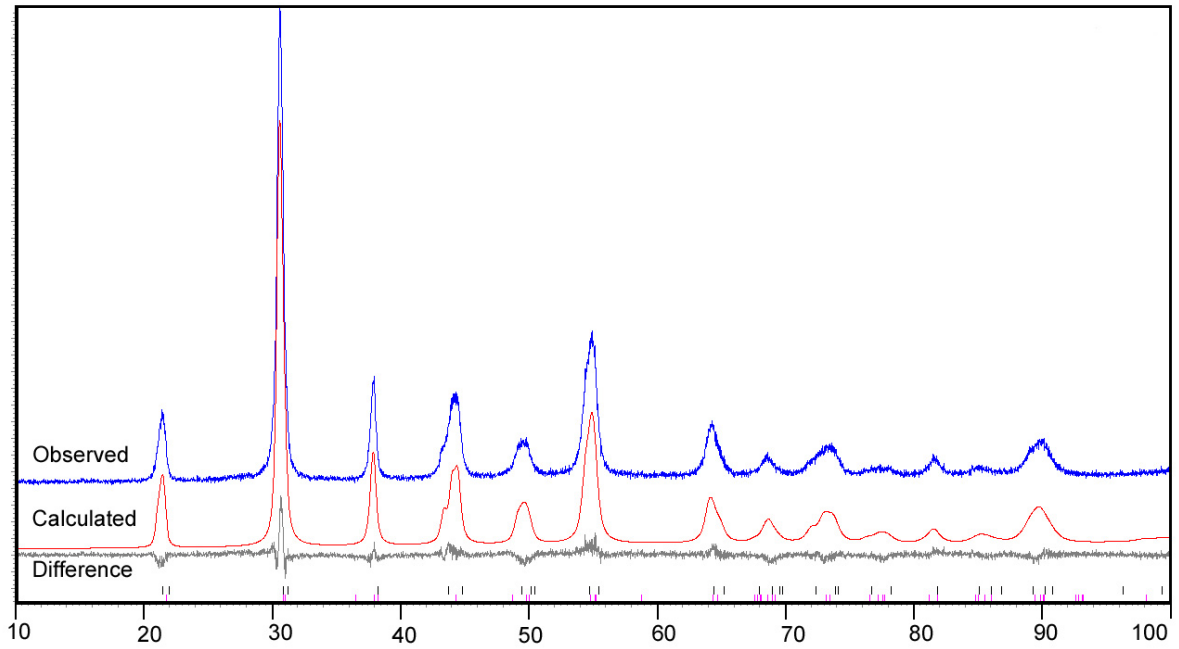


Figure 3.1 Refined pattern with observed, calculated and difference profiles in the 2-theta range 10-100° for HM $\text{Pb}(\text{Zr}_{0.53}\text{Ti}_{0.47})\text{O}_3$ using tetragonal and rhombohedral coexistence model. Bars represent the peak positions.

3.2 Image analysis

Image analysis was done on quenched samples at different sintering stages and sintered samples to obtain the grain size and the homogeneity of the microstructure.

3.2.1 Grain size measurement

Grain size was analyzed using the SEM images of thermally etched PZT samples. Mean chord length of the grains was determined using lineal intercept analysis with Image C (ImageC, Imtronic GmbH, Berlin) software on at least 300 grains. According to Mendelson (Mendelson 1969), the relation between average grain size and average intercept size was determined by equation 3.1.

$$G = k_G I_a \quad (3.1)$$

Where G is the average grain size, k_G is a proportionality constant which varies with the particle shape and I_a is the average chord length. For spherical particles, k_G was estimated to be 1.56.

3.2.2 Homogeneity evaluation

Homogeneity characterization was carried out on PZT samples with different porosities to follow the evolution of inhomogeneity during sintering. The homogeneity of the pore distribution was measured according to a variance analysis method described by Missiaen and Thomas (Missiaen

and Thomas 1995). The SEM images were converted to binary images and the pore fraction p was determined in several quadratic sections with predefined edge length l_s . The variance σ^2 of the pore fraction was scaled by the variance σ_{ran}^2 that was expected for a 2D random distribution of pores according to equation 3.2

$$\frac{\sigma^2}{\sigma_{ran}^2} = \frac{\sigma^2 l_s^2}{p l_p^2} \quad (3.2)$$

With l_p average chord length of pores determined by lineal intercept analysis. The scaled variance was calculated from more than 10 images and plotted versus the edge length of the sections. The curves were fitted by a parabola ($y=ax^2+bx+c$) where the parameter “a” in the parabola function is a measure of the inhomogeneity at a certain fractional density.

3.3 Sintering behavior of PZT ceramics in TOMMI

3.3.1 Temperature calibration

As a closed crucible was used in our experiments and the thermo couple was outside the crucible, it was expected that the real temperature inside the crucible was different due to the heat capacity of the closed crucible. In order to describe the sintering behavior and interpret our data more precisely, it is necessary to transform the temperature obtained from the thermo couple to the real temperature at which the sintering actually happened.

The temperature calibration was done by an additional thermo couple. During a heating cycle, the additional thermo couple was inserted into the closed crucible from a little hole drilled into the cover and recorded the temperature. In the meantime, the temperature of the furnace was recorded by the controller as well. Two runs with heat rates of 1K/min and 10K/min were conducted and further processed with in-house software to generate a temperature calibration file, which can be used to calibrate the temperature of heating cycles with heating rates from 1K/min to 10K/min.

3.3.2 Correction of thermal expansion

The dimensional change recorded by the software is comprised by two contributions. One is the shrinkage caused by the densification process. The other is ascribed to the thermal expansion of the compact during the heating process. Since our interest is only on the densification process, the measured data were corrected for thermal expansion, using a second order polynomial fitted to the thermal expansion curve of a sintered PZT sample.

3.3.3 Calculation of sintering temperatures

To simplify the interpretation of shrinkage curves from TOMMI, the sintering temperatures will be presented with T_{onset} and T_{50} in the following chapters. As plotted in Figure 3.2, onset temperatures (T_{onset}) for sintering were defined by the temperature where 0.1% of total shrinkage had occurred. The temperatures where samples had reached 50 % of the total shrinkage (T_{50}) were recorded as well. With 5 measurements on different pure PZT samples, the standard errors of measuring T_{onset} and T_{50} were ± 12 °C and ± 6 °C, respectively.

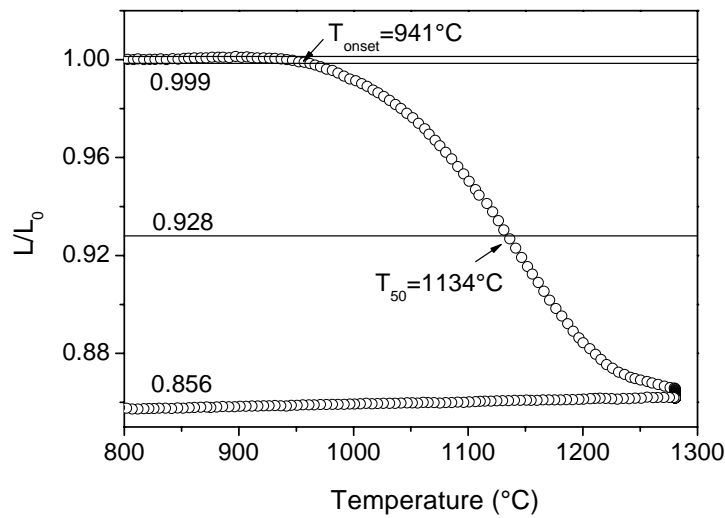


Figure 3.2 Shrinkage of a PZT sample made from highly pure materials (HM) as function of temperature (The way to derive temperatures for the onset of shrinkage (T_{onset}) and 50 % of total shrinkage (T_{50}) is indicated in the diagram.)

3.3.4 Kinetic field and activation energy for sintering of PZT

The kinetic field, which was introduced by Palmour in 1987, allows an estimation of the activation energy which controls shrinkage without knowing details of the underlying mechanisms (Palmour III and Hare 1987). It has been widely used by other groups (Zimmer, Raether et al. 1998; Raether and Schulze Horn 2009). In solid state sintering, the equation for the densification rate can be separated into temperature-dependent, grain size dependent and density dependent quantities as follows:

$$-\frac{d\varepsilon}{dt} = \frac{C_1(\rho)\gamma}{kG^n} \frac{D_0 e^{-E_a/RT}}{T} \quad (3.3)$$

ε -strain rate, ρ -density, t -time, C_1 -function of the density, γ -solid gas interface energy, D_0 -diffusion coefficient, E_a -apparent activation energy, R -gas constant, k -Boltzmann constant, T -absolute temperature, G -mean grain diameter, n -exponent depending on the densification mechanism.

The equation 3.3 can be transformed to the following equation.

$$\ln\left(-T \frac{d\varepsilon}{dt}\right) = \ln\left(\frac{C_1(\rho)\gamma D_0}{k}\right) - n \ln G - \frac{E_a}{RT} \quad (3.4)$$

A plot of the left-hand side versus $1/T$ would give a value for E_a provided the data points are taken at a constant value of ρ and G . If the grain size is not changing significantly during the experiments, points for a constant value of ρ are obtained by changing the heating rate. The measurements lead to values of E_a at different values of ρ .

The kinetic field is constructed from the measured shrinkage curves obtained from heating ramps with different heating rates. These shrinkage curves are shown exemplarily for sample HM in Figure 3.3. Then, the logarithm of the shrinkage rate is plotted in an Arrhenius plot versus the reciprocal absolute temperature. Points of equal shrinkage on the different curves are connected and form the so called iso-density lines. The iso-density lines for the PZT sintering could be fitted by straight lines. From their slopes activation energy for the respective density has been derived using equation 3.4 (Figure 3.4).

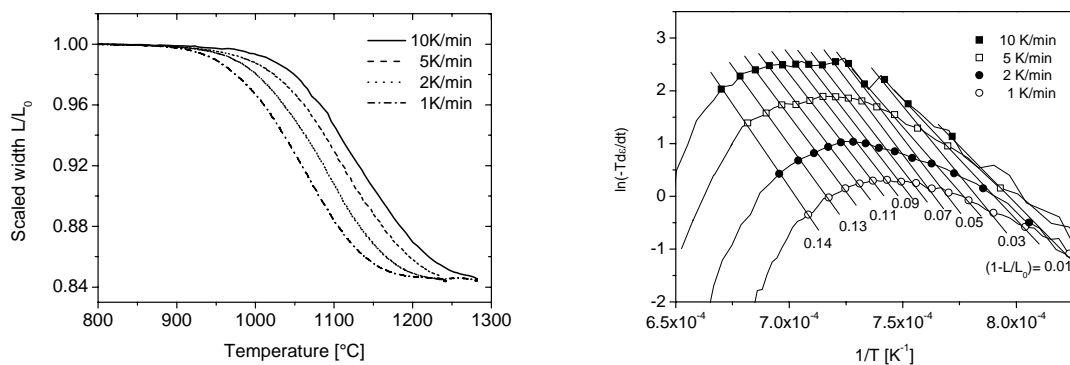


Figure 3.3 Scaled width L/L_0 of PZT prepared from highly pure materials sintered at different heating rates

Figure 3.4 Kinetic field of PZT prepared from highly pure raw materials

Chapter 4 Lead zirconate titanate ceramics from different raw materials and with lead nonstoichiometry

4.1 Introduction

As has been mentioned, the final properties of PZT ceramics are affected by raw materials and processing factors (Hiremath, Kingon et al. 1983). In the Chapter 2, effects of mixing methods on these highly pure raw materials have been described. The preparation process of PZT ceramics has been optimized. In this section, comparison of PZT prepared from two sources of raw materials (industrial raw materials and highly pure raw materials) is made in terms of sintering behavior, microstructure and electrical properties to have an overall impression of the total effect of impurities.

4.2 Comparison of PZT ceramics prepared from industrial-used and highly pure raw materials

4.2.1 Differential Thermal Analysis

Figure 4.1 presents DTA curves of $\text{PbO-ZrO}_2\text{-TiO}_2$ synthesized from different raw materials. These curves show the expected transitions of PbO and the formation of PbTiO_3 at approximately 600 °C (Chandratreya, Fulrath et al. 1981). The transition temperature of PbO to form PbTiO_3 varied in the two mixtures. The HM mixture showed a transition temperature of 625°C, while that temperature of the IM mixture shifted to a lower value, 587°C. It is known that polymorphic forms exist in TiO_2 such as rutile phase and anatase phase. From Table 2.1, the modification of HM TiO_2 was rutile, different from the modification of IM TiO_2 , anatase. The anatase phase transforms to rutile at above 900°C and is considered to be metastable (Chen, Cheng et al. 1990), which could explain the shift in the formation temperature of PbTiO_3 . A detailed discussion will be presented in the following chapter.

4.2.2 X-ray Diffraction Analysis

XRD diffraction patterns of the powder mixtures calcined at 850°C are shown in Figure 4.2. The XRD results indicate that a single perovskite phase existed in both PZT samples prepared from different raw materials. In addition, the splitting of the (200) diffraction peak is observed. Usually

the (200) line is used for phase identification. It splits into two in the tetragonal structure and no splitting occurs in the case of rhombohedral structure. Three peaks suggest the coexistence of rhombohedral and tetragonal phases (Chen, Long et al. 2003). Thus, the diffraction peak at (200) together with the other two split peaks confirm the compositions of these samples were within the morphotropic phase boundary (Chen, Long et al. 2003). Since the composition of $\text{Pb}(\text{Zr}_{0.53}\text{Ti}_{0.47})\text{O}_3$ was designated to be within the MPB, the desired phases were achieved after the calcination.

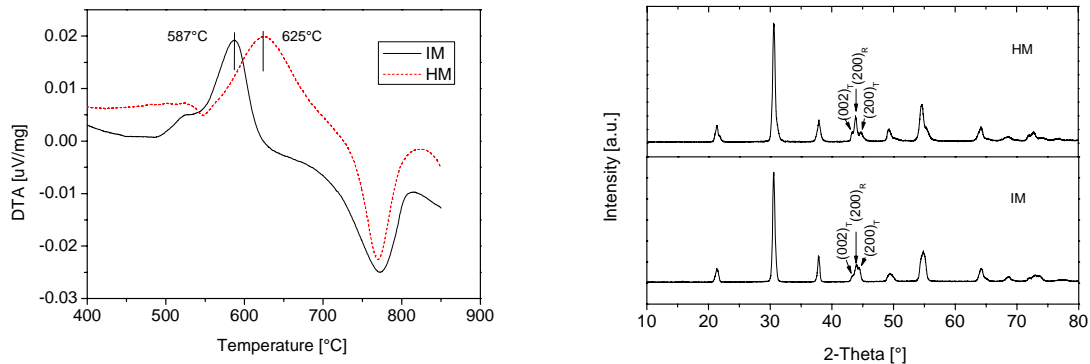


Figure 4.1 DTA study of IM and HM mixtures

Figure 4.2 XRD patterns of IM and HM mixtures after calcination at 850°C for 2 hours

4.2.3 *In situ* sintering behavior

The green samples with a composition of $\text{Pb}(\text{Zr}_{0.53}\text{Ti}_{0.47})\text{O}_3$ were prepared from calcined HM and IM powder and sintered in TOMMI device at 1280°C for 1h with a heating rate of 10 K/min to study the sintering behavior. Their shrinkage curves are illustrated as a function of temperature in Figure 4.3a. Shrinkage of a sample made from IM materials with 1.5 wt% additional PbO is also plotted for comparison. The onset temperatures of shrinkage increase from 745 °C to 865 °C and to 960 °C for sample IM with excess PbO, sample IM and HM, respectively. In addition, the temperature that HM sample requires to be fully densified is approximately 1280°C, which is much higher than that of IM sample (1100°C) and IM sample with 1.5wt% additional PbO (1000°C). The large difference in sintering activity between the samples can be seen from the densification rates as well (Figure 4.3b), which is calculated from time derivative of the shrinkage data. The densification rate of sample HM is much lower than that of sample IM and reaches its maximum at 1190 °C whereas sample IM shows the highest densification rate at 950 °C. The differences in the sintering behavior between the HM and IM samples are attributed to the differences in raw materials. Since the particle sizes of those two samples are similar (refer to Table 2.5), the reason for the distinctive sintering behavior of the two samples is explained by the impurity level. As listed in Table 2.1, all the impurity concentrations in IM raw materials are higher than that in HM raw materials.

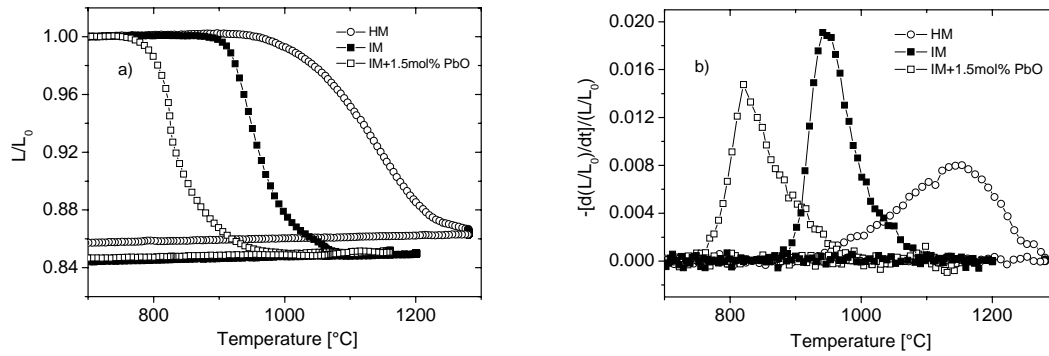


Figure 4.3 Scaled width L/L_0 (a) and densification rate dL/dt (b) of PZT samples made from different raw materials at a heating rate of 10 K/min (HM-highly pure materials, IM- industrially used materials)

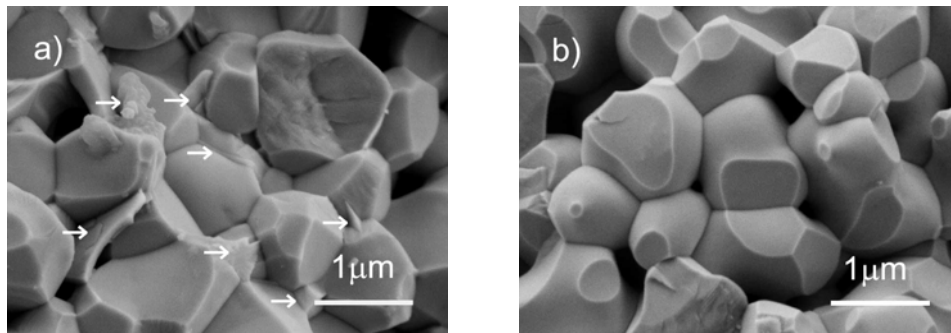


Figure 4.4 SEM images of pure PZT samples quenched at a linear shrinkage of 10% made from industrially used raw materials (a) and highly pure raw materials (b). (Arrows indicate secondary phase)

It is well known that a small amount of liquid phase can significantly stimulate rapid densification and reduce the sintering temperatures (Marion, Hsueh et al. 1987). Liquid phase sintering in PZT containing excess PbO has already been reported and its effect is attributed to the low melting point of lead oxide (Snow 1974; Fan and Kim 2001). Thus, the similar sintering behavior of IM samples with and without PbO excess indicates that liquid phase has been formed even in stoichiometric IM sample. Figure 4.4 shows the microstructure of samples IM and HM which were quenched after a linear shrinkage of 10% during the sintering with a heating rate of 10 K/min. Secondary phases were observed at grain boundaries and triple junctions as pointed out by arrows in Figure 4.4a. Unlike the IM sample, the HM sample showed no secondary phase after quenching (Figure 4.4b). Although – due to its small size– it was difficult to measure the composition using EDX, a brighter color of the secondary phase than the grains was observed using the QBSD detector of SEM. It indicated a PbO-rich phase, which has already been found in PZT samples with PbO excess or additives purposely introduced by other researchers (Snow 1974). Therefore, it is assumed that the impurities in IM mixture formed a melt phase with the PbO at low temperature.

The effect of secondary phase on sintering of PZT is emphasized by Figure 4.3b, as the densification rate of sample IM reaches a maximum which is about two times higher than that of sample HM.

4.2.4 Sintering behavior with uniaxial load

The comparison of sintering with and without load of PZT samples from different raw materials is shown in Figure 4.5. With the load the strain in the axial direction, i.e. the height change of the cylindrical samples, is increased while the strain in the radial direction is significantly decreased compared to free sintering. During cooling the strain rate is nearly zero. Samples sintered without load showed exactly the same shrinkage in axial and radial direction. Note that the used external stress of 0.4 MPa is smaller than the sintering stress which is usually between 1 and 10 MPa for the used powders. Previous experiments on many ceramic systems have shown that the anisotropy which is caused by small uniaxial stresses during loading dilatometry depends on the sintering mechanism: very small plastic deformation is observed for solid state sintering whereas a drastic increase by more than an order of magnitude was found for all liquid phase sintered systems (Scherer 1986). The anisotropy observed in the loading experiments indicates that sintering of both types of samples, HM and IM, was dominated by a liquid phase mechanism. Although a liquid phase sintering mechanism is expected for sample IM (referring to the previous section) it is surprising for sample HM exhibiting such anisotropic sintering behavior.

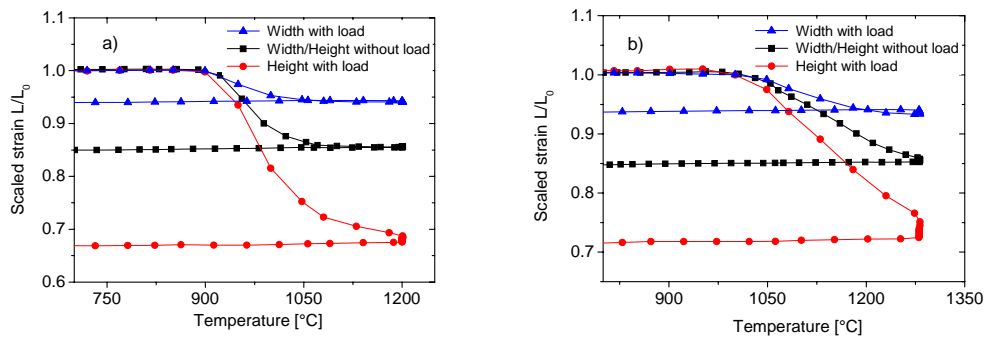


Figure 4.5 Axial and radial strain of PZT samples with or without uniaxial load of 0.4 MPa at a heating rate of 10 K/min made from industrially used raw materials (a) and highly pure raw materials (b)

4.2.5 Dielectric and piezoelectric properties

The dielectric and piezoelectric properties of HM and IM samples are given in Table 4.1. Within the experimental error, the mechanical quality factor shows no significant variation between these two samples. IM PZT exhibits a lower coupling factor, dielectric loss factor as well as lower

piezoelectric coefficient d_{33} than HM sample. However, the dielectric constant of IM sample is much higher than that of HM PZT. Previous investigations have demonstrated that the dielectric and piezoelectric characteristics can be easily tailored by doping (Hammer, Monty et al. 1998). The smaller coupling factor and piezoelectric coefficient imply a “soft” characteristic of IM sample comparing to HM sample, whereas the higher dielectric constant suggests the “hard” side of IM sample as well. The combination of “soft” and “hard” characteristics of IM sample could be attributed to the different impurities in the raw materials. In order to understand the mixed behavior, further investigations on the impurities will be presented in the next chapter.

Table 4.1 Dielectric and piezoelectric properties of pure PZT samples prepared from different raw materials

Sample	Chord length (μm)	Planar coupling factor k_p (%)	Dielectric loss $\tan\delta$ (10^{-3})	Mechanical quality factor Q_m	Piezoelectric coefficient d_{33} (pC/N)	Dielectric constant ϵ_r
Pure IM	16.5 \pm 0.4	51.3 \pm 0.2	17.4 \pm 1.6	96 \pm 10	270 \pm 0.2	863 \pm 11
Pure HM	13.4 \pm 0.4	53.3 \pm 0.9	20.6 \pm 0.8	84 \pm 15	322 \pm 5	754 \pm 22

4.2.6 Ferroelectric properties

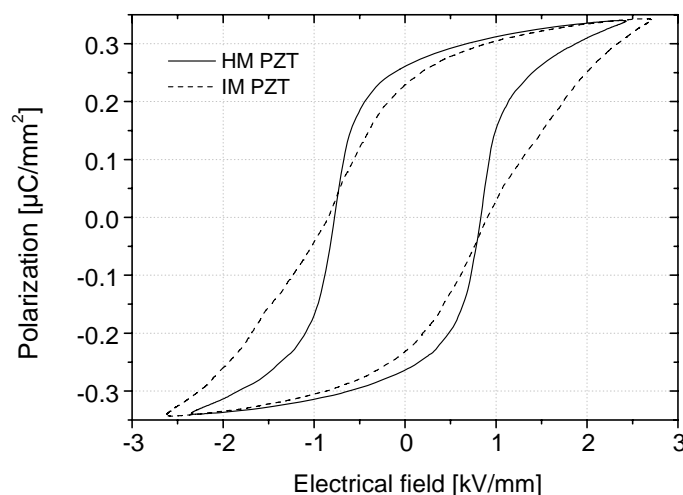


Figure 4.6 Comparison of hysteresis loops obtained from HM PZT and IM PZT

Differences on the hysteresis loops were also observed. Figure 4.6 plots the polarization hysteresis (P-E) loops of both samples. The shape of the P-E loops differs significantly with the ceramic compositions. A well saturated loop is observed with the highly pure sample, while a less “square”

shaped loop is found for the IM sample. "Hard" behavior in IM sample is suggested as its remnant polarization is smaller and coercive field is relative larger than in the highly pure sample. Because of the impurities in IM sample, defects may be introduced to the system. This phenomenon reveals pinned domain motion in IM sample and is believed to be related to the strong interaction between point defects and domain walls (Chaisan, Yimnirun et al. 2007). Antiferroelectric behavior could result from this interaction (Takahashi 1970). No antiferroelectric phenomena were observed in our samples.

4.3 Effect of lead nonstoichiometry on highly pure PZT

Because lead loss has always been an issue of sintering or electrical properties, effects of lead nonstoichiometry on PZT ceramics are investigated in this section before the study on the specific impurities is carried out in Chapter 5 (Webster, Weston et al. 1967; Holman and Fulrath 1972; Akbas, McCoy et al. 1995). Lead oxide excess is usually introduced to the PZT systems to lower the temperature as well as to compensate the lead loss from evaporation of lead oxide during sintering. Liquid phase from lead oxide is formed due to its low melting point (Garg and Agrawal 1999). Moreover, it could be formed at even lower temperatures if some of the impurities have a eutectic point with lead oxide (Zhilun, Longtu et al. 1989). It is known that lead oxide can exhibit a eutectic point from the binary systems with SiO_2 (Calvert and Shaw 1970), Fe_2O_3 (Mountvala and Ravitz 1962), and Bi_2O_3 (Yoo, Lee et al. 2005). Pérez et al also reported PbO-SiO_2 as a sintering additive to produce highly dense materials (Pérez, Soares et al. 2005). Therefore, liquid phase sintering was investigated in the highly pure system with lead oxide excess to exclude the impurity effect. Additionally, PZT systems with lead oxide deficiency were investigated as well because lead oxide deficiency happens in PZT systems without enough precautions to maintain its stoichiometry. In this study, the level of lead oxide nonstoichiometry is within a range of -1.0-3.0%, which is similar to the level in industrial production.

4.3.1 Phase determination

XRD patterns of PZT with different lead nonstoichiometry (0.5, 1.5, 3mol% lead excess and 0.5, 1.0 mol% lead deficiency) are compared in Figure 4.7. In all cases, the splitting of the broad diffraction peak (200) is observed, which reveals that both rhombohedral and tetragonal phases are present and is consistent with the composition close to the MPB. It was reported that a secondary phase of ZrO_2 could result from lead deficiency considering the phase diagram of $\text{PbO-ZrO}_2\text{-TiO}_2$ (Webster, Weston et al. 1967). However, no peaks from additional phase are observed in the lead deficient

PZT samples. This may be due to the inefficiency of XRD to detect a small quantity of secondary phase.

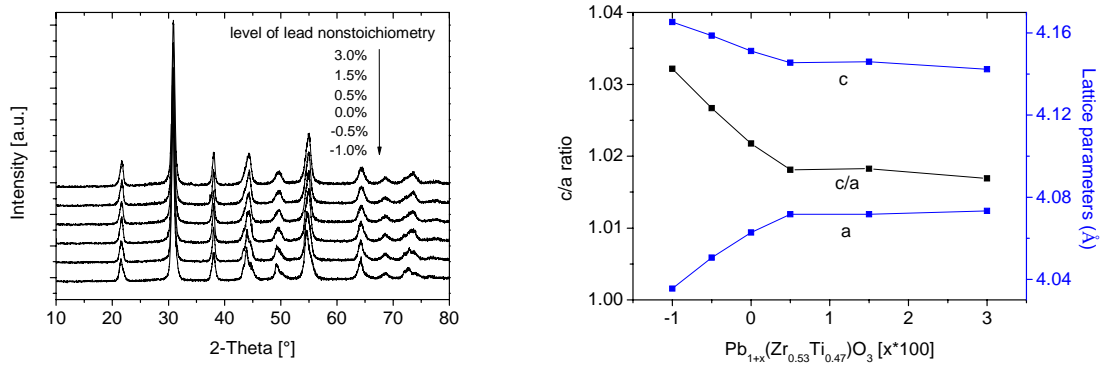


Figure 4.7 XRD patterns of PZT with different levels of lead nonstoichiometry

Figure 4.8 Evolution of the unit cell distortion of tetragonal phase, c/a ratio with lead nonstoichiometry

From the XRD data, the patterns were refined using Rietveld method. The lattice parameters and c/a ratio are shown in Figure 4.8 as a function of lead nonstoichiometry. It is seen that higher c/a ratio was introduced to the lattices of lead deficient samples, whereas the tetragonal distortion was initially decreased with small amount of lead excess, and then remained constant with further addition of lead oxide. Soares et al reported results on the lattice change with PZT composition (Soares, Senos et al. 2000). It was found that the values of the lattice parameters c and a were closing to each other with the increase of Zr/Ti ratio in the entire composition range where the tetragonal phase was present. The significant reduction of the lattice distortion with increasing Zr-content was also reported by Hoffmann and Hammer (Hoffmann, Hammer et al. 2001). In their report, the c/a ratio for morphotropic (54/46) and tetragonal (45/55) compositions differed by about 30%. If ZrO₂ was precipitated as secondary phase in the lead deficient samples as assumed, the Zr/Ti ratio would decrease with increasing lead deficiency, therefore higher tetragonal distortion would be expected. Based on the above discussions, it is believed that the drastic tetragonal distortion in lead deficient PZT results from the change in composition caused by the precipitation of ZrO₂. Comparing stoichiometric PZT with the samples with lead oxide excess, the c/a ratio slightly decreases. It indicates a slightly lead deficient composition in the stoichiometric HM PZT which was caused by lead loss during the calcination. In the present study, no attempt was made to quantify the amount of rhombohedral and tetragonal phases present in the samples, as comparison of the peak intensity may not give accurate phase concentrations (Gupta and Viehland 1998).

4.3.2 Sintering behavior

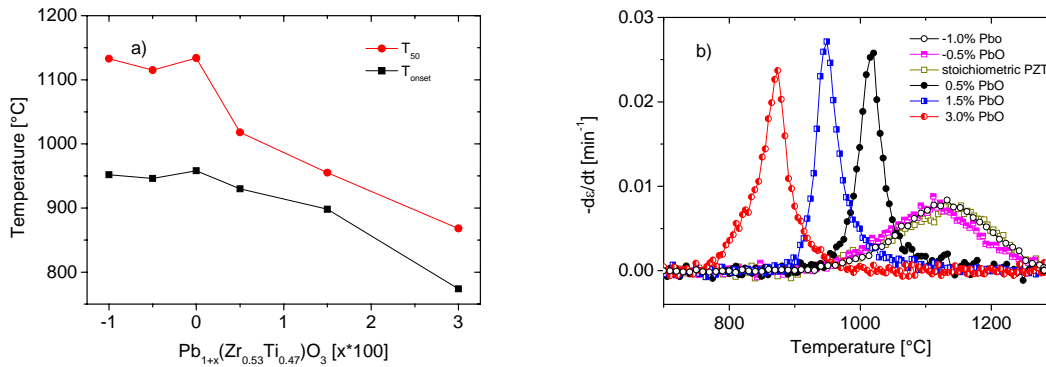


Figure 4.9 Sintering temperatures (a) and densification rates (b) of PZT samples with different levels of lead nonstoichiometry (-1.0, -0.5, 0, 0.5, 1.5, 3%; heating rate 10K/min)

Figure 4.9 presents the sintering temperatures of PZT ceramics with different levels of lead oxide nonstoichiometry. It is evidenced that densification was highly improved by addition of PbO excess. Both temperatures T_{onset} and T₅₀ decrease dramatically with increasing amount of lead oxide excess. The sample with 1.5 mol% PbO excess started to sinter below 900°C and had a T₅₀ of 955°C, comparing to 958°C and 1130°C of the pure PZT sample. In contrast to the samples with lead oxide excess, the temperatures of PZT sample with 0.5 mol % and 1.0 mol % lead oxide deficiency showed only few variations.

It might be expected that the lead deficiency (leading to oxygen vacancies) would increase the diffusion rate and improve the densification, but this was not the case. Beside the oxygen vacancies, an equal number of lead vacancies was introduced as well as a pair of uncharged Schottky vacancies (Shackelford and Holman 1975). These Schottky vacancies cannot move freely in the crystal to enhance the diffusion and densification process. Owing to the lead oxide evaporation, thermal Schottky vacancies were introduced to the stoichiometric sample according to the following equation.



The observed independence of densification rate on the lead deficiency was in disagreement to Kingon and Clark's findings, in which a sample with 1.6% lead oxide deficiency showed a higher densification rate than that of a sample with 3.5% PbO excess (Kingon and Clark 1983). They believed that an increase of oxygen vacancy concentration contributed to the surprisingly improved densification behavior of 1.6 mol % lead deficient sample. However, their sample with 0.8% lead deficiency exhibited a quite low densification rate.

The improvement in sintering of samples with lead oxide excess can be easily explained by two reasons. Primarily, the formation of Schottky vacancies during sintering was suppressed by lead oxide excess which compensated part of the lead loss. Moreover, liquid phase formed during sintering from the excess lead oxide, due to which the materials transport was accelerated. Nevertheless, it is noted that with 3mol% PbO excess, the onset temperature was reduced to approximately 770°C, which is far below the melting point of pure lead oxide (888°C). Since it is difficult to detect the liquid phase at the initial stage of sintering due to the relatively low quantity and small particle size, the sample with 3.0 mol% lead oxide was sintered with a quite small load (0.01MPa). If there is no liquid phase formed during the initial stage of sintering, such small load will not affect the sintering behavior, as the sintering stress without liquid phase is already between 1-10MPa (German 1996). However, anisotropic sintering behavior is expected if a liquid phase is present, similar to the load experiments of IM and HM samples (as shown in Figure 4.5). Figure 4.10 shows the comparisons of PZT with 3.0mol% of lead oxide during free sintering and sintering with a load of 0.01 MPa at a heating rate of 2K/min. An early densification maximum was observed on the shrinkage rate curve during loaded sintering. Kingery et al. studied the hot press sintering with the presence of liquid phase. It is suggested that the applied pressure is most effective in giving rapid densification by the rearrangement process. Once this process has been completed, densification continues with other sintering mechanisms (Kingery, Woulbroun et al. 1963), which is in a good agreement with our results. Therefore, liquid phase was believed to form already at 770°C, far below the melting point of PbO. In order to elucidate the reason, additional experiments are required in the future.

In Hammer and Hoffmann's former study, two densification maxima on the shrinkage curves were observed in the samples with the same amount of lead oxide excess during free sintering (Hammer and Hoffmann 1998). The reason may be related to the way in which their shrinkage data were obtained. Customary dilatometers were used in their study, which unintentionally allowed the push rod of the dilatometer to apply a small force on the measuring sample and enhance the rearrangement process (Kingery, Woulbroun et al. 1963). Similar results were reported by Wang et al. on PZT ceramics using LaBiO₂+CuO as sintering aid which could form a liquid phase (Wang, Murakami et al. 2001). One peak was seen in the shrinkage curve of pure PZT ceramics, while two peaks were observed in the shrinkage curves when the sintering aid was present. A load of 0.01N from their thermo-mechanical analyzer (TMA) was acknowledged.

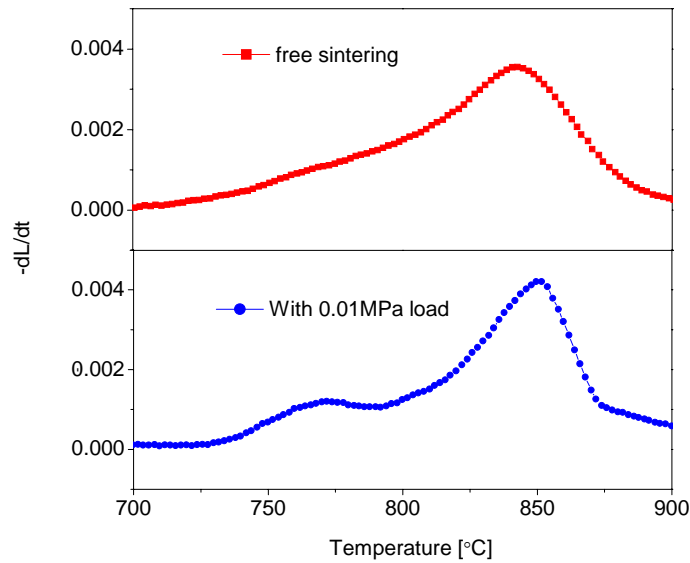


Figure 4.10 Comparison of shrinkage rate of PZT sample with 3.0 mol% PbO excess during free sintering and sintering with 0.01MPa load (heating rate 2K/min)

4.3.3 Microstructure properties

The sample with 1.5 wt% PbO excess was quenched at a fractional density of 85%, to detect the morphology of liquid phase formed by lead oxide during sintering. Figure 4.11 shows the TEM study of the quenched sample. A thin film was seen along the grain boundaries. The thickness of this film is about 2 nm. No change in composition by EDS analysis was observed at the grain boundaries and the grains, which could be due to the small size of the interlayer. From the wetting experiments we have done, it is seen that the wetting angle of PbO melting phase on PZT is nearly zero. This suggests that the liquid phase formed from lead oxide would be able to generate a thin film to cover the individual PZT grains. The grain size of the quenched sample was obtained through chord length method on SEM images and to be 1.25 μm . Assuming that the thin film is pure PbO, the weight fraction of the liquid phase is 1.15 wt%, calculated from its thickness and PZT grain size. Considering the evaporation of lead oxide during sintering, the result is in good agreement with the actual content of lead oxide excess (1.5 wt%) added in the preparation. Goo et al. have reported that the nature of the liquid phase on the grain boundary of pure $\text{Pb}(\text{Zr}_{0.52}\text{Ti}_{0.48})\text{O}_3$ with 3 wt% excess PbO is amorphous (Goo, Mishra et al. 1981). In contrary, no clear sign of amorphous phase was observed in the present highly pure sample. Since PbO, ZrO_2 , and TiO_2 , are not glass-formers, the grain-boundary phase is expected to be crystalline. The amorphous nature in Goo's report was believed to result from impurities of the raw materials. Glass formers, such as SiO_2 , B_2O_3 , Bi_2O_3 are common impurities in the raw materials that could change the nature of liquid

phase in PZT samples with lead oxide excess into glassy phase. For example, SiO₂ was detected in our industrial raw materials (refer to Table 2.2).

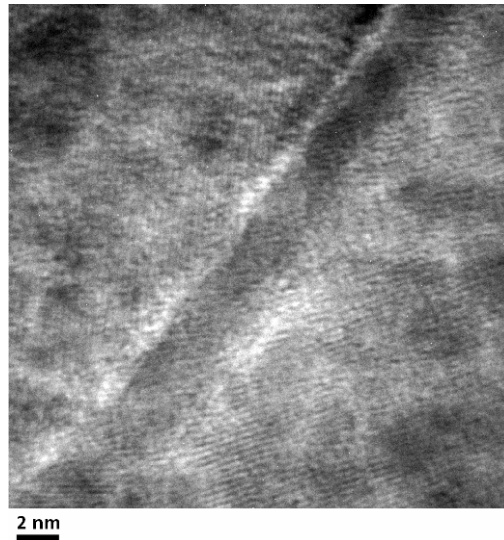


Figure 4.11 TEM study on the PZT sample with 1.5% excess PbO quenched at a fractional density of 82%

Figure 4.12 presents the density of PZT ceramics sintered at 1280°C for 2 h as a function of lead nonstoichiometry. In the case of lead deficient samples, a smaller density than the pure PZT sample is observed. The reason should be associated with reduced molecular weight in the lead deficient samples because lead is the heaviest element in PZT. As known from the last section, densification was highly enhanced with lead oxide excess, while being independent of lead oxide deficiency. Therefore, the density was increased by a small amount of lead oxide excess and to some extent was reduced by the lead deficiency. The relatively low density of the sample containing the maximum excess of lead oxide (3.0 mol %) should be related to overfiring. Clusters of large pores appeared after sintering, as seen from the SEM image (Figure 4.13a). However, much smaller pores were observed in the samples with 1.5% PbO (Figure 4.13b). The sintering temperatures required to densify the sample containing 3.0%PbO was much lower than that of the sample with 1.5% PbO. When both samples were sintered at the same temperature (1280°C for 2h), overfiring is likely to be expected in the one containing more liquid phase. Because pore coarsening occurred concurrently with the grain growth at the final stage of sintering, the average pore size increased with sintering time (Kim, Kim et al. 1990). Pore growth and density decrease in liquid phase sintering were also reported and were interpreted in terms of two possible mechanisms, pore coalescence and pore coarsening, due to the difference in curvature between small and large pores (Oh, Chung et al. 1988).

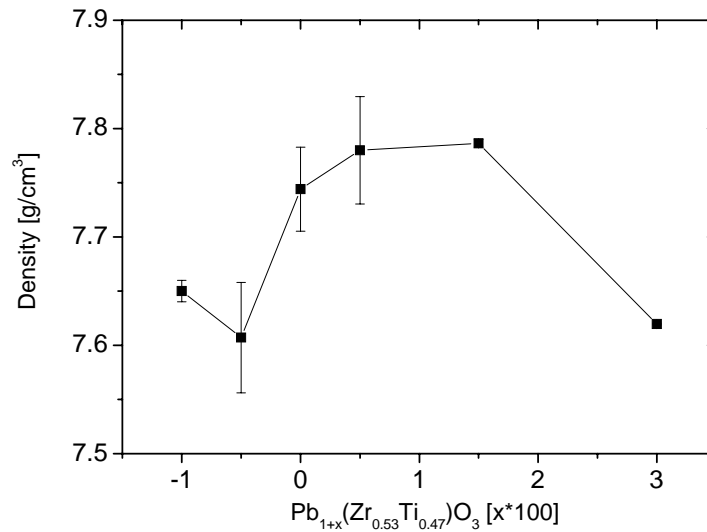


Figure 4.12 Densities of PZT samples with different amount of lead oxide excess (-0.5, 0, 0.5, 1.5, 3) sintered at 1280°C for 2 h with a heating rate of 5K/min

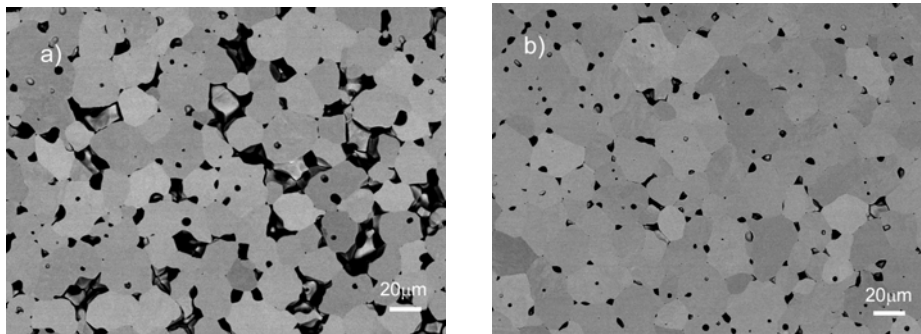


Figure 4.13 SEM images of PZT samples containing 3.0%PbO (a) and 1.5% PbO (b) sintered at 1280°C for 2 h with a heating rate of 5K/min

4.3.4 Dielectric and Ferroelectric properties

Figure 4.14 displays the electrical properties of samples with different levels of lead nonstoichiometry. Lead excess shows no significant impact on the planar coupling factor k_p , while it is reduced when lead deficiency was introduced. The dielectric loss factor $\tan\delta$ and d_{33} followed the tendency of density (Figure 4.12). With increasing amount of nonstoichiometry, they increased at first to a maximum and then started to descend with further lead excess. The mechanical quality factor Q_m experiences a decrease with raised lead excess. An upward trend with increased lead deficiency was observed in the dielectric constant at room temperature.

In a polycrystalline system, dielectric and piezoelectric properties are dependent on the addition of two contributions, named in the literature as intrinsic and extrinsic (Zhang, Pan et al. 1988). The

intrinsic contribution comes from the deformation of the unit cell, while the remaining extrinsic contribution is the result of the existence of domain walls and defect dipoles (Garcia, Perez et al. 2008). As seen from Figure 4.8, the tetragonal distortion of the perovskite unit cell increased with lead deficiency, which translated to a reduction in the volume of the unit cell. Randall stated that these dimensional changes were the result of internal stress when the transition from the paraelectric to ferroelectric phase occurred (Randall, Kim et al. 1998). Therefore, the high distortion of the tetragonal cell in lead deficient samples can create strong local internal stress that made domain wall motion difficult. Moreover, internal stress was strong enough to switch the polarization back after the electrical field was removed, which increased the difficulty to polarize the sample and reduced the contribution of the domains. Consequently, the mechanical quality factor was increased and piezoelectric, dielectric loss and coupling factor were reduced.

It is well known that the dielectric constant depends largely on the composition of PZT samples, especially the Zr/Ti ratio. M.R. Soares (Soares, Senos et al. 2000) investigated the dielectric properties of PZT ceramics with the coexistence of tetragonal and rhombohedral phases. Within the MPB region, the dielectric constant of the ceramic increased as the composition approaching the tetragonal phase side (Ti-rich region). From the discussions in section 4.3.1, it is known that the Zr/Ti ratio is reduced due to the precipitation of ZrO_2 in the lead deficient samples. Therefore, as the lead deficiency increased, the composition moved towards the Ti-rich region, resulting in higher dielectric constant. Webster and Weston reported the dielectric properties of lead deficient samples with Zr/Ti ratio of 0.497 and 0.539. In the PZT with the molar ratio of 0.539, the dielectric constant generally increased with decreasing PbO content, which is in a good agreement with our results. This effect was explained by the shift of compositions to the tetragonal-rhombohedral boundary (Webster, Weston et al. 1967). Moreover, the strong internal stress caused by the lattice distortion in lead deficient samples could also be attributed to the high dielectric constant. In fine grained $BaTiO_3$, high dielectric constant is always observed with the grain size around 1 μm , which was reported to be the consequence of the strong internal stress in the fine grained samples (Buessem, Cross et al. 1966; Bell, Moulson et al. 1984).

In samples with excess lead oxide, as the tetragonality was reduced and held constant when the concentration of PbO excess was beyond 0.5 mol% (refer to Figure 4.8), the switching of spontaneous polarization became easier, which resulted in a decrease in the coercive field and an increment in the electromechanical coupling factor, together with a reduction in the dielectric constant. Moreover, the higher density of samples with lead oxide excess could contribute to their better properties as well. The deteriorated properties of the sample with 3.0% lead oxide excess

should be associated to the high porosity and the secondary phase. It also implies the optimal amount of the lead oxide excess in PZT ceramics should be less than 3.0 mol% in order to maintain the partial pressure and compensate the lead evaporation as well as achieve high quality of PZT ceramics.

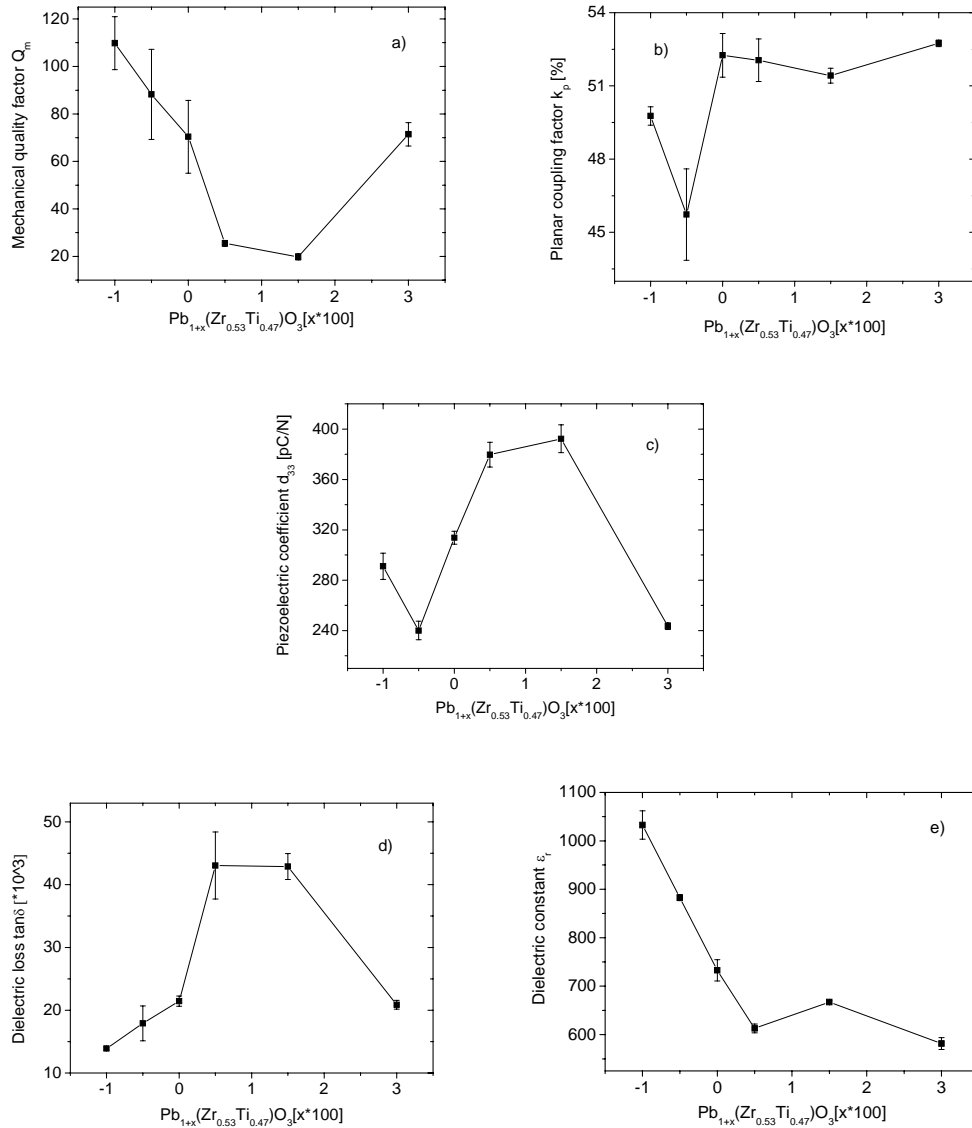


Figure 4.14 (a) Mechanical quality factor Q_m (b) Planar coupling factor k_p (c) Piezoelectric coefficient d_{33} (d) Dielectric loss $\tan \delta$ (e) Dielectric constant ϵ_r of PZT with different level of lead nonstoichiometry

Figure 4.15 displays the P-E loops of the PZT samples with lead nonstoichiometry. It is obvious that the samples with lead oxide excess smaller than 1.5 mol% have higher polarization than the samples with lead deficiency and 3.0% PbO excess. The lead deficient samples required, however, higher coercive field. This is consistent with the results regarding their piezoelectric properties and further confirms the assumption that the internal stress was caused by the increased tetragonal distortion due to the lead deficiency.

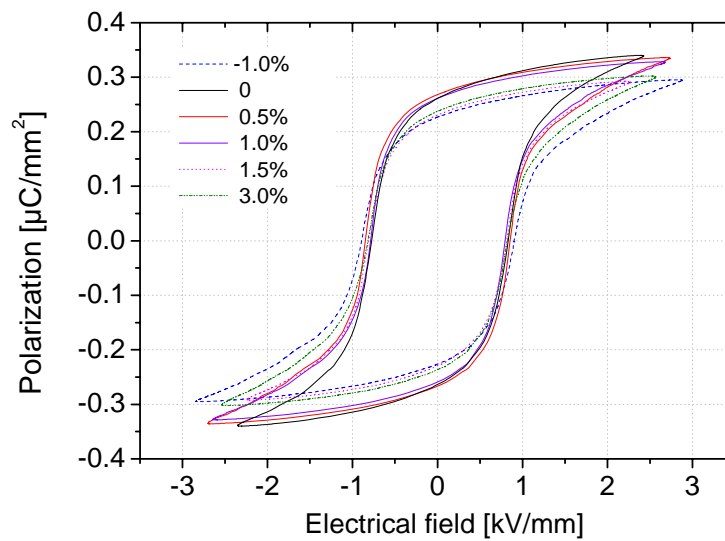


Figure 4.15 P-E loops of PZT ceramics with different levels of lead nonstoichiometry

4.4 Summary

In this chapter, it has been demonstrated that PZT samples prepared from raw materials with different impurities showed distinct variations in terms of sintering behavior, microstructure, dielectric and piezoelectric properties. Sintering of specimen prepared from industrially used raw materials (IM) was highly enhanced by PbO-rich secondary phase and a liquid phase sintering mechanism is proposed. High sintering (about 1280°C) temperature was required for full densification of PZT samples prepared from highly pure raw materials (HM). No secondary phase was observed in the quenched HM sample. Compared to the IM sample, the HM sample had a higher piezoelectric coefficient and planar coupling factor. Mixed “soft” and “hard” characteristics were observed in the IM sample. This was explained by the oppositional effects of different impurities from the raw materials. The following chapter will extend the investigations to gain a deeper view of these effects.

The results obtained with PZT samples with different levels of lead nonstoichiometry reveal that the lead content in the PZT ceramics played a crucial role in the sintering. Sintering temperatures were reduced and densification rates were strongly enhanced by the introduction of lead oxide excess. The reason was believed to be related to the liquid phase formed by PbO during sintering due to its low melting point. A sluggish rearrangement process with low densification rate occurred in the PZT with 3.0% lead excess at a temperature below the melting point. A small force such as 0.1MPa on the sample could result in rapid densification and an additional densification maximum was found on the shrinkage curve. Lead deficiency was not favorable to the sintering of

PZT ceramics. Their sintering behavior was similar to the stoichiometrically prepared PZT sample, which was assumed to be due to the lead deficiency in the sample caused by the evaporation of lead oxide during sintering. Generally, lead excess is favorable to improve both the microstructure and electrical properties of PZT ceramics. Deteriorated properties were found in the samples in which the lead oxide excess is beyond a certain level (3mol %). Among all the compositions investigated, the lead deficiencies caused high tetragonal distortion and shift the compositions to the Ti-rich side, which in turn improved the dielectric constant.

Chapter 5 Systematic study of the impurity effect on lead zirconate titanate ceramics

5.1 Introduction

To describe ferroelectric ceramics, several parameters need to be characterized. Each stands for one of the properties, such as mechanical quality factor, dielectric constant, piezoelectric coefficient and so on. It is known that PZT ceramic has been applied in various fields, which require different emphasis on specified properties (Xu 1991). In order to achieve the requirements in different applications, the common approach is to introduce dopants or substituents for tailoring the properties of PZT ceramics. They can be categorized into isovalent and aliovalent substituents according to the comparison of their own valence to the valence of the replaced ion (Atkin, Holman et al. 1971; Lal, Gokhale et al. 1989). Two general types of aliovalent dopants, donor dopant and acceptor dopant, have been identified (Majumder, Roy et al. 2001). As described in the introduction chapter, oxygen vacancies caused by acceptor doping to maintain electrical neutrality result in domain wall pinning, consequently, increase the mechanical quality factor, coercive field and reduce the dielectric constant and piezoelectric coefficient, which is called “hardening” effect (Tan, Li et al. 1999). The sample with acceptor doping is called “hard” PZT. On the contrary, donor doping results in Pb vacancies and reduces the mechanical quality factor, coercive field, while increases the dielectric constant and piezoelectric coefficient. Thus, the PZT sample with these properties is called “soft” PZT (Hoffmann, Hammer et al. 2001). When samples are doped with several substituents at one time, the behavior certainly becomes much more complicated, because defects may interact with each other, which is believed to be the cause of the mixed characteristics of IM sample as presented in the previous chapter. In addition, PZT samples prepared from industrially used raw materials showed different sintering kinetics compared to those prepared from highly pure raw materials. Rapid densification was observed at low temperatures (about 900 °C) for PZT prepared from industrially used materials, while much higher sintering temperatures were required for samples from highly pure materials. Variations in the properties of these two samples were evidenced as well.

These studies have been extended in present chapter in order to describe the mechanisms how the impurities influence the sintering process and the product properties. At first, the individual impact of industrially used raw materials was studied. The differences were investigated among different components (PbO, ZrO₂ and TiO₂) to identify the one contributing to the variations.

Thereafter, impurities were categorized into certain groups according to their valences and radii and doped into the highly pure samples. The most important species was identified and its effect on the ceramics properties was investigated as a function of dopant concentration.

5.2 Impurities originating from customary raw materials

5.2.1 Sintering behavior of PZT prepared with mixed raw materials

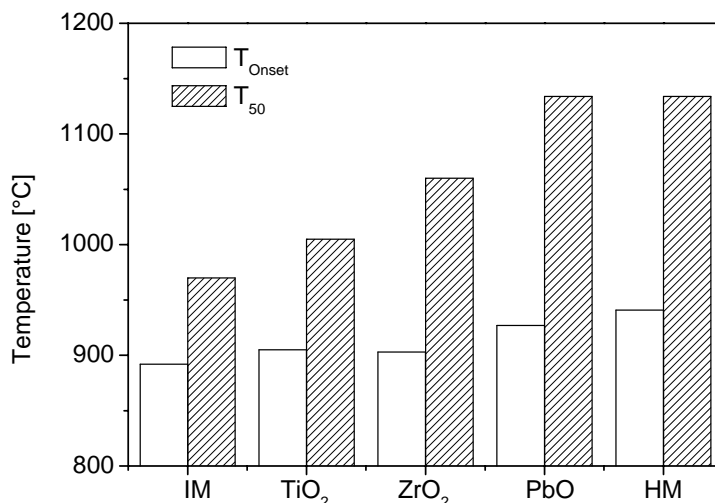


Figure 5.1 Temperatures for the onset of shrinkage (T_{onset}) and 50 % of total shrinkage (T_{50}) of PZT samples made from highly pure (HM) and industrially used (IM) raw materials and mixtures with one oxide component being replaced by the IM material

Sintering behavior was recorded for samples prepared from HM and IM powders. In addition, one of the three oxide powders, PbO, TiO₂ and ZrO₂ which are required for green sample production was replaced each time by an industrial used powder, whereas the other two were still highly pure powders. Figure 5.1 presents a summary of the sintering temperatures, T_{onset} and T_{50} of these measurements. It is clearly shown that T_{onset} and T_{50} depend largely on the purity of the raw materials. As was already observed in the previous chapter, the PZT sample from HM materials has the highest T_{onset} and T_{50} . When ZrO₂ or TiO₂ in the system were replaced by less pure IM material, T_{onset} and T_{50} sharply decrease, together with the difference between T_{onset} and T_{50} , which suggests an improved sintering process and enhanced densification rate. This behavior is attributed to the higher concentration of impurities in IM ZrO₂ and TiO₂. As expected, the substitution of PbO by less pure IM material did not change the sintering behavior owing to the low concentrations of impurities in IM PbO (as shown in Table 2.2). Furthermore, it is interesting to notice that the effect of TiO₂ substitution on the sintering temperatures is more significant than that of ZrO₂ substitution, providing the concentration levels of nearly all impurities were higher in IM

ZrO₂. Therefore, it implies that other properties of the components rather than only purity must have affected the sintering behavior as well.

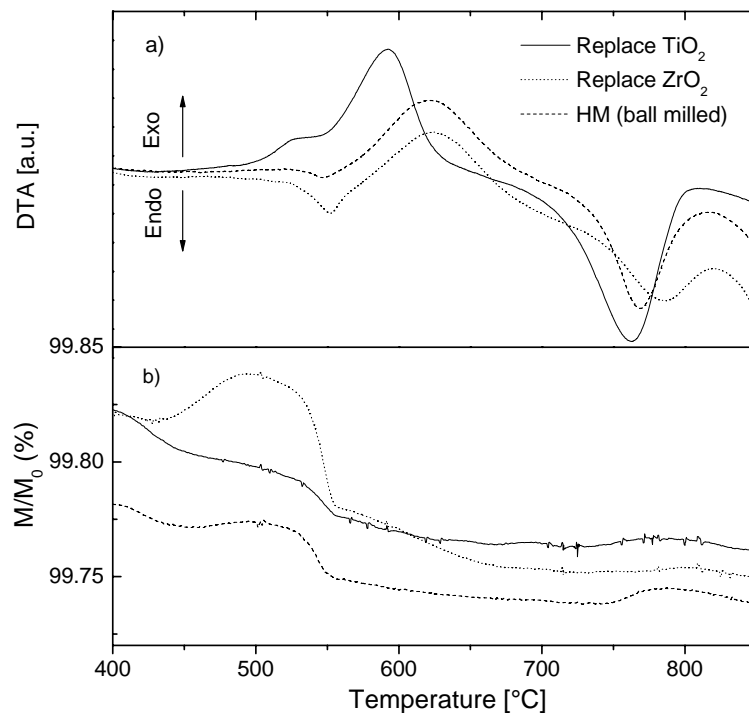


Figure 5.2 DTA (a) and TG (b) study of a mixture from highly pure oxide powders (HM) and mixtures where TiO₂ or ZrO₂ were replaced by industrially used oxides respectively

Figure 5.2 shows the changes in the DTA-TG curves during calcination of mixtures from different raw materials. It is observed that the first exothermic peaks of HM PZT and the sample with ZrO₂ replaced by IM counterpart are located at the same temperature (620 °C). It shifted to a lower temperature (590 °C) when TiO₂ is replaced. Note that the individual oxides had been separately ball milled before this experiment to obtain similar particle sizes (Table 5.1). Many scientists studied the reaction sequence during PZT formation via the mixed oxide route (Chandratreya, Fulrath et al. 1981; Kingon, Terblanché et al. 1982). Agreement was achieved that the first step was the reaction of PbO and TiO₂ to form PbTiO₃. Accordingly, the first exothermic peak seen in the DTA curves is attributed to the formation of PbTiO₃. The shift was also observed when comparing the DTA curves of pure IM and HM materials in Figure 4.1 in the previous chapter. At this point, it should be clear that it was the TiO₂ component to be ascribed to the shift of their first exothermic peak. Since HM and IM TiO₂ had comparable particle sizes of 1.52 μm and 0.96 μm after ball milling (Table 5.1), the higher reactivity of the IM TiO₂ than HM TiO₂ should be attributed to their different crystalline phases. As far as it concerned, IM powder was in the form of anatase which is metastable (Chen, Cheng et al. 1990) and is therefore considered to be more reactive than rutile which is the crystalline phase of HM-TiO₂. A similar trend was reported by Chen as well (Chen,

Cheng et al. 1990). In their DTA curves of 2PbO-TiO₂, the formation temperature of PbTiO₃ shifted from 593 °C to 585 °C when anatase was used instead of rutile.

Table 5.1 Particle size (d_{50}) of the individual powders after ball milling

	PbO		ZrO ₂		TiO ₂	
	IM	HM	IM	HM	IM	HM
d_{50} (μm)	6.52	5.96	0.99	1.14	0.96	1.52
Phase	Massicot	Massicot	Monoclinic	Monoclinic	Anatase	Rutile

Differences in the TG curve are also observed. A distinct weight loss is found right before the formation of the PbTiO₃ phase in the HM sample as well as in the mixture where HM ZrO₂ was replaced by IM ZrO₂. However, such weight loss is not evidenced in the curve of the mixture in which HM TiO₂ was replaced by IM powder. According to Härdtl's and Rau's report, PbTiO₃ has a PbO vapor pressure approximately two order of magnitude lower than pure PbO (Härdtl and Rau 1969). Therefore, it is assumed that formation of PbTiO₃ at lower temperature reduced the PbO partial pressure and consequently the evaporation of PbO during calcination. Since even small changes in PbO concentration have a large impact on sintering activity as discussed in the previous chapter, the relative higher concentration of lead oxide content in the sample with TiO₂ replaced by IM component is considered to account for its improved densification behavior (refer to Figure 5.1).

5.2.2 Sintering behavior of highly pure PZT doped with impurities

To study the effects of the impurities, they were added into the highly pure materials with twice the concentration identified in IM materials. Their concentrations are as follows: Al-0.076 mol%; Ba-0.0094 mol%; Ca-0.08 mol%; Fe-0.029 mol%; Hf-0.73 mol%; Na-0.21 mol%; Si-0.18 mol%; Y-0.13 mol%. Table 5.2 gives the ionic radii of the various constituents in doped PZT ceramics. According to ionic radii and valencies, the impurities were roughly grouped into two categories to reduce the number of experiments. One of low valency and large ion radius (Na, Ba, Ca) was considered to replace Pb - if incorporated into the PZT lattice. The other group (Fe, Al, Y, Hf, Si) was formally assumed to substitute Zr/Ti in the PZT lattice. This second group was further divided into two groups of middle (Fe, Al, Y) and high valency (Hf, Si) impurities respectively. When the impurities were added, the concentration of PbO, TiO₂ and ZrO₂ was adapted to the stoichiometric concentration, according to the formal attribution of the impurities to their respective sites in the PZT lattice.

Table 5.2 Ionic radii of the various constituents in the doped PZT ceramics

Ionic Species	Ionic radius / \AA	Ionic Species	Ionic radius/ \AA
Pb ²⁺	1.43	Zr ⁴⁺	0.86
Na ⁺	1.32	Ti ⁴⁺	0.75
Ba ²⁺	1.56	Si ⁴⁺	0.54
Ca ²⁺	1.26	Hf ⁺	0.85
Y ³⁺	1.04	Fe ³⁺	0.72
		Al ³⁺	0.68

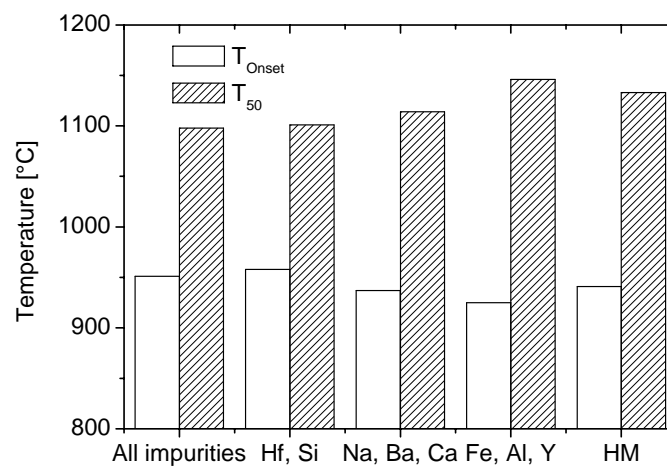


Figure 5.3 Temperatures for the onset of shrinkage T_{onset} and 50 % of total shrinkage (T_{50}) of PZT samples doped with different groups of impurities

Figure 5.3 illustrates the sintering temperatures of PZT doped with grouped impurities. The sample with all the impurities exhibits a similar T_{onset} but a lower T_{50} temperature than the HM sample. Doping the HM sample with the Na/Ba/Ca group leads to a significant decrease in T_{50} . In this group, it is believed that Na incorporated at a Pb site in the PZT lattice and increased the concentration of oxygen vacancies (Lee and Lee 2006). Because oxygen vacancies were the rate-limiting species in the system, the increased concentration further enhanced both the diffusion flux and the densification rate (Atkin and Fulrath 1971). Ba and Ca have the same valency as Pb. It is known that isovalent substitution usually has little influence on PZT ceramic during the period of sintering (Huang, Chen et al. 2004). Thus, Na is assumed to mainly account for the effect of doping Na/Ba/Ca. On the other hand, doping with Fe/Al/Y shows nearly no improvement of densification kinetics in this study, although Fe and Al are usually reported to substitute Zr/Ti and be compensated by oxygen vacancies similar to Na as discussed above (Weston, Webster et al. 1969; Atkin and Fulrath 1971). It is however disputed which site (Pb or Zr/Ti) Y would substitute (Yoon,

Kim et al. 1993; Beitollahi and Abedini 2006). If Y together with Fe and Al substituted Zr/Ti, oxygen vacancy concentration and hence the densification rate should have been increased. If Y had substituted Pb the positive charge could have been compensated by substitution of a neighboring Zr/Ti atom by Fe or Al. Therefore, only small net effect of co-doping Y, Fe and Al could result from charge compensation. Atkin demonstrated a similar pairwise substitution with co-doping of Al and Nb in PZT (Atkin and Fulrath 1971). Doping with Al or Nb kept the grain size small and expedited densification, whereas codoping did not lead to improvements on sintering.

The prevailing effect of impurities on the sintering temperatures results from doping with Hf and Si, which almost takes up the total effect of adding all impurities at one time. On one hand, it is assumed that Hf simply substituted Zr atoms in the PZT lattice and did not change the sintering kinetics, as it is chemically similar to Zr. On the other hand, SiO₂ could form liquid phase with PbO during sintering as a eutectic exists in their binary phase diagram (Smart and Glasser 1974). Figure 5.4 displays the SEM image of the fracture surface of the sample doped with Hf and Si. An intergranular fracture mode was observed and a secondary phase was identified along the grain boundaries. EDS measurement showed that this secondary phase had a high concentration of PbO and contained Si, which indicates that PbO and Si may have formed a melt phase during sintering. Si is, therefore, mainly ascribed to the decrease of sintering temperature when adding both impurities. The assumption is confirmed by an additional experiment where only Si was introduced (as will be discussed in the following section). Palkar et al reported the use of Si as sintering aid to improve the sintering behavior of PbTiO₃ (Palkar, Purandare et al. 2000). It was observed that it was possible to obtain a relative density of 95% at 1000°C for 1 h using 2 mol% of Si.

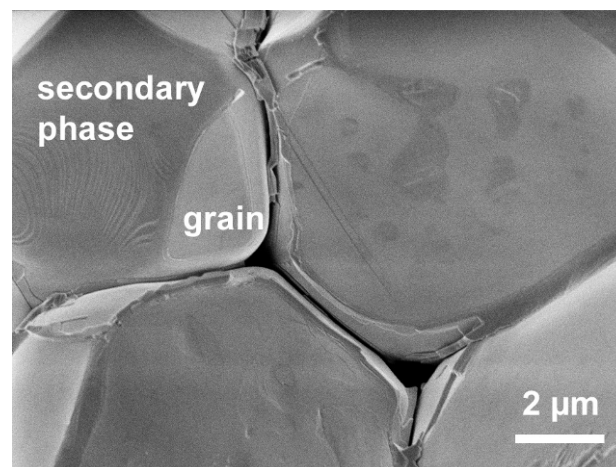


Figure 5.4 SEM picture of fracture surface of sample doped with Hf and Si (one grain is partly covered with secondary phase)

In the experiments described above, the impurities were doped in the PZT system with a stoichiometric composition. However, the composition is nonstoichiometric in the industrial production chain, because usually the impurities are not taken into account when weighing the raw materials. If they are incorporated in the PZT lattice, deviations from stoichiometric composition are expected. It is seen from Table 2.2 that HfO_2 dominated among the impurities in the IM raw materials. Since it is believed that Hf replaces Zr/Ti and it has nearly double molecular weight than ZrO_2 , about 0.7 mol % PbO excess could result from not considering this contribution. In the previous chapter, it was already shown that small concentrations of excess PbO could drastically decrease sintering temperature. As plotted in Figure 5.5, when the impurities were doped without considering stoichiometry, i.e. similar to the industrial process, densification was significantly enhanced with a reduction of T_{50} by more than 50 K compared to the sample with stoichiometric composition. This phenomenon verifies that the PbO concentration is one of the most important parameters, controlling sintering kinetics of PZT.

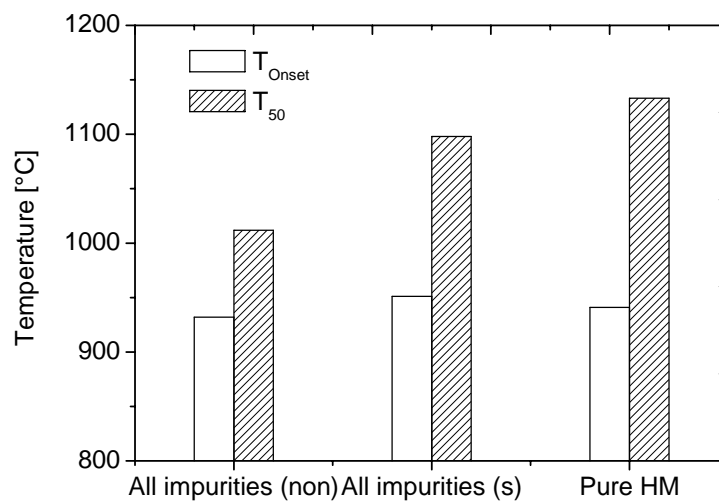


Figure 5.5 Temperatures for the onset of shrinkage T_{Onset} and 50 % of total shrinkage (T_{50}) of pure (HM) PZT samples without impurities and stoichiometric (s) and nonstoichiometric (non) samples doped with all impurities

5.2.3 Microstructural and electrical properties of PZT doped with impurities

Figure 5.6 shows the microstructures of thermally etched PZT samples. The mean chord lengths of PZT grains derived from lineal intercept analysis are shown in Table 5.3. Large grains are observed in the pure IM and HM samples and the HM material doped with Hf and Si, while relatively smaller grains are found in the samples doped with Fe/Al/Y and Na/Ba/Ca, respectively. The smallest grain size is seen in the samples doped with all impurities. According to former studies, Y is known as a grain growth inhibitor in other systems, such as SrTiO_3 or ZrO_2 (Stoto, Nauer et al.

1991; Huang, Zhao et al. 2006). It is also reported that grain growth has been slowed down by doping with Fe, Al or Na in PZT systems (Weston, Webster et al. 1969; Atkin and Fulrath 1971). The mechanism is believed to be that the doping ions concentrate near the grain boundaries and substantially reduce their mobility. The reason for the large chord lengths observed for the IM samples produced by freeze drying is not clear (refer to Table 5.3). For IM samples produced by standard processing much smaller chord lengths of $7.8 \mu\text{m}$ had been observed. Grain growth normally becomes prominent in the final sintering stage when the fractional density reaches 90% and pores are isolated (Rahaman 2003). As shown in Figure 5.6a and Figure 5.6b, large grain growth occurred in pure HM sample and the sample doped with Hf and Si. Apparently, grain boundary mobility had exceeded pore mobility and pores were enclosed inside the grains, which is well known as retarded densification (Stoto, Nauer et al. 1991).

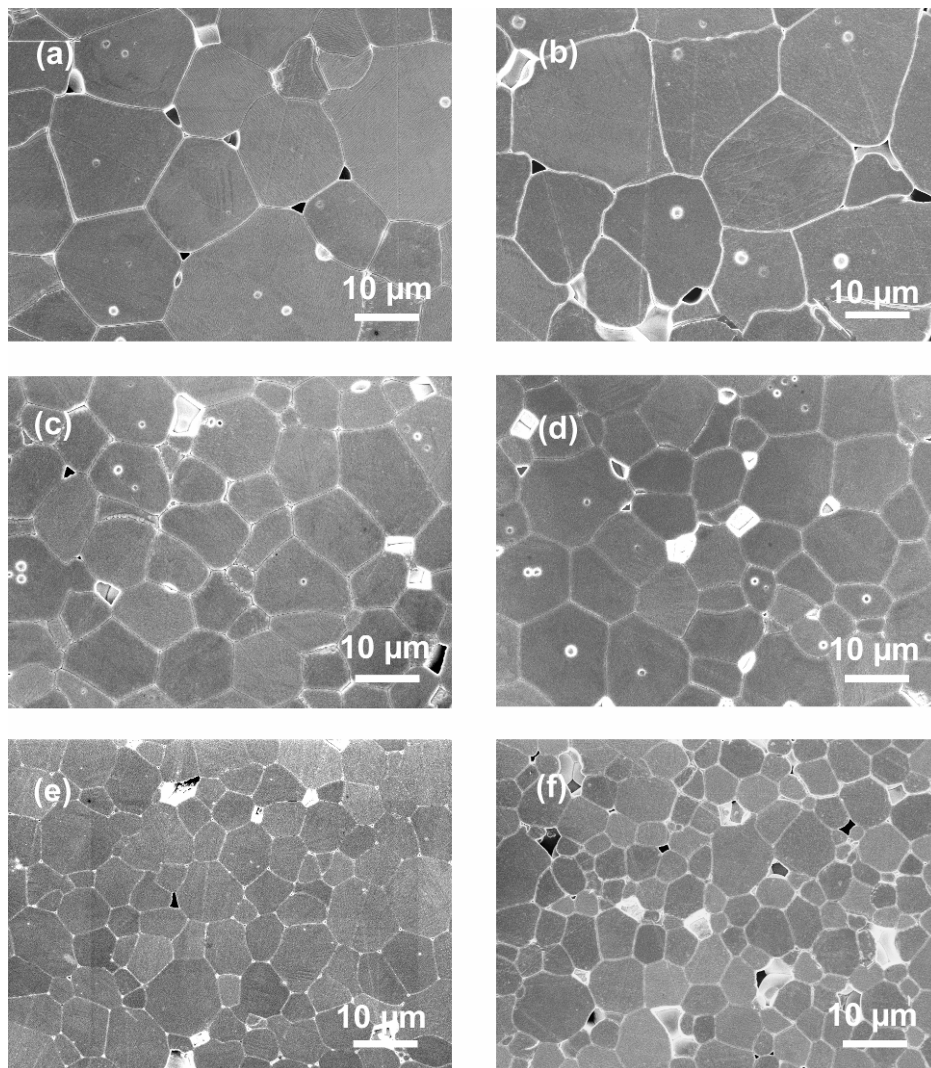


Figure 5.6 SEM images of polished surfaces of the pure HM sample (a) and samples from HM material doped with different impurities: Hf/Si (b), Na/Ba/Ca (c), Fe/Al/Y (d), all impurities nonstoichiometric (e), all impurities stoichiometric (f)

Table 5.3 shows the dielectric and piezoelectric properties of the pure HM and IM sample and HM material doped with different impurities. Doping with Na/Ba/Ca resulted in a higher mechanical quality factor, higher coercive field, lower dielectric loss and lower dielectric constant. These changes can be explained by the acceptor doping effect. On the one hand, Na⁺ substituted Pb²⁺ at the Pb-site and acted as acceptor ion. The positive charge was compensated by oxygen vacancies. On the other hand, oxygen vacancies restricted the domain motion and pinned the domain walls by introducing space charges and internal fields inside PZT grains (Moulson and Herbert 2003), which reduced the contributions of domains to the dielectric and piezoelectric properties. Research group He and Vanderbilt used first-principles density functional calculations to investigate the interaction of oxygen vacancies and 180° domain walls in tetragonal PbTiO₃. Their results indicated that the vacancies had lower formation energy in the domain wall than in the bulk, thus, exhibited the tendency of these defects to migrate to, and pin, the domain walls (He and Vanderbilt 2003). Thereby, they increase the mechanical quality factor and coercive field and decrease the dielectric constant and piezoelectric coefficient (Moulson and Herbert 2003). Smaller dielectric constants were measured in the sample doped with Hf and Si. The reason should be related to the secondary phase on the grain boundaries, because it was noted that the secondary phase formed from Si and PZT had low dielectric and piezoelectric properties (Ursic, Hrovat et al. 2008). Additions of Fe/Al/Y led to a higher mechanical quality factor and lower dielectric loss similar to the sample doped with Na/Ba/Ca. However, a higher dielectric constant was obtained as well. The mixed properties of PZT doped with Fe/Al/Y could be explained as the results of combined effects of acceptor doping and donor doping, which is consistent with the assumption that Y³⁺, at least part of the ions, substituted Pb and served as donor ion other than acceptor ion as Fe³⁺ and Al³⁺ replacing Zr/Ti. Lee studied the co-doping of La³⁺ and Nb⁵⁺ in PZT ceramics (Lee and Lee 2006). Mixed effects on electrical properties were achieved as well. The properties of the IM sample were similar to the HM sample doped with all impurities non-stoichiometrically with the exception of chord length. The reason is not clear. However, the chord length of IM sample is greatly influenced by the processing procedure. Without the freeze-drying process, much smaller chord length of 7.84 μm was observed, while large grain size of 13.8 μm was still found in HM PZT sample. Increasing piezoelectric constants with increasing grain size were reported previously (Martirena and Burfoot 1974). However, no obvious effect of grain size on d_{33} can be identified in Table 5.3. It is attributed to the large grain diameter of the present samples.

Table 5.3 Mean chord length, dielectric and piezoelectric properties of sintered IM and HM samples and samples made of HM powder doped with different impurities: Hf/Si, Na/Ba/Ca, Fe/Al/Y, all impurities nonstoichiometric(non), all impurities stoichiometric (S)

Sample	Chord length (μm)	Planar coupling factor k_p (%)	Dielectric loss $\tan\delta$ (10^{-3})	Mechanical quality factor Q_m	Piezoelectric coefficient d_{33} (pC/N)	Dielectric constant ϵ_r	Remnant polarization P_r ($\mu\text{C}/\text{mm}^2$)	Coercive Field E_c (kV/mm)
Pure IM	16.5 \pm 0.4	51.3	17.4	96	270	863	0.23	0.91
Pure HM	13.4 \pm 0.4	53.3	20.6	84	322	754	0.26	0.84
Hf/Si	11.8 \pm 0.3	47.6	15.7	126	209	616	0.27	0.93
Na/Ba/Ca	7.9 \pm 0.2	51.0	12.2	142	267	736	0.26	0.95
Fe/Al/Y	7.4 \pm 0.2	41.0	15.5	112	228	1012	0.25	0.89
All (Non)	6.4 \pm 0.1	50.5	13.2	100	277	940	0.19	0.91
All (S)	4.4 \pm 0.1	42.0	14.9	106	202	751	0.15	0.87
Uncertainty	-	0.5	0.6	17	3	13	-	-

5.3 Individual impurities, Na, Y or Si in highly pure PZT ceramics

As known from the previous section, the impurities Na, Y and Si had predominant effects among all of the impurities. It is desirable to investigate their individual role in sintering and the effect on properties of PZT ceramics in detail. In present section, Na, Y and Si were doped into PZT ceramics with different concentration varying from 0 to 1mol%, which is in the typical range of concentration of impurities involved in production. For the purpose of weighing the components, Na and Y were assumed to replace Pb ions, while Si was located on Zr/Ti site. XRD results suggested single perovskite structure in all present samples.

5.3.1 Microstructure properties

Figure 5.7(a) illustrates the chord length measured on the sintered samples versus the compositional variation. The error bar represents the standard error of the chord length distribution. It can be seen that grain growth was suppressed by the addition of Na within the studied compositional range. The chord length of pure HM PZT is 13.4 μm . Upon Na modification, it decreases significantly to 6.3 μm with 0.2 mol % and 2.9 μm with 1 mol%. Doping with Y showed grain size inhibition behavior as well, with the chord length descending steadily to 10.7 μm . Grain growth suppression has been reported in La or Nb doped PZT systems. Yet, the reason for grain

growth inhibition is not clear. It is suggested to be the consequence of the solute drag effect, where dopants congregate on the grain boundary and reduce its mobility leading to a reduction in grain growth rate (Rahaman 2003). In the case of SiO₂ doping, little effect on the grain size were observed. According to Rahaman, the liquid phase facilitated the grain growth by increasing the solubility of solid in the liquid using the capillary force between two grains during sintering (Rahaman 2003). Based on this reason, discontinuous or abnormal grain growth often occurs in the systems involving liquid phase sintering (Hennings, Janssen et al. 1987). In Si doped samples, no sign of abnormal grain growth was observed. Figure 5.7(b) plots the density of PZT samples as function of impurity levels. All the samples showed relative densities higher than 94%. At low concentration of Y or Na, samples showed no significant changes on the density. It decreased slightly with further doping with 0.5, 1.0 mol% Na or Y. Doping with Si, however, resulted in a dramatic decrease of the sample density, from 7.73 g/cm³ to 7.5 g/cm³ with 1 mol% Si.

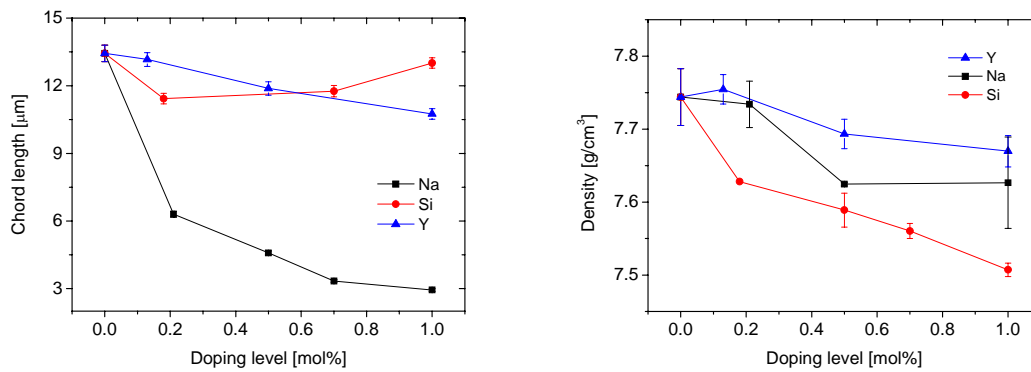


Figure 5.7 Chord length and density dependence on the doping level of impurities in PZT ceramics

SEM images of fracture surfaces of samples with different impurities are shown in Figure 5.8. Well faceted grains are observed in the samples doped with Na. Similar phenomenon was found in Y-doped samples, only with larger grain size. In Si doped PZT, the grains were covered with the melt phase and it is difficult to distinguish the real grain surface and the secondary phase. To some extent, it also indicates the good wetting between the grains and the melt phase. The fracture mode of all the samples is intergranular. This suggests that the strength of the grain boundaries is weaker than the grains.

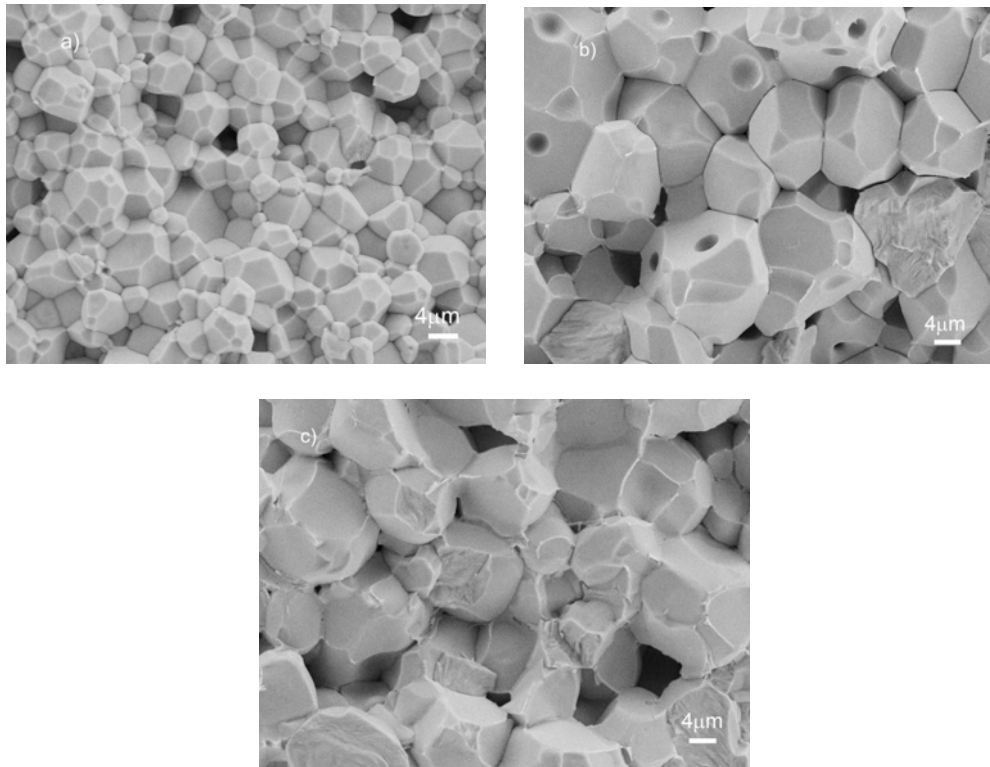


Figure 5.8 SEM images of fracture surfaces of PZT samples doped with 0.5mol% Na (a), Y (b) and Si(c), respectively

The fresh fractured surface and the surface sputtered by Ar⁺ ion for 4020s of Na and Y doped PZT samples were investigated by XPS to detect the doped impurities on the grain boundaries and inside the grains. Because the fracture mode of these samples is intergranular, the compositions obtained by the XPS measurement of the fresh fractured surface represent the condition of grain boundaries. After sputtering for 4000s, XPS reveals mostly the composition of the bulk regions. Figure 5.9 shows the results of 0.21 mol% (a) and 0.70 mol% (b) Na doped samples. It is seen that the concentration of Na is beyond the detection limit both on the grain boundaries and the bulk regions in 0.21 mol% Na doped sample. However, as the doping level increased to 0.7mol%, Na was detected on the grain boundaries while no trace of Na was detected in the bulk regions after sputtering for 4020s. Figure 5.10 presents the XPS spectrum of 0.13 mol% and 1.0 mol% doped samples. Similar results as Na doped sample was obtained. Although Y was detected both on the grain boundaries and in the bulk regions due to the relative high doping level, the concentration was much higher on the grain boundaries after comparing the intensity of the peaks of Y and O. These results suggest that the impurities, Na and Y had the tendency to congregate on the grain boundaries at high doping level. It also provided the foundation for the theory of drag effect that may explain the grain size inhibition in Na and Y doped samples.

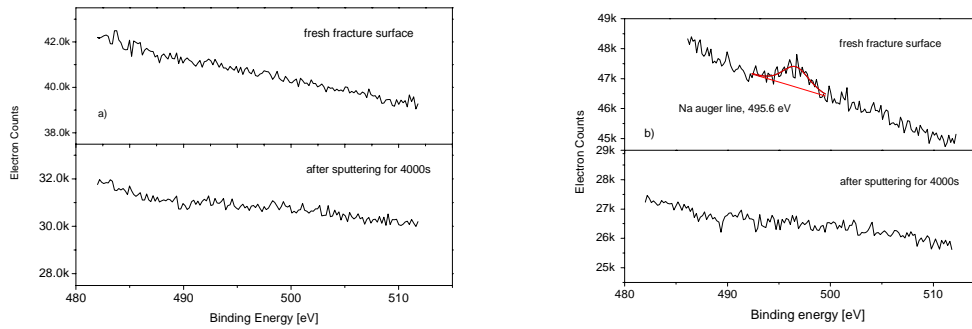


Figure 5.9 XPS spectra of Na KLL Auger line of 0.21mol % and 0.7mol% Na doped PZT ceramics

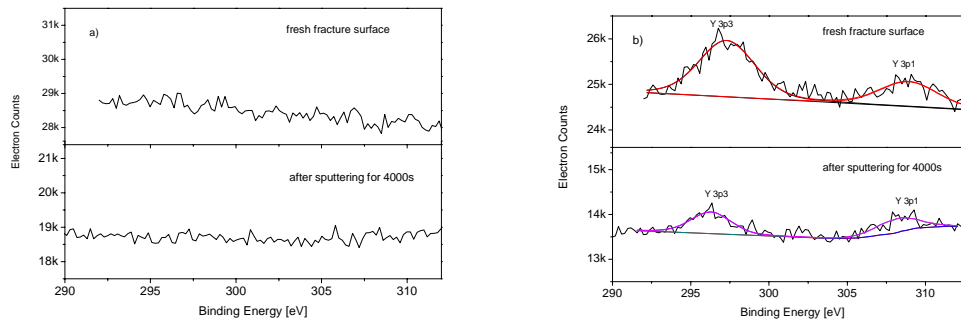


Figure 5.10 XPS spectra of Y 3p lines of 0.13 mol% and 1.0mol% Y doped PZT ceramics

Figure 5.11 displays the TEM image of 0.5 mol% SiO₂ doped PZT quenched at a shrinkage of 10%. Amorphous phase is observed on the triple junctions of the grains. EDX results revealed that the amorphous phase contained Si, which provided the direct proof that glassy phase formed during sintering from SiO₂ and PbO. It is noted that no amorphous phase is seen along the grain boundaries. This could be associated with the small quantity of the melt phase and relative small grain size, hence, large surface area. Figure 5.12 presents the SEM images of polished surfaces of sintered samples with 0.5 mol % impurity ions. The grain size increased to more than 10 μm . Because of the relative larger grain size, secondary phase is visible not only on the triple junctions but also on the grain boundaries.

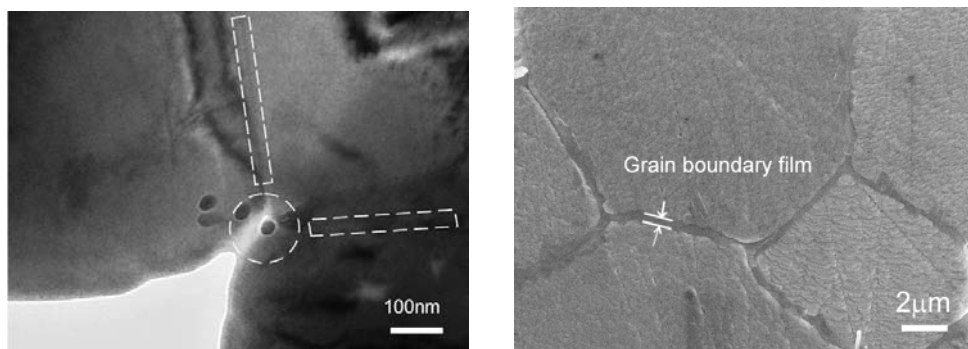
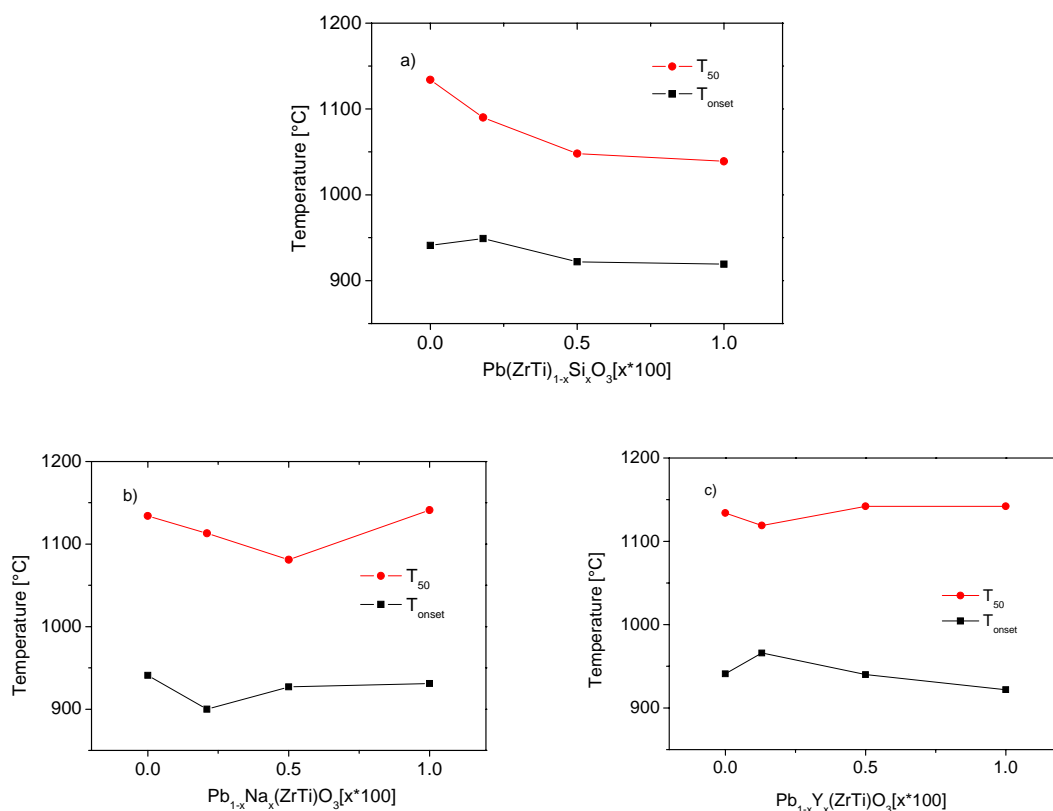


Figure 5.11 TEM image of 0.5 mol% SiO₂ modified PZT quenched at shrinkage of 10% (the black dots are where the EDX analysis has been performed)

Figure 5.12 SEM image of sintered sample with 0.5 mol% SiO₂

5.3.2 Sintering behavior of PZT ceramics with Na, Y and Si modification

Figure 5.13a shows T_{onset} and T_{50} as a function of SiO₂ doping level. T_{onset} increases at first, then decreases steadily with increasing amount of SiO₂. T_{50} decrease sharply with SiO₂ modification. As know from Section 5.2.2, secondary phase could form from PbO and SiO₂. On one hand, due to the low eutectic point of PbO and SiO₂, liquid phase may exist during the sintering as the sintering temperature is much higher than the eutectic point. On the other hand, because the amount of SiO₂ is rather low, the composition of SiO₂ and PbO is far away from the eutectic composition according to the phase diagram (Smart and Glasser 1974). With increasing amount of SiO₂, the composition is moving toward the eutectic concentration, thus the amount of liquid phase is expected to soar, which enhanced the mass transfer and reduced the sintering temperatures.

Figure 5.13 T_{onset} and T_{50} temperatures of sintering PZT ceramics with compositional variations (a: doped with Si; b: doped with Na; c: doped with Y)

The sintering temperatures (T_{onset} and T_{50}) of PZT are shown in Figure 5.13b as function of Na concentration. Both T_{onset} and T_{50} decrease at low level of Na doping. However, they increase steadily with further addition. This phenomenon is believed to be the consequence of two

competing effects from oxygen vacancy and lead deficiency on sintering. As explained earlier, oxygen vacancies are usually created with Na doping in PZT systems to maintain charge neutrality and they are rate-limiting species (Atkin and Fulrath 1971). Thus, the sintering rate of Na doped samples was controlled by the diffusion of oxygen vacancies. The increased concentration of oxygen vacancies facilitated the diffusion as well as sintering (Ahn, Song et al. 2006). However, since Na substituted Pb site, lead deficiency in the system increased as Na had the tendency to congregate on the grain boundaries (refer to Figure 5.9). Therefore, the lead deficiency may take over the control of sintering from oxygen vacancies at high level of Na doping. With lead deficiency, the samples became difficult to be sintered and showed a similar sintering behavior to stoichiometric PZT as demonstrated in the last chapter. Comparing to Na doped samples, less noticeable changes of the sintering temperatures are seen in the sintering curves of Y-doped PZT samples (Figure 5.13c). Only the sample with 0.13mol% Y exhibits little variation. It shows a decreased T_{50} , however, together with an increased T_{onset} . Its low T_{50} should be related to the increased concentration of defects that were introduced by Y doping, while the high sintering temperatures of PZT sample doped with 0.5% and 1.0% Y are also believed to be the outcome of increased lead deficiency similar to Na substitution. The increased T_{onset} of 0.13% Y doped sample is believed to be related to the measuring method.

Figure 5.14 plots the densification rates of samples doped with different impurities. It is clearly shown that the densification rate of PZT samples doped with Na or Y exhibited a similar trend as their sintering temperatures, especially T_{50} . At low level of substitution (Na: $\leq 0.5\text{mol}\%$, Y : $\leq 0.13\text{mol}\%$), the densification rates of both samples increased due to the dominant effect of increased concentrations of vacancies, whereas downgraded to the level of pure PZT sample upon further modification as a result of prevailing effect of increased level of lead deficiency. Given the drastically reduced sintering temperatures of samples doped with Si, it is surprising to notice that the densification rate did not change much with Si doping and the concentration of melt phase. In a system with liquid phase sintering, the viscosity plays a very important role. The transport of matter through the liquid could be impeded with increased viscosity (Bateman, Bennison et al. 1989). It is known that the viscosity of a melt phase is increased with decreasing temperatures (Fontana and Plummer 1979). Furthermore, as Hallse and Cook pointed out, the higher silica content results in higher viscosity of lead silicate phase (Hallse and Cook 1958). Therefore, the samples with Si doping showed no improvement on densification rate due to their relative low sintering temperature, thus high viscosity. The slight increment in densification rate of samples doped with only 0.18mol% Si is attributed to its lower viscosity because of the lower content of melt phase and higher sintering temperature than the samples doped with 0.5 and 1.0mol% Si.

Contrarily, the densification rates of systems with lead oxide excess were highly increased by the PbO liquid phase even at low temperatures (refer to Figure 4.3). Thus, the kinetics of liquid phase sintering of PZT varies with the nature of liquid phase.

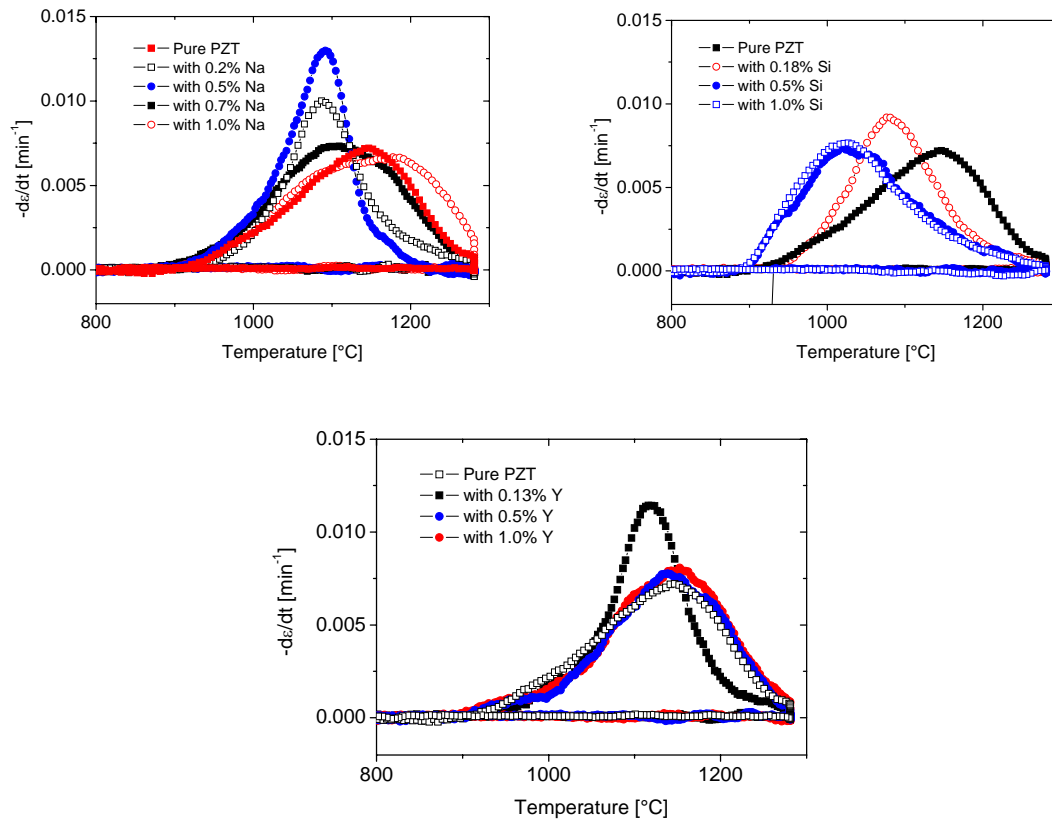


Figure 5.14 Densification rate of samples doped with different impurities

5.3.3 Impurity level dependent piezoelectric and dielectric properties

The dielectric and piezoelectric properties, Q_m , $\tan\delta$, k_p , d_{33} and ε_r as a function of the concentration of Na, Y and Si impurities are presented in Figure 5.15, Figure 5.16 and Figure 5.17, respectively. Mechanical quality factor Q_m decreased with Y doping level over the investigated range of concentration. Both Na and Si doping increased Q_m . However, it increased significantly from 70 to 350 with 0.5 mol% Na and then increased slightly upon increment of Na, whereas with increasing Si concentration Q_m remained at low values (less than 160) over the whole range of modification and exhibited a maximum at 0.5%, followed by a slight decrease. Correspondingly, these impurities showed contrary behavior in dielectric loss. The dielectric constant ε_r increased considerably with Y doping and slightly with increasing modification of Na. Si resulted in a decrease of dielectric constant. Upon increment of the Na or Y or Si concentration, k_p decreased by

20% with impurity (Na or Y or Si) doping. The d_{33} value decreased from 300 pC/N to 150 pC/N upon Na substitution and to 260pC/N upon Y or Si substitution.

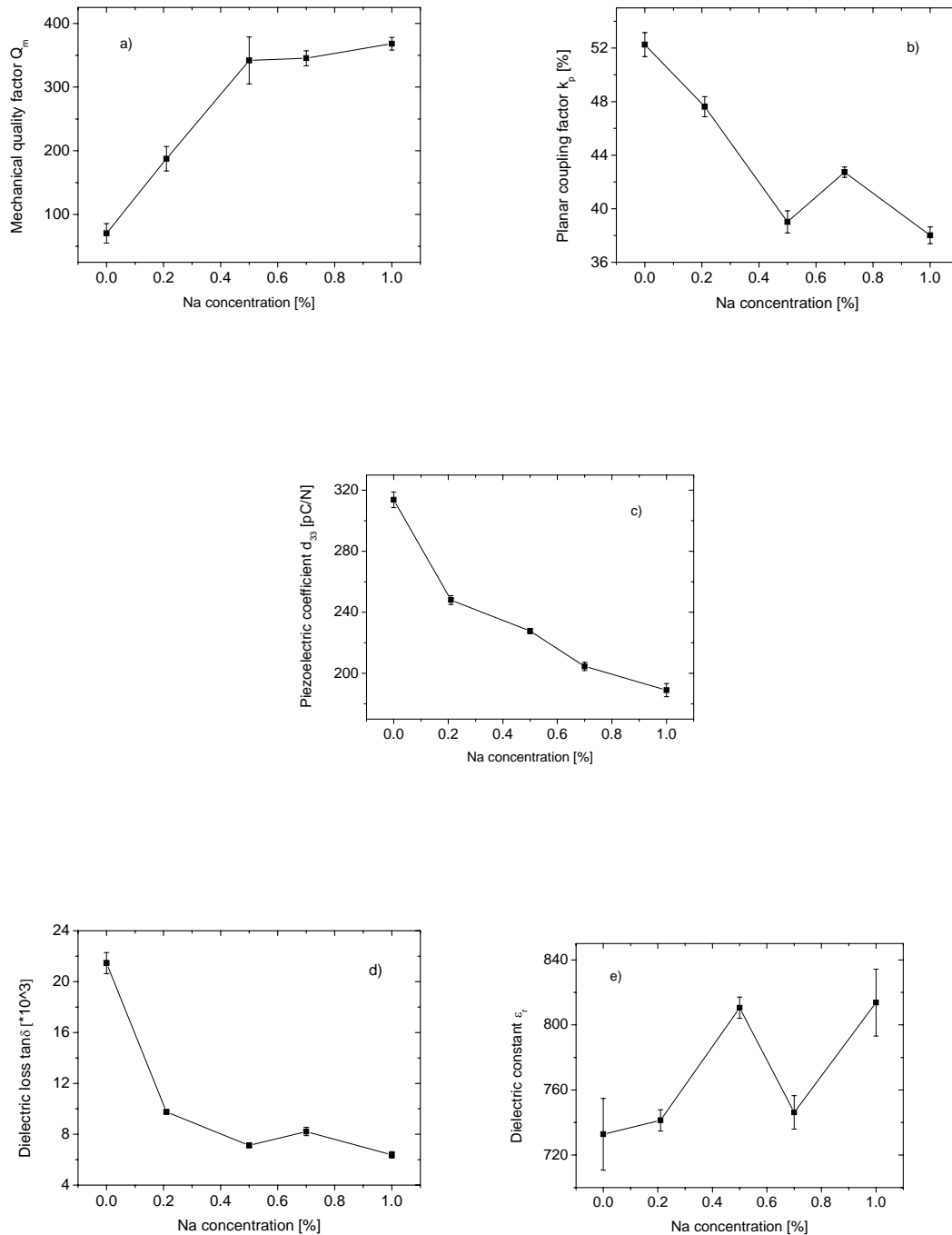


Figure 5.15 (a) Mechanical quality factor Q_m (b) Planar coupling factor k_p (c) Piezoelectric coefficient d_{33} (d) Dielectric loss (e) Dielectric constant ϵ_r of PZT doped with 0, 0.21, 0.5, 0.7, 1.0 mol% Na

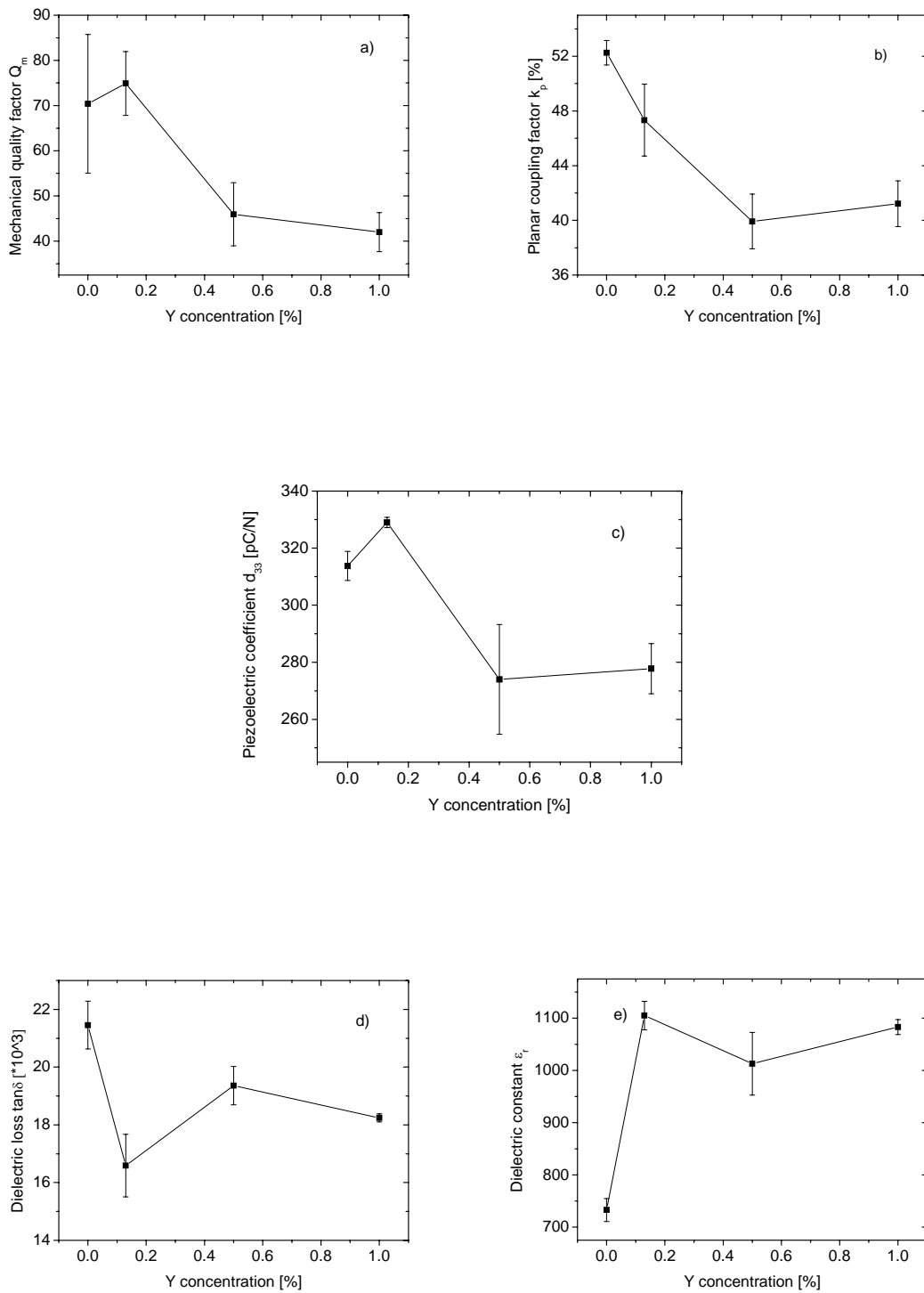


Figure 5.16 (a) Mechanical quality factor Q_m (b) Planar coupling factor k_p (c) Piezoelectric coefficient d_{33} (d) Dielectric loss (e) Dielectric constant ϵ_r of PZT doped with 0, 0.13, 0.5, 0.7, 1.0 mol% Y

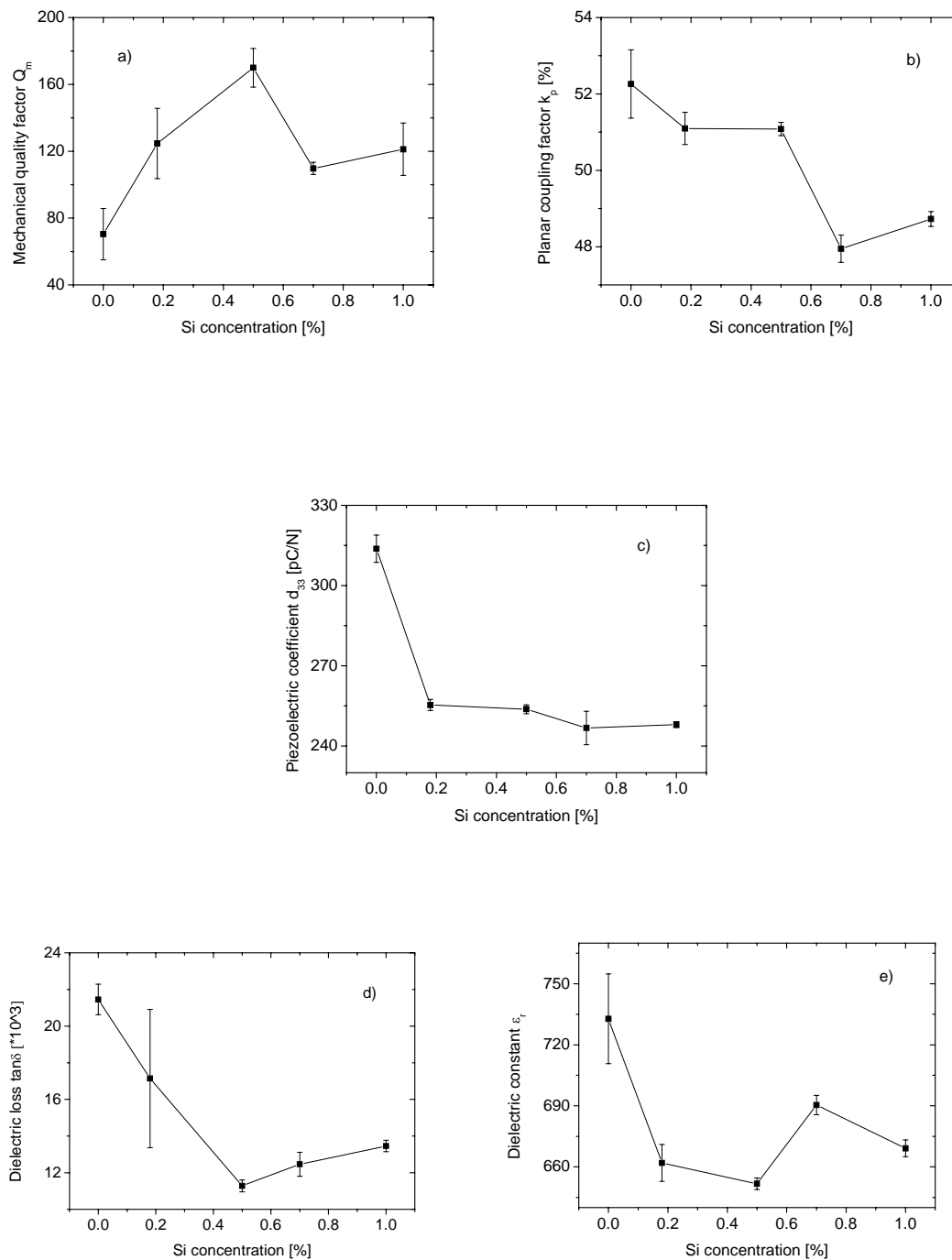


Figure 5.17 (a) Mechanical quality factor Q_m (b) Planar coupling factor k_p (c) Piezoelectric coefficient d_{33} (d) Dielectric loss (e) Dielectric constant ϵ_r of PZT doped with 0, 0.18, 0.5, 0.7, 1.0 mol% Si

Previous investigations established that PZT doped with aliovalent substitutions could result in different piezoelectric behaviors (Liang and Wu 1993; Donnelly, Shrout et al. 2007). The data presented in Figure 5.16(a) and (e) demonstrate that Y substitution increase the degree of “soft”

characteristics, as mechanical quality factor was decreased and dielectric constant was increased (Huang, Chen et al. 2004; Deng, Yin et al. 2005). However, Figure 5.16(b) and (c) imply that Y doping has a “hardening” side as well, since both k_p and d_{33} decreased upon Y substitution (Suwannasiri and Safari 1993). As mentioned in the last chapter, the ionic radius of Y^{3+} is smaller than that of Pb^{2+} , but bigger than Zr^{4+} or Ti^{4+} . Moreover, although Y is confirmed to substitute Pb site in the previous section 5.2.3, the possibility that Y could substitute Zr/Ti site was not ruled out. In fact, the valence of Y is between Pb and Zr or Ti. Thus, substitution on both sites might be expected. In other words, both A-site and oxygen vacancies could result from Y substitution, so are the combinatory “soft” and “hard” piezoelectric characteristics. Gao studied the effects of rare earth metal (Ce, Eu and Yb) substitution on the piezoelectric properties of PZT-PSM ceramics. Combinatory “hard” and “soft” characteristics were observed in all the samples regardless of the ionic radii of the rare earth metal (Gao, Uchino et al. 2002).

Figure 5.15 (a), (b), (c) and (d) present the PZT samples with increasing Q_m , decreasing k_p , d_{33} and $\tan\delta$ upon Na modification due to the acceptor doping of Na^+ on Pb^{2+} . As a result, sample doped with Na^+ showed typical “hard” characteristics. With the exception of the dielectric constant, it exhibited uncertain behavior and slight increment with increasing Na concentration. The properties of all PZT system are dictated by a broad range of factors, namely type of dopants (Huang, Chen et al. 2004), their concentration (Durruthy, Fuentes et al. 2000) and grain size of ceramics (Zhang and Raj 1995). As shown in Figure 5.7, Na had a remarkable effect on grain growth inhibition. Therefore, microstructure should be taken into account when discussing the effect of Na on the electrical properties of PZT. Randall et al. reported the effects of grain size on ferroelectric properties of undoped and niobium-doped PZT (52/48). Although piezoelectric properties d_{33} and k_p as well as dielectric constant at high temperatures was reported to decrease monotonously with grain size reduction, the dielectric constant at room temperature showed a reversed tendency and increased with grain size reduction. This is also in agreement with the studies from Haertling and Sundar et al. (Haertling 1964; Sundar, Kim et al. 1996). One of the intrinsic microstructural characteristics in PZT ceramics are the internal stresses occurring during the paraelectric-ferroelectric transition (Kamel and de With 2008). According to the internal stress model proposed by Buessem et al (Buessem, Cross et al. 1966), the large internal stress developed during cooling of PZT is released by the formation of a polydomain structure. However, as the grain size decreases, the formation of polydomains may not occur, rather monodomains are expected. As a result, the internal stresses increase during cooling with the grain size reduction. It increases the dielectric constant by applying a compression along the c axis according to Buessem’s

internal stress model ((Buessem, Cross et al. 1966)). The internal stress was also attributed to the high dielectric constant in the lead deficient samples (refer to Figure 4.14e).

From the results regarding sintering behavior and microstructure of Si doped PZT, it is evident that the liquid phase formed from PbO and SiO₂ in an early sintering stage due to the eutectic point of these two phases at low temperatures and remained along the grain boundaries in the sintered samples (as shown Figure 5.12). Because of this non-ferroelectric melt phase, the sample showed detrimental properties. As plotted in Figure 5.17, the dielectric constant, k_p and d_{33} are all reduced together with slightly increased Q_m . The melt phase on the PZT grain boundaries may also have small effect on restricting the domain motion along the grain boundaries, thus reduced the dissipated energy and increased Q_m .

5.3.4 Ferroelectric properties

In order to understand hysteretic losses and their relationship with impurity doping, the P-E responses were investigated. Figure 5.18(a), (b) and (c) show the P-E hysteresis loops of undoped highly pure PZT and PZT doped with different concentration of Na, Si and Y, respectively. It can be seen that the degree of switchable polarization decreases sharply upon Na modification. Double-loop like characteristics are observed with the samples doped with more than 0.2mol% Na and a roughly linear loop is found in sample doped with 1mol% Na. The samples doped with Y and Si all show well saturated P-E loops. The coercive field (E_c) increases steadily upon Y modification, while remnant P_R and spontaneous polarizations P_s remain almost unchanged after the reduction from pure PZT. Thus, the area of hysteresis loop increased upon Y substitution, which is consistent with the observed reduction in Q_m . The samples with Si, on the other hand, show an independent coercive field and substantially decreased polarization with the increase of Si level. Similarly, the area of loop is reduced in agreement with the increase in Q_m upon Si substitution.

The hysteresis arises from the energy needed to reverse the metastable dipoles during each excursion of the electrical field (Xu 1991). For non-ferroelectric samples a straight line results in, while for a ferroelectric sample a hysteresis loop is generated. The area of the loop represents energy that is dissipated within the sample as heat. Smith and Hom reported that the polarization depends largely on the domain wall motion (Smith and Hom 1999). The dipoles of acceptor ions and oxygen vacancies result from acceptor doping and pin the domain motion by aligning along the spontaneous polarization. Higher coercive field results in, consequently. Thus, the increased coercive field of Y doped samples indicates that oxygen vacancies played a predominant role

during polarization. In some cases, it is even difficult to obtain a well saturated P-E loop because of the presence of oxygen vacancies-acceptor complexes as well as high conductivity in measured compounds (Gerson 1960), such as the sample doped with 1 mol% Na. The grain size effect should also be accounted for the difference between the shapes of P-E loops of Na and Y doped samples. As the grain size decreases, one expects the domain walls to be inhibited in their movement, because grain boundaries will contribute additional pinning effects for the moving walls. If the walls become less mobile, their contribution to the properties will also decrease (Martirena and Burfoot 1974). Double loop like hysteresis loop were also reported on K^+ doped PZT by Tan et al. (Tan, Li et al. 1997). It was explained by the presence of an increasing domain density whose polarization becomes increasingly difficult to switch with K^+ concentration. In their report, the inhibition effect on the grain growth was demonstrated in K^+ doped samples. This is in a good agreement with our assumptions that both oxygen vacancies and grain size should be responsible for double-loop like hysteresis of Na^+ modified samples. In the case of Si doped PZT, the decreased polarization is due to the increasing amount of non-ferroelectric melt phase, consequently the contribution from the remaining PZT phase decreased. The melt phase, however, showed no significant effect on the coercive field.

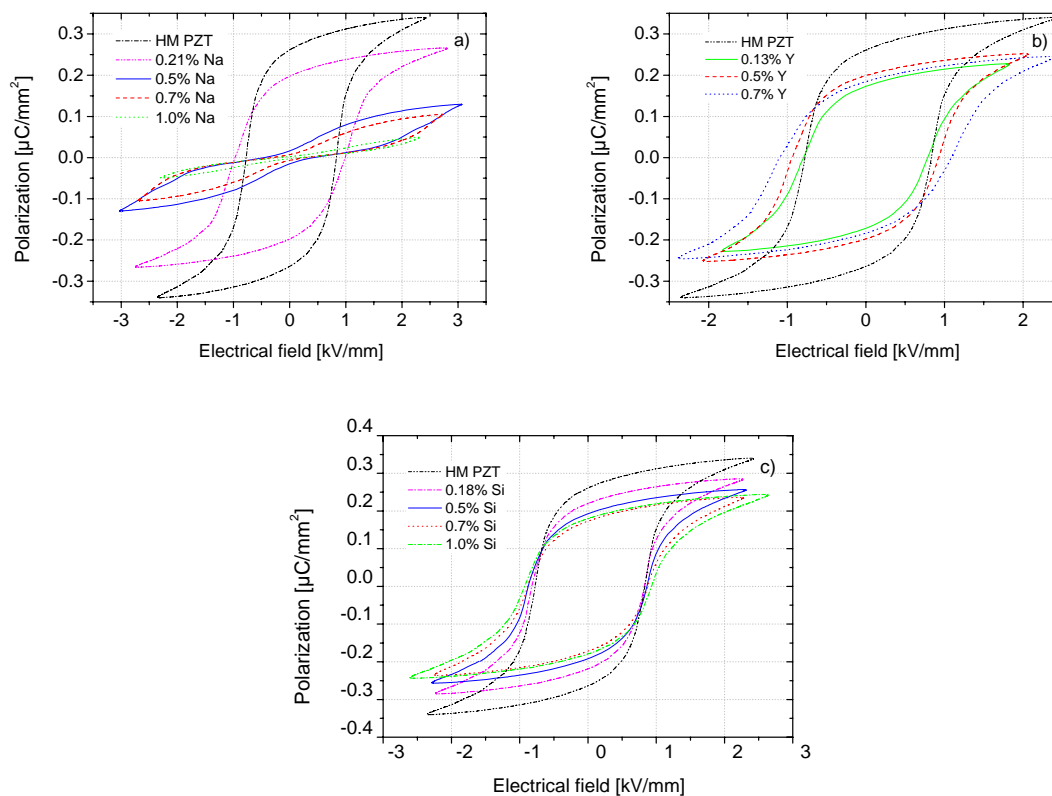


Figure 5.18 Hysteresis loops for PZT ceramics doped with different concentration of Na (a), Y (b) and Si(c)

5.4 Summary

Various impurities which were identified in industrially used raw materials for PZT production showed distinct effects on sintering behavior and properties of PZT ceramics. Although the impurities were added in small concentrations, sintering temperatures considerably decreased, final grain size changed and also the dielectric and piezoelectric properties were affected. Part of this variation can be attributed to deviations from the PZT composition close to the morphotropic phase boundary when the impurities were not considered in the weight fractions of the PbO-TiO₂-ZrO₂ raw materials. Especially with Hf - which is a typical impurity in the used zirconia raw materials - large deviations from the morphotropic composition occur, if its proportion is not considered adequately. Some impurities (such as Na) require oxygen vacancies for charge compensation when they are incorporated in the PZT lattice. These vacancies increase diffusion and accelerate sintering. Others (Si) are considered most effective via the PbO melt phase. This melt phase has a large impact on sintering and any change of the PbO concentration – even indirectly via impurities that substitute Pb in the PZT lattice – changes sintering activity. PbO concentration can already be affected by evaporation during calcination which depends critically on the formation kinetics of intermediate lead oxides (PbTiO₃).

In addition to sintering behavior the microstructure and the dielectric and piezoelectric properties of sintered PZT ceramics also considerably change when impurities are added to highly pure raw materials. A careful routine measurement of impurity concentration in the raw materials and the adaptation of the target composition are required to obtain PZT ceramics with small product variation via the mixed oxide route.

The effects of the individual impurity (Na, Y and Si) on the sintering behavior and properties of PZT ceramics prepared from highly pure raw materials have been investigated. Distinct responses have been observed on these PZT samples upon the modification of different impurities (Na, Y and Si). Doping with Na and Y at low levels (less than 0.5%) reduced the sintering temperatures, as well as the densification rate. With higher concentration of the impurities, they were increased again and close to the pure ceramics. This was attributed to the competing effects of vacancies and lead content. The sintering temperatures were substantially reduced upon Si modification due to the melt phase formed from PbO and SiO₂. But, the melt phase played no significant role in increasing the densification rate.

Substitution of Na on Pb site resulted in “softening” effect in mechanical quality factor, piezoelectric constant, planar coupling factor of investigated ceramics, with the exception of the dielectric constant. It increased with increasing doping level because of its powerful effect on grain growth inhibition. As a result of oxygen vacancies and small grain size, the full polarization of Na doped PZT was difficult to achieve. Double-loop like hysteresis was observed on the samples doped with more than 0.5 mol% Na. Combinative “soft” and “hard” characteristics in PZT ceramics resulted from Y doping. The dielectric constant increased considerably from 725 to 1000 and Q_m , k_p and d_{33} all decreased upon Y addition. Well saturated P-E loops were achieved in all investigated samples, with increased coercive field and decreased polarization. In general, samples doped with Si showed similar electrical properties to soft PZT, with slightly increased Q_m . The polarization of the samples was reduced upon Si modification. The coercive field, however, remain nearly unaffected.

Chapter 6 Studies on sintering kinetics of PZT by the kinetic field method

6.1 Introduction

A better understanding of densification during sintering is essential for assuring dense and reproducible PZT ceramics and for optimizing their mechanical and electrical properties. Activation energy has been widely applied in describing sintering of alumina or zirconia, zinc oxide systems (Chen, Shen et al. 1991; Wang and Raj 1991; Bernard-Granger and Guizard 2007). However, few attempts in obtaining the activation energy for sintering of PZT have been made. He and Ma employed a constitutive model to determine the activation energy for sintering of stoichiometric PZT to be 390 kJ/mol (He and Ma 2003). It was suggested that both grain boundary diffusion and interfacial reaction were the processes controlling densification of the sample. Grain growth and densification of hot-pressed PZT ceramics containing Bi were studied by Haertling (Haertling 1966). The activation energies of grain growth and densification were 397 kJ/mol and 157 kJ/mol respectively. No activation energy data on samples sintering with liquid phase has been reported.

In contrast to the previous studies, optical dilatometry was used to investigate the sintering behavior of PZT ceramics and samples with excess PbO or doped with Na or Si. The concentration of the additives was chosen to be close to those of industrial PZT ceramics. The samples were sintered using the constant-heating-rate method. The microstructure homogeneity was quantified by image analysis. A kinetic-field approach proposed by Palmour (Palmour III and Hare 1987) was utilized to investigate the sintering kinetics of PZT ceramics with lead oxide excess or doped with an impurity (Na or Si). The activation energy was calculated to study the contribution of coarsening and diffusion at different stage of sintering.

6.2 Sintering behavior at different heating rate

The samples were sintered at different heating rates. Based on the shrinkage data, a kinetic field was built to obtain the activation energy. Figure 6.1(a) exemplarily displays the shrinkage curves of PZT samples with 1.5wt% PbO excess obtained from heating ramps with different heating rates (1K/min, 2K/min, 5K/min, and 10K/min). T_{onset} and T_{50} are obtained from the shrinkage curves and listed in Table 6.1. The logarithm of true strain rate is plotted in an Arrhenius plot versus the

reciprocal absolute temperature, shown in Fig.6.1 (b). Points of equal shrinkage on different curves are connected to form the so-called iso-strain lines. The iso-strain lines for the PZT sintering could be fitted by straight lines. From the slope of each line, the apparent activation energy for the correspondent shrinkage can be derived using the Arrhenius equation (Eq.3.4).

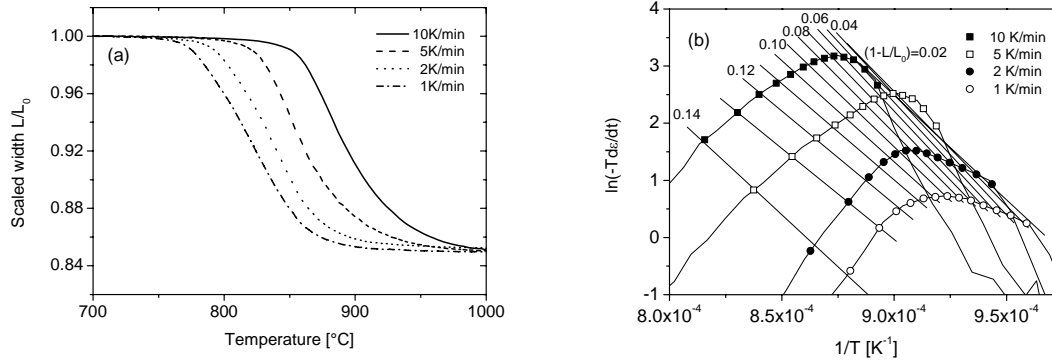


Figure 6.1 Shrinkage curves (a) and the kinetic field (b) of PZT with 1.5 wt% PbO excess sintered at different heating rates

As seen from Table 6.1, the sintering temperatures are drastically affected by the heating rate. When the heating rate was increased from 1K/min to 10K/min, T_{onset} and T_{50} increased from 738°C to 781°C and from 821°C to 892°C, respectively. Part of this increase may be related to the large thermal gradients in the sample during fast heating. However, the increasing difference between T_{onset} and T_{50} should be attributed to the sintering kinetics rather than temperature gradients, because temperature gradients are expected to decrease at constant heating rate as the thermal diffusivity usually increases in ceramic samples after the onset of sintering. In fact, similar behavior is often observed for sintering of zirconia and alumina that the lower the heating rate, the higher the shrinkage for a given temperature (Wang and Raj 1990; Sato and Carry 1996). It is assumed that at a lower heating rate, the compact is exposed for a longer time and shrinks more until reaching a certain temperature.

Table 6.1 The sintering temperatures T_{onset} and T_{50} of PZT with 1.5wt%PbO at different heating rates

Heating rate	1K/min	2K/min	5K/min	10K/min
T_{onset} [°C]	738	748	769	781
T_{50}	821	837	859	892
$T_{50}-T_{\text{onset}}$ [°C]	83	89	90	111

6.3 Kinetic field and apparent activation energy for sintering of PZT

The shrinkage curves of PZT ceramics with different compositions are plotted in Figure 6.2. It is seen that the shrinkage curves were shifted to lower temperatures when added with Na, Si or excess PbO. The latter two were believed to have introduced liquid phase into the system which led to a decrease in the sintering temperature, while the densification behavior was improved through the oxygen vacancies created to maintain charge neutrality when Na was added in the system.

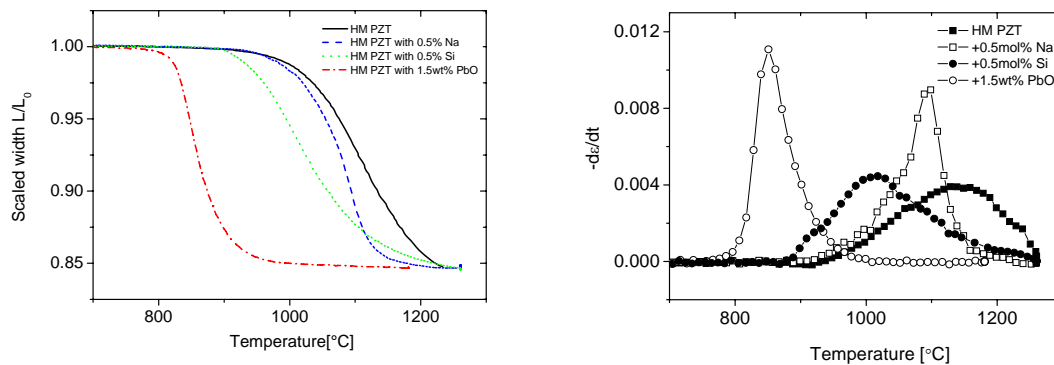


Figure 6.2 Shrinkage curves and shrinkage rate of PZT samples with different compositions at a heating rate of 5K/min

The apparent activation energies for sintering of PZT ceramics with different compositions are calculated from the kinetic field and presented in Figure 6.3. They exhibited distinct dependence on the shrinkage. An upward trend of the apparent activation energy with the shrinkage was observed in the pure sample and samples doped with 0.5mol% Na and Si. A plateau of approximately 460 kJ/mol and 420kJ/mol was seen of the pure PZT sample and the one doped with 0.5mol% Si respectively. An increasing trend of apparent activation energy was also observed in the sample with 1.5wt% lead oxide excess; however, a decrease was evidenced with further densification. Note that the four plots in Figure 6.3 were drawn on the same scale. Thus, it can be seen that the pure PZT sample had the highest apparent activation energy while the sample with 1.5wt% lead oxide excess showed the smallest apparent activation energy with the values below 350 kJ/mol. It implies that the apparent activation energy could be reduced by a wide range of additives.

In sintering of ceramics, surface diffusion, grain boundary diffusion and lattice diffusion are the main mechanisms for the transport of materials. Only the last two contribute to densification. Although surface diffusion does not contribute to densification, it increases the particle contact, decreases the surface curvature and leads to coarsening. Because the apparent activation energy is only an overall expression of all the thermally activated processes during sintering, the coarsening process could also affect the iso-strain lines. Recently, Raether and Schulze Horn reported that the

rotation of iso-density or iso-strain lines indicated the trend of variation in apparent activation energies with shrinkage and provided information on the extent of coarsening and the related activation energy compared to the activation energy for densification (Raether and Schulze Horn 2009). A clockwise rotation of the iso-strain lines indicates the activation energy for the coarsening mechanism is smaller than that for densification. Vice versa, a counter clockwise rotation is obtained when the activation energy for coarsening is larger than that for densification. Therefore, it is assumed that the variations in apparent activation energy in different samples are due to the differences in activation energy of densification and grain growth.

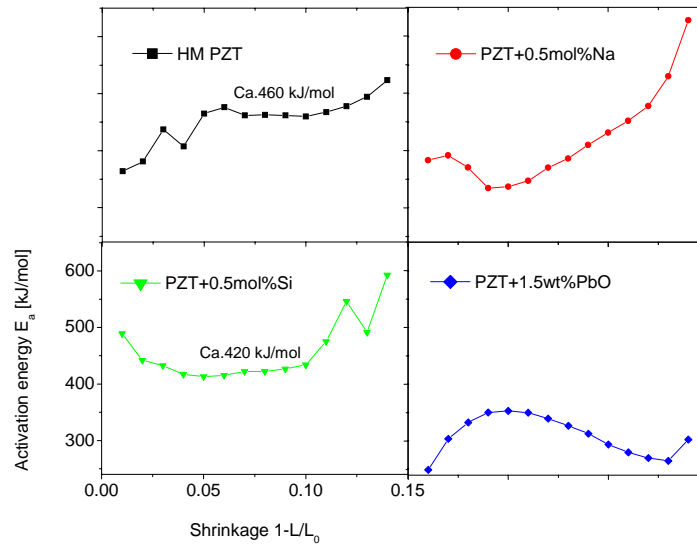


Figure 6.3 Apparent activation energies calculated from shrinkage curves using the kinetic field method (All four plots on the same scale)

6.4 The fitting of iso-strain lines

To obtain more information regarding the coarsening and densification in PZT systems, equation 3.4 was fitted to the experimental iso-strain lines using an in-house least square fitting software which was based on a gradient search algorithm, by which activation energy for grain growth as well as for densification can be calculated separately. Grain growth was described by:

$$G^m = G_0^m + C_2(T)t; \quad C_2(T) = C_0(\rho) \exp\left(-\frac{E_G}{RT}\right) \quad (6.1)$$

with G_0 as initial grain size; m as grain growth exponent; C_2 as frequency factor depending on microstructure; E_G as activation energy for grain growth.

As known from the previous chapters, liquid phase was introduced in the system doped with Si or with lead oxide excess. Therefore, equation 3.4 was transformed to

$$\ln\left(-\delta T \frac{d\varepsilon}{dt}\right) = \ln\left(\frac{C'D_0\gamma_{ls}}{G^n}\right) - \frac{E_D}{RT} \quad (6.2)$$

$$\delta = \frac{\Delta L^2 L}{L_0^3}$$

During the fit, a start particle size of 0.8 μm was used. The activation energy and exponents (refer to equation 3.4, 6.1) for grain growth and densification were varied to achieve the best fit, i.e. the lowest value of chi square χ^2 . The results from samples with liquid phase involved during sintering were fitted with both the solid and liquid phase model.

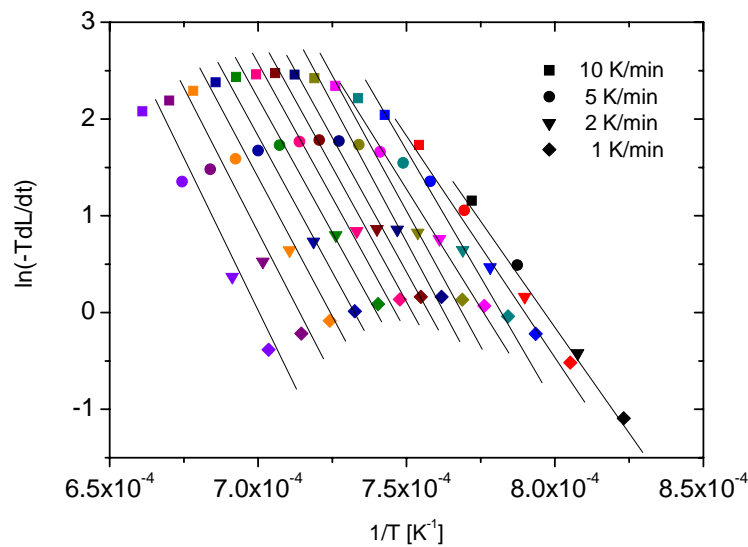


Figure 6.4 Kinetic field diagram reproduced by fitting the iso-density lines

Figure 6.4 presents the fit of the iso-strain lines for the pure HM sample with the scatters as the fitted results. The χ^2 values of the fits and the calculated activation energy for grain growth E_G and densification E_D are listed in Table 6.2. It is demonstrated that a good agreement between the experimental iso-strain lines and the fitted results is achieved. Good fits, i.e. small value of χ^2 (<0.08), were obtained in the pure PZT sample and the one doped with Na or Si when fitted using solid state sintering model. Relatively higher values were acquired for the sample doped with Si when using the liquid phase model and for the sample with 1.5wt% PbO lead oxide excess fitted with both sintering models. It suggests that better fitting behavior could be achieved using the solid state sintering model even in the systems involving liquid phase. This phenomenon is

assumed to be associated with the wetting behavior between the liquid phase and PZT grains. To testify the assumption, separate wetting experiments have been conducted. Loosely pressed PbO powder compact was placed on a sintered PZT plate. When heating them to high temperature, it was seen that PbO powder melt at the melting point 889°C, spread and covered the surface of the plate, which indicated that the contact angle of PbO liquid phase and PZT was close to zero. Owing to the perfect wetting behaviour and small quantity, the liquid phase formed a thin film on the surfaces of grains during sintering as seen from the SEM image (Figure 4.11). It makes it possible that the diffusion could happen through the thin film to the pores. Therefore, grain boundary or surface diffusion through the thin film is more likely to occur instead of the main mechanisms of liquid phase sintering such as Ostward ripening or contact flattening.

The activation energy of densification exhibited a value of approximately 360kJ/mol, while the one for grain growth varies in different systems, 320kJ/mol, 310kJ/mol and 340kJ/mol for pure PZT, PZT doped with Na and Si, respectively.

Table 6.2 Fitted activation energies for diffusion E_D and grain growth E_G during sintering of PZT samples with different compositions

Systems	HM PZT	PZT+0.5mol% Na	PZT+0.5mol% Si		PZT +1.5wt% PbO	
Fitting model	Solid	Solid	Solid	Liquid	Solid	Liquid
χ^2	0.059	0.075	0.059	0.1832	0.842	1.415
E_D kJ/mol	354	358	358	589	371	572
E_G kJ/mol	320	311	340	600	365	596
Growth exponent	2	0.9	2	4	3	4
Size exponent	3	3.1	3	4	4	4

6.5 Microstructure analysis

Homogeneity characterization was carried out on the PZT samples with different compositions during sintering. Figure 6.5 shows the SEM images of partially sintered PZT samples with different fractional densities. The scaled variance (refer to Chapter 3) was calculated to characterize inhomogeneity of microstructure. The results from the pure PZT sample, the samples doped with 0.5 mol%Na, Si and 1.5wt% PbO excess are presented in Figure 6.6. The inhomogeneity in all samples increases during sintering due to the coarsening effect. The scaled variance of the sample with lead oxide excess shows a nearly linear relationship with fractional density within the

experimentally studied range. The pure PZT sample and the samples doped with 0.5 mol% Na and Si exhibit a much smaller scaled variance, thus more homogeneous microstructure. In these samples, the variance starts to increase sharply after the relative density reaches 90%, which is correspondent to the prominent grain growth at the late stage of sintering. A suppressing role on the grain growth and inhomogeneous microstructure was observed in the 0.5mol% Na doped PZT sample, in which the variance remained at the lowest level.

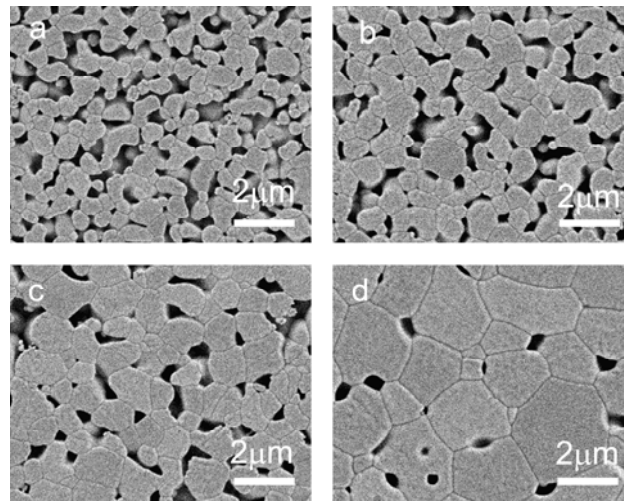


Figure 6.5 Microstructure evolution of pure PZT ceramics at different fractional densities (a-78%; b-83%; c- 90%; d- 95%)

It is common that inhomogeneous microstructure exists in the green body of the ceramics because of the local stress distribution during forming, the particle size distribution, and surface properties of the particles. As a result, locally differentiated microstructure with some region revealing a higher density than others is formed during sintering. The presence of a liquid phase could enhance such inhomogeneous structure. Guha and Anderson investigated the microstructure inhomogeneity in sintered PMN-PT ceramics (Guha and Anderson 1987). The inhomogeneity was characterized by the formation of a dense, localized region containing PbO-rich liquid, which is in agreement with our results. The variance was higher in the samples containing liquid phase (the sample with 1.5%wt excess PbO and 0.5 mol% Si) and was increased with the amount of liquid phase.

From Figure 6.1 a rapid densification can be seen in the PZT sample with 1.5%PbO due to the liquid phase caused by the PbO excess. It can be seen that the strain rate reached the maximum at the shrinkage of 6% (corresponding to a fractional density of 72%). After that, the densification rate slowed down and the variance was increased from 0.13 to 0.88. Therefore, the increased variance in the PZT sample with 1.5wt% PbO may account for the difficulty in fitting its iso-strain lines,

because inhomogeneity was not considered in Eq (6.1). However, a reasonable fitting was still achieved in the sample doped with Si because of the relative low densification rate and variance.

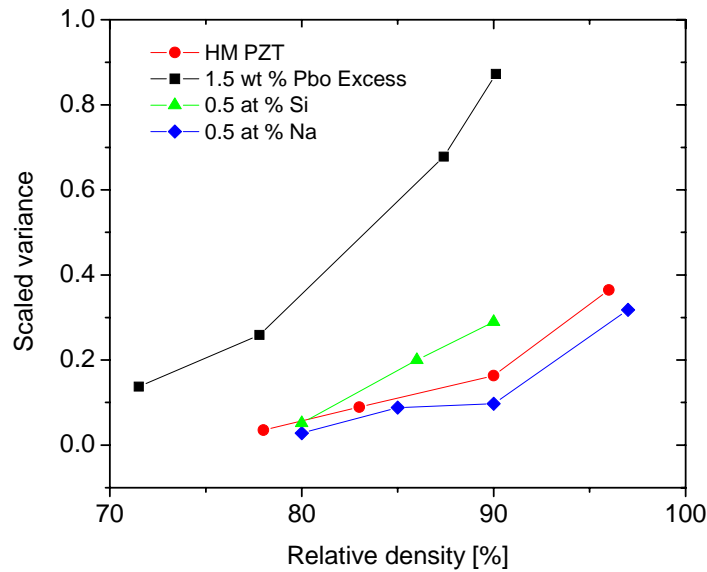


Figure 6.6 The scaled variance as function of fractional density of PZT samples with different compositions

6.6 Summary

The apparent activation energy in sintering of PZT ceramics with different compositions was calculated via the kinetic-field approach. The activation energy for densification and grain growth was obtained by fitting the iso-strain lines. The activation energy for densification maintains a value of approximately 360 kJ/mol upon the addition of impurities, 0.5% Si or 0.5% Na. Smaller values were acquired for grain growth and varied in different systems, with the lowest value of 310 kJ/mol in Na doped PZT. Although liquid phase was present in Si doped sample and the sample with excess PbO, a better fit can be achieved using solid state sintering model. It was explained by the good wetting behavior between PZT and the small amount of liquid phase, which enable the matter transport similar to the solid state sintering, such as surface diffusion and grain boundary diffusion. However, the increased amount of liquid phase in the system is not favorable to the fit due to the enhanced inhomogeneity of the microstructure.

Chapter 7 Conclusions

- 1) A comparison between the PZT samples prepared from industrially used and highly pure raw materials was made. Reduced sintering temperatures and higher densification rates were observed with the sample prepared from industrially used raw materials.
- 2) Various impurities, which were identified in the industrial raw materials, were added in the highly pure samples. The sintering behavior was affected through two ways. First, the charged vacancies were created through substitution of impurities on the site where the valence is different (such as Na, Y, Fe, Al). However, with increased substitution at Pb site, the increased lead deficiency dominates in the systems, because of which the sample exhibited a sintering behavior similar to highly pure systems. Second, sintering can be affected by elements that have a low eutectic temperature with lead oxide (such as Si). The sintering temperatures were drastically reduced due to the formation of the liquid phase.
- 3) The lead content in PZT can be affected by the crystalline phase of starting component TiO_2 . PbO concentration was changed during calcination depending on the formation kinetics of intermediate lead oxide. Deviations from the stoichiometric composition can result when the impurities were not considered in the weight fractions of the raw materials.
- 4) The crucial role of lead content in sintering of PZT ceramics was demonstrated. Sintering temperatures were dramatically reduced and densification rates were strongly enhanced by the introduction of lead oxide excess. The reason was believed to be associated with the liquid phase formed by PbO during sintering because of its low melting point. Rapid densification was observed at low level of PbO excess. However, a sluggish rearrangement process with low densification rate occurred in PZT with 3.0% PbO excess at a temperature below the melting point of PbO. A small force (as small as 0.1MPa) on the sample could result in rapid densification and an additional densification maximum was evidenced.
- 5) Although sintering temperatures were reduced by Si-doping, it exhibits no strong effect on the densification rate as the lead oxide excess. This phenomenon was attributed to the nature of the liquid phase introduced by the addition of SiO_2 , an amorphous glass phase.

- 6) Different dependence of activation energy on the fractional density was observed. It is attributed to the variation in the activation energies in densification and grain growth. By fitting the iso-strain lines, an activation energy of approximately 360 kJ/mol was obtained for densification of pure PZT sample and samples doped with 0.5% Na or Si. Smaller values were acquired for grain growth. Although liquid phase was present in Si-doped sample and the one with PbO excess, a better fitting can be achieved using solid state sintering model. The enhanced inhomogeneity was suggested to explain the difficulty in fitting the sintering curves of 1.5wt%PbO added sample.
- 7) Because of the charged vacancies created by doping the impurities, the samples showed either “soft” or “hard” behaviour in the case of donor or acceptor doping respectively. The rare earth impurity, such as Y, with a valence and ion radius between A site and B site elements in PZT lattice, result in a combinative “soft” and “hard” characteristics. The grain size inhibition effect was observed upon the doping of Na, Si, Y. Doping with Na showed the strongest effect on the grain size, which resulted in the high dielectric constant in the fine-grained samples.
- 8) Internal stress was suggested to explain the high dielectric constant in lead deficient PZT samples, which was introduced by the tetragonal lattice distortion in the lead deficient samples. Moreover, the increasing amount of lead deficiency could result in the segregation of ZrO_2 . It shifts the Zr/Ti ratio to the Ti-rich side, which may cause a higher dielectric constant as well. The lead excess is favorable in improving both the microstructure and electrical properties of PZT ceramics. However, deteriorated properties were found in samples in which the lead oxide excess is beyond a certain level (1.5mol%PbO).

References

- Ahn, C.-W., H.-C. Song, et al. (2006). "Effect of ZnO and CuO on the Sintering Temperature and Piezoelectric Properties of a Hard Piezoelectric Ceramic." *Journal of the American Ceramic Society* **89**(3): 921-925.
- Akbas, M. A., M. A. McCoy, et al. (1995). "Microstructural Evolution during Pressureless Sintering of Lead Lanthanum Zirconate Titanate Ceramics with Excess Lead(II) Oxide." *Journal of the American Ceramic Society* **78**(9): 2417-2424.
- Arlt, G. (1990). "Twinning in ferroelectric and ferroelastic ceramics: stress relief." *Journal of Materials Science* **25**(6): 2655-2666.
- Atkin, R. B. and R. M. Fulrath (1971). "Point Defects and Sintering of Lead Zirconate-Titanate." *Journal of the American Ceramic Society* **54**(5): 265-270.
- Atkin, R. B., R. L. Holman, et al. (1971). "Substitution of Bi and Nb Ions in Lead Zirconate-Titanate." *Journal of the American Ceramic Society* **54**(2): 113-115.
- Bateman, C. A., S. J. Bennison, et al. (1989). "Mechanism for the Role of Magnesia in the Sintering of Alumina Containing Small Amounts of a liquid Phase." *Journal of the American Ceramic Society* **72**(7): 1241-1244.
- Beitollahi, A. and M. Abedini (2006). "Effect of the level of the addition of $\text{Pb}(\text{Y}_{0.5}\text{Nb}_{0.5})\text{O}_3$ on the structure, microstructure and ferroelectric properties of PZT(53/47)." *Journal of Materials Science* **41**(12): 3671-3677.
- Bell, A. J., A. J. Moulson, et al. (1984). "The effect of grain size on the permittivity of BaTiO_3 ." *Ferroelectrics* **54**(1): 147.
- Berlincourt, D. and H. H. A. Krueger (1959). "Domain Processes in Lead Titanate Zirconate and Barium Titanate Ceramics." *Journal of Applied Physics* **30**(11): 1804-1810.
- Bernard-Granger, G. and C. Guizard (2007). "Apparent Activation Energy for the Densification of a Commercially Available Granulated Zirconia Powder." *Journal of the American Ceramic Society* **90**(4): 1246-1250.
- Buessem, W. R., E. Cross, et al. (1966). "Effect of Two-Dimensional Pressure on the Permittivity of Fine- and Coarse-Grained Barium Titanate." *Journal of the American Ceramic Society* **49**(1): 36-39.
- Buessem, W. R., L. E. Cross, et al. (1966). "Phenomenological Theory of High Permittivity in Fine-Grained Barium Titanate." *Journal of the American Ceramic Society* **49**(1): 33-36.
- Calvert, P. D. and R. R. Shaw (1970). "Liquidus Behavior in the Silica-Rich Region of the System PbO-SiO_2 ." *Journal of the American Ceramic Society* **53**(6): 350-352.
- Cao, W. and L. E. Cross (1993). "Theoretical model for the morphotropic phase boundary in lead zirconate-lead titanate solid solution." *Physical Review B* **47**(9): 4825.
- Chaisan, W., R. Yimnirun, et al. (2007). "Dielectric and ferroelectric properties of lead zirconate titanate-barium titanate ceramics prepared by a modified mixed-oxide method." *Materials Chemistry and Physics* **104**(1): 113-118.
- Chandratreya, S. S., R. M. Fulrath, et al. (1981). "Reaction Mechanisms in the Formation of PZT Solid Solutions." *Journal of the American Ceramic Society* **64**(7): 422-425.

- Chen, H., J. Long, et al. (2003). "Effect of Zr/Ti ratio on the properties of PMMN-PZT ceramics near the morphotropic phase boundary." *Materials Science and Engineering B* **99**(1-3): 433-436.
- Chen, S.-Y., S.-Y. Cheng, et al. (1990). "Polymorphic Phase Transformation of Lead Monoxide and Its Influence on Lead Zirconate Titanate Formation." *Journal of the American Ceramic Society* **73**(2): 232-236.
- Chen, Y.-C., C.-Y. Shen, et al. (1991). "Grain growth processes in ZnO visitors with various valence states of manganese and cobalt." *Journal of Applied Physics* **69**(12): 8363-8367.
- Corker, D. L., R. W. Whatmore, et al. (2000). "Liquid-phase sintering of PZT ceramics." *Journal of the European Ceramic Society* **20**(12): 2039-2045.
- Damjanovic, D. (1998). "Ferroelectric, dielectric and piezoelectric properties of ferroelectric thin films and ceramics." *Reports on Progress in Physics* **61**(9): 1267.
- Deng, G., Q. Yin, et al. (2005). "High Piezoelectric and Dielectric Properties of La-Doped $0.3\text{Pb}(\text{Zn}_{1/3}\text{Nb}_{2/3})\text{O}_3-0.7\text{Pb}(\text{Zr}_x\text{Ti}_{1-x})\text{O}_3$ Ceramics Near Morphotropic Phase Boundary." *Journal of the American Ceramic Society* **88**(8): 2310-2314.
- Dih, J. J. and R. M. Fulrath (1978). "Electrical Conductivity in Lead Zirconate-Titanate Ceramics." *Journal of the American Ceramic Society* **61**(9-10): 448-451.
- Donnelly, N. J., T. R. Shrout, et al. (2007). "Addition of a Sr, K, Nb (SKN) Combination to PZT(53/47) for High Strain Applications." *Journal of the American Ceramic Society* **90**(2): 490-495.
- Du, H., S. Qu, et al. (2007). "Effect of Zr/Ti ratio on piezoelectric and dielectric properties of PNW-PMS-PZT ceramics." *Journal of Electroceramics*: DOI:10.1007/s10832-007-9253-9
- Durruthy, M. D., L. Fuentes, et al. (2000). "Influence of the niobium dopant concentration on the $\text{Pb}(\text{Zr}_{0.54}\text{Ti}_{0.46})\text{O}_3$ ceramics sintering and final properties." *Journal of Materials Science* **35**(9): 2311-2317.
- Fan, H. and H.-E. Kim (2001). "Effect of Lead Content on the Structure and Electrical Properties of $\text{Pb}((\text{Zn}_{1/3}\text{Nb}_{2/3})_{0.5}(\text{Zr}_{0.47}\text{Ti}_{0.53})_{0.5})\text{O}_3$ Ceramics." *Journal of the American Ceramic Society* **84**(3): 636-638.
- Fontana, E. H. and W. A. Plummer (1979). "A Viscosity-Temperature Relation for Glass." *Journal of the American Ceramic Society* **62**(7-8): 367-369.
- Fousek, J. and V. Janovec (1969). "The Orientation of Domain Walls in Twinned Ferroelectric Crystals." *Journal of Applied Physics* **40**(1): 135-142.
- Gao, Y., K. Uchino, et al. (2002). "Effects of rare earth metal substituents on the piezoelectric and polarization properties of $\text{Pb}(\text{Zr,Ti})\text{O}_3\text{-Pb}(\text{Sb,Mn})\text{O}_3$ ceramics." *Journal of Applied Physics* **92**(4): 2094-2099.
- Garcia, J. E., R. Perez, et al. (2008). "Evaluation of domain wall motion in lead zirconate titanate ceramics by nonlinear response measurements." *Journal of Applied Physics* **103**(5): 054108-8.
- Garg, A. and D. C. Agrawal (1999). "Effect of net PbO content on mechanical and electromechanical properties of lead zirconate titanate ceramics." *Materials Science and Engineering B* **60**(1): 46-50.
- German, R. M. (1985). *Liquid Phase Sintering*, Plenum Press, London.
- German, R. M. (1996). *Sintering Theory and Practice*, John Wiley & Sons, Inc, New York.
- Gerson, R. (1960). "Variation in Ferroelectric Characteristics of Lead Zirconate Titanate Ceramics Due to Minor Chemical Modifications." *Journal of Applied Physics* **31**(1): 188-194.

- Goo, E. K. W., R. K. Mishra, et al. (1981). "Transmission Electron Microscopy of $\text{Pb}(\text{Zr}_{0.52}\text{Ti}_{0.48})\text{O}_3$." *Journal of the American Ceramic Society* **64**(9): 517-519.
- Guha, J. P. and H. U. Anderson (1987). "Microstructural Inhomogeneity in Sintered $\text{Pb}(\text{Mg}_{1/3}\text{Nb}_{2/3})\text{O}_3$ - PbTiO_3 Based Dielectrics." *Journal of the American Ceramic Society* **70**: C-39.
- Guo, R., L. E. Cross, et al. (2000). "Origin of the High Piezoelectric Response in $\text{PbZr}_{1-x}\text{Ti}_x\text{O}_3$." *Physical Review Letters* **84**(23): 5423-5423.
- Gupta, S. M. and D. Viehland (1998). "Tetragonal to rhombohedral transformation in the lead zirconium titanate lead magnesium niobate-lead titanate crystalline solution." *Journal of Applied Physics* **83**(1): 407-414.
- Haertling, G. H. (1964). "Hot-pressed lead zirconate-lead titanate ceramics containing bismuth." *American Ceramic Society Bulletin* **43**(12): 875-879.
- Haertling, G. H. (1966). "Grain Growth and Densification of Hot-Pressed Lead Zirconate-Lead Titanate Ceramics Containing Bismuth." *Journal of the American Ceramic Society* **49**(3): 113-118.
- Haertling, G. H. (1999). "Ferroelectric Ceramics: History and Technology." *Journal of the American Ceramic Society* **82**(4): 797-818.
- Hallse, R. L. and R. L. Cook (1958). "Volatility Studies of Lead Silicate Melts." *Journal of the American Ceramic Society* **41**(9): 331-336.
- Hammer, M. and M. J. Hoffmann (1998). "Sintering Model for Mixed-Oxide-Derived Lead Zirconate Titanate Ceramics." *Journal of the American Ceramic Society* **81**(12): 3277-3284.
- Hammer, M., C. Monty, et al. (1998). "Correlation between Surface Texture and Chemical Composition in Undoped, Hard, and Soft Piezoelectric PZT Ceramics." *Journal of the American Ceramic Society* **81**(3): 721-724.
- Hankey, D. L. and J. V. Diggers (1981). "Solid-State Reactions in the System $\text{PbO-TiO}_2\text{-ZrO}_2$." *Journal of the American Ceramic Society* **64**(12): C-172-C-173.
- Härdtl, K. H. (1982). "Electrical and mechanical losses in ferroelectric ceramics." *Ceramics International* **8**(4): 121-127
- Härdtl, K. H. and H. Rau (1969). "PbO vapour pressure in the $\text{Pb}(\text{Ti}_{1-x})\text{O}_3$ system." *Solid State Communications* **7**(1): 41-45.
- He, L. and D. Vanderbilt (2003). "First-principles study of oxygen-vacancy pinning of domain walls in PbTiO_3 ." *Physical Review B* **68**(13): 134103
- He, Z. and J. Ma (2003). "Constitutive modeling of the densification of PZT ceramics." *Journal of Physics and Chemistry of Solids* **64**(2): 177-183.
- Hennings, D. F. K., R. Janssen, et al. (1987). "Control of Liquid-Phase-Enhanced Discontinuous Grain Growth in Barium Titanate." *Journal of the American Ceramic Society* **70**(1): 23-27.
- Hiremath, B. V., A. I. Kingon, et al. (1983). "Reaction Sequence in the Formation of Lead Zirconate-Lead Titanate Solid Solution: Role of Raw Materials." *Journal of the American Ceramic Society* **66**(11): 790-793.
- Hoffmann, M. J., M. Hammer, et al. (2001). "Correlation between microstructure, strain behavior, and acoustic emission of soft PZT ceramics." *Acta Materialia* **49**(7): 1301-1310.
- Holman, R. L. and R. M. Fulrath (1972). "Intrinsic Nonstoichiometry in Single-Phase $\text{Pb}(\text{Zr}_{0.5}\text{Ti}_{0.5})\text{O}_3$." *Journal of the American Ceramic Society* **55**(4): 192-194.

- Holman, R. L. and R. M. Fulrath (1973). "Intrinsic nonstoichiometry in the lead zirconate-lead titanate system determined by Knudsen effusion." *Journal of Applied Physics* **44**(12): 5227-5236.
- Huang, C.-L., B.-H. Chen, et al. (2004). "Variability of impurity doping in the modified $\text{Pb}(\text{Zr,Ti})\text{O}_3$ ceramics of type ABO_3 ." *Solid State Communications* **130**(1-2): 19-23.
- Huang, X., H. Zhao, et al. (2006). "Effect of fabrication parameters on the electrical conductivity of $\text{Y}_x\text{Sr}_{1-x}\text{TiO}_3$ for anode materials." *Journal of Physics and Chemistry of Solids* **67**(12): 2609-2613.
- Jaffe, B., W. R. Cook, et al. (1971). *Piezoelectric Ceramics*. London and New York, Academic Press Inc.
- Jaffe, B., R. S. Roth, et al. (1954). "Piezoelectric Properties of Lead Zirconate-Lead Titanate Solid-Solution Ceramics." *Journal of Applied Physics* **25**(6): 809-810.
- Jin, B. M., J. Kim, et al. (1997). "Effects of grain size on the electrical properties of $\text{PbZr}_{0.52}\text{Ti}_{0.48}\text{O}_3$ ceramics." *Applied Physics A: Materials Science & Processing* **65**(1): 53-56.
- Kamel, T. M. and G. de With (2008). "Grain size effect on the poling of soft $\text{Pb}(\text{Zr,Ti})\text{O}_3$ ferroelectric ceramics." *Journal of the European Ceramic Society* **28**(4): 851-861.
- Kaneko, S., D. Dong, et al. (1998). "Effect of Simultaneous Addition of BiFeO_3 and $\text{Ba}(\text{Cu}_{0.5}\text{W}_{0.5})\text{O}_3$ on Lowering of Sintering Temperature of $\text{Pb}(\text{Zr,Ti})\text{O}_3$ Ceramics." *Journal of the American Ceramic Society* **81**(4): 1013-1018.
- Kim, S.-B., D.-Y. Kim, et al. (1990). "Effect of Grain Size and Poling on the Fracture Mode of Lead Zirconate Titanate Ceramics." *Journal of the American Ceramic Society* **73**(1): 161-163.
- Kingery, W. D., J. M. Woulbroun, et al. (1963). "Effects of Applied Pressure on Densification During Sintering in the Presence of a Liquid Phase." *Journal of the American Ceramic Society* **46**(8): 391-395.
- Kington, A. I. and J. B. Clark (1983). "Sintering of PZT Ceramics: I, Atmosphere Control." *Journal of the American Ceramic Society* **66**(4): 253-256.
- Kington, A. I. and J. B. Clark (1983). "Sintering of PZT Ceramics: II, Effect of PbO Content on Densification Kinetics." *Journal of the American Ceramic Society* **66**(4): 256-260
- Kington, A. I., P. J. Terblanché, et al. (1982). "Effect of reactant dispersion on formation of PZT solid solutions." *Ceramics International* **8**(3): 108-114.
- Kong, L. B., W. Zhu, et al. (2000). "Preparation and characterization of $\text{Pb}(\text{Zr}_{0.52}\text{Ti}_{0.48})\text{O}_3$ ceramics from high-energy ball milling powders." *Materials Letters* **42**(4): 232-239.
- Kulcsar, F. (1959). "Electromechanical Properties of Lead Titanate Zirconate Ceramics Modified with Certain Three-or Five-Valent Additions." *Journal of the American Ceramic Society* **42**(7): 343-349.
- Lal, R., N. Gokhale, et al. (1989). "Effect of sintering parameters on the microstructure and properties of strontium modified PZT ceramics prepared using spray-dried powders." *Journal of Materials Science* **24**(8): 2911-2916.
- Lange, U. (2003). Einfluß der Korngröße auf die morphotrope Phasengrenze in Sol-Gel abgeleiteten Nd-dotierten PZT-Keramiken (in German). Würzburg, Germany, PhD dissertation of Bayerischen Julius-Maximilians-Universität Würzburg.
- Lee, B. and E. Lee (2006). Effects of complex doping on microstructural and electrical properties of PZT ceramics, *Journal of Electroceramics*. **17**: 597-602
- Li, F. X., D. N. Fang, et al. (2006). "Theoretical saturated domain-orientation states in ferroelectric ceramics." *Scripta Materialia* **54**(7): 1241-1246.

- Li, J.-F., S. Wang, et al. (2000). "Properties of Modified Lead Zirconate Titanate Ceramics Prepared at Low Temperature (800°C) by Hot Isostatic Pressing." *Journal of the American Ceramic Society* **83**(4): 955-957
- Liang, C.-K. and L. Wu (1993). "Microstructure and Properties of Cr₂O₃-Doped Ternary Lead Zirconate Titanate Ceramics." *Journal of the American Ceramic Society* **76**(8): 2023-2026.
- Majumder, S. B., B. Roy, et al. (2001). "Effect of acceptor and donor dopants on polarization components of lead zirconate titanate thin films." *Applied Physics Letters* **79**(2): 239-241.
- Mal, J. and R. N. P. Choudhary (1997). "Structural and dielectric properties of sol-gel prepared PZT(La, K) ferroelectric ceramics." *Journal of Physics and Chemistry of Solids* **58**(3): 421-425.
- Marion, J. E., C. H. Hsueh, et al. (1987). "Liquid-Phase Sintering of Ceramics." *Journal of the American Ceramic Society* **70**(10): 708-713.
- Martirena, H. T. and J. C. Burfoot (1974). "Grain-size effects on properties of some ferroelectric ceramics." *Journal of Physics C: Solid State Physics* **7**(17): 3182-3192.
- Matsuo, Y. and H. Sasaki (1965). "Formation of Lead Zirconate-Lead Titanate Solid Solutions." *Journal of the American Ceramic Society* **48**(6): 289-291.
- Mendelson, M. I. (1969). "Average grain size in polycrystalline ceramics." *Journal of the American Ceramic Society* **52**(8): 443-446.
- Merz, W. J. (1953). "Double Hysteresis Loop of BaTiO₃ at the Curie Point." *Physical Review* **91**(3): 513.
- Missiaen, J. M. and G. Thomas (1995). "Homogeneity characterization of binary grain mixtures using a variance analysis of two-dimensional numerical fractions." *Journal of Physics: Condensed Matter*(15): 2937.
- Moulson, A. J. and J. M. Herbert (2003). *Electroceramics: Materials, Properties, Applications*, John Wiley & Sons, Ltd. Second edition.
- Mountvala, A. J. and S. F. Ravitz (1962). "Phase Relations and Structures in the System PbO-Fe₂O₃." *Journal of the American Ceramic Society* **45**(6): 285-288.
- Nelmes, R. J. and W. F. Kuhs (1985). "The crystal structure of tetragonal PbTiO₃ at room temperature and at 700 K." *Solid State Communications* **54**(8): 721-723.
- Noheda, B., D. E. Cox, et al. (1999). "A monoclinic ferroelectric phase in the Pb(Zr_{1-x}Ti_x)O₃ solid solution." *Applied Physics Letters* **74**(14): 2059-2061.
- Noheda, B., J. A. Gonzalo, et al. (2000). The monoclinic phase in PZT: New light on morphotropic phase boundaries. *FUNDAMENTAL PHYSICS OF FERROELECTRICS 2000: Aspen Center for Physics Winter Workshop*, AIP.
- Oh, U.-C., Y.-S. Chung, et al. (1988). "Effect of Grain Growth on Pore Coalescence During the Liquid-Phase Sintering of MgO-CaMgSiO₄ Systems." *Journal of the American Ceramic Society* **71**(10): 854-857.
- Palkar, V. R., S. C. Purandare, et al. (2000). "Breakthrough in densification of ferroelectric PbTiO₃ with Si as sintering aid." *Materials Letters* **43**(5-6): 329-334.
- Palmour III, H. and T. H. Hare (1987). *Sintering 85*, Plenum Press, New York.
- Park, J.-K., U.-J. Chung, et al. (2001). "Preparation of Dense Lead Magnesium Niobate-Lead Titanate (Pb(Mg_{1/3}Nb_{2/3})O₃;PbTiO₃) Ceramics by Spark Plasma Sintering." *Journal of the American Ceramic Society* **84**(12): 3057-3059.
- Pérez, J. A., M. R. Soares, et al. (2005). "Microstructural design of PZT ceramics." *Journal of the European Ceramic Society* **25**(12): 2207-2210.

- Raether, F. and P. Schulze Horn (2009). "Investigation of sintering mechanisms of alumina using kinetic field and master sintering diagrams." *Journal of the European Ceramic Society* **29**(11): 2225-2234
- Raether, F., R. Springer, et al. (2001). "Optical dilatometry for the control of microstructure development during sintering." *Materials Research Innovations* **4**(4): 245-250.
- Raether, F. G. (2009). "Current State of *In Situ* Measuring Methods for the Control of Firing Processes." *Journal of the American Ceramic Society* **92**(s1): S146-S152.
- Rahaman, M. N. (2003). *Ceramic Processing and Sintering*, CRC Press.
- Randall, C. A., N. Kim, et al. (1998). "Intrinsic and Extrinsic Size Effects in Fine-Grained Morphotropic-Phase-Boundary Lead Zirconate Titanate Ceramics." *Journal of the American Ceramic Society* **81**(3): 677-688.
- Ryu, J., J.-J. Choi, et al. (2001). "Effect of Heating Rate on the Sintering Behavior and the Piezoelectric Properties of Lead Zirconate Titanate Ceramics." *Journal of the American Ceramic Society* **84**(4): 902-904.
- Sato, E. and C. Carry (1996). "Yttria Doping and Sintering of Submicrometer-Grained α -Alumina." *Journal of the American Ceramic Society* **79**(8): 2156-2160.
- Scherer, G. W. (1986). "Viscous Sintering under a Uniaxial Load." *Journal of the American Ceramic Society* **69**(9): C-206-C-207.
- Shackelford, J. F. and R. L. Holman (1975). "Nonstoichiometry in ABO_3 compounds similar to $PbTiO_3$." *Journal of Applied Physics* **46**(4): 1429-1434.
- Shirane, G., E. Sawaguchi, et al. (1951). "Dielectric Properties of Lead Zirconate." *Physical Review* **84**(3): 476.
- Smart, R. M. and F. P. Glasser (1974). "Compound Formation and Phase Equilibria in the System $PbO-SiO_2$." *Journal of the American Ceramic Society* **57**(9): 378-382.
- Smith, R. C. and C. L. Hom (1999). "Domain Wall Theory for Ferroelectric Hysteresis." *Journal of Intelligent Material Systems and Structures* **10**(3): 195-213.
- Snow, G. S. (1974). "Elimination of Porosity in $Pb(Zr, Ti)O_3$ Ceramics by Liquid-Phase Sintering." *Journal of the American Ceramic Society* **57**(6): 272.
- Soares, M. R., A. M. R. Senos, et al. (2000). "Phase coexistence region and dielectric properties of PZT ceramics." *Journal of the European Ceramic Society* **20**(3): 321-334.
- Stoto, T., M. Nauer, et al. (1991). "Influence of Residual Impurities on Phase Partitioning and Grain Growth Processes of Y-TZP Materials." *Journal of the American Ceramic Society* **74**(10): 2615-2621.
- Subbarao, E. C., M. C. McQuarrie, et al. (1957). "Domain Effects in Polycrystalline Barium Titanate." *Journal of Applied Physics* **28**(10): 1194-1200.
- Sundar, V., N. Kim, et al. (1996). The effect of doping and grain size on electrostriction in $PbZr_{0.52}Ti_{0.48}O_3$. *Applications of Ferroelectrics, 1996. ISAF '96., Proceedings of the Tenth IEEE International Symposium on*. **2**: 935-938 vol.2.
- Suwannasiri, T. and A. Safari (1993). "Effect of Rare-Earth Additives on Electromechanical Properties of Modified Lead Titanate Ceramics." *Journal of the American Ceramic Society* **76**(12): 3155-3158.
- Takahashi, M. (1970). "Space Charge Effect in Lead Zirconate Titanate Ceramics Caused by the Addition of Impurities." *Japanese Journal of Applied Physics* **9**: 1236-1246.

- Tan, Q., J.-F. Li, et al. (1997). "Ferroelectric behaviours dominated by mobile and randomly quenched impurities in modified lead zirconate titanate ceramics." *Philosophical Magazine B* **76**(1): 59-74.
- Tan, Q., J. Li, et al. (1999). "Role of lower valent substituent-oxygen vacancy complexes in polarization pinning in potassium-modified lead zirconate titanate." *Applied Physics Letters* **75**(3): 418-420.
- Uchino, K. (2000). *Ferroelectric Devices*, Marcel Dekker Inc.
- Ursic, H., M. Hrovat, et al. (2008). "Microstructural and electrical characterisation of PZT thick films on LTCC substrates." *Journal of the European Ceramic Society* **28**(9): 1839-1844.
- Venkataramani, S. B., James V. (1980). "Reactivity of zirconia in calcining of lead zirconate-lead titanate compositions prepared from mixed oxides " *American Ceramic Society Bulletin* **59**(4): 462-466.
- Wang, J. and R. Raj (1990). "Estimate of the Activation Energies for Boundary Diffusion from Rate-Controlled Sintering of Pure Alumina, and Alumina Doped with Zirconia or Titania." *Journal of the American Ceramic Society* **73**(5): 1172-1175.
- Wang, J. and R. Raj (1991). "Activation Energy for the Sintering of Two-Phase Alumina/Zirconia Ceramics." *Journal of the American Ceramic Society* **74**(8): 1959-1963.
- Wang, X. X., K. Murakami, et al. (2001). "Piezoelectric properties, densification behavior and microstructural evolution of low temperature sintered PZT ceramics with sintering aids " *Journal of the European Ceramic Society* **21**(10-11): 1367-1370.
- Webster, A. H., T. B. Weston, et al. (1967). "Effect of PbO Deficiency on the Piezoelectric Properties of Lead Zirconate-Titanate Ceramics." *Journal of the American Ceramic Society* **50**(9): 490-491.
- Weston, T. B., A. H. Webster, et al. (1969). "Lead Zirconate-Lead Titanate Piezoelectric Ceramics with Iron Oxide Additions." *Journal of the American Ceramic Society* **52**(5): 253-257.
- Wittmer, D. E. and R. C. Buchanan (1981). "Low-Temperature Densification of Lead Zirconate-Titanate with Vanadium Pentoxide Additive." *Journal of the American Ceramic Society* **64**(8): 485-490.
- Wu, L., T.-C. Wu, et al. (1983). "The DC resistivity of modified PZT ceramics." *J.Phys. C: Solid State Phys.* **16**: 2923-2832.
- Xu, Y. (1991). *Ferroelectric Materials and Their Applications*, Elsevier Science Publishers B.V.
- Yimnirun, R., Y. Laosiritaworn, et al. (2006). "Effect of uniaxial compressive pre-stress on ferroelectric properties of soft PZT ceramics." *Journal of Physics D: Applied Physics* **39**(4): 759-764.
- Yoo, J., C. Lee, et al. (2005). "Microstructural and piezoelectric properties of low temperature sintering PMN-PZT ceramics with the amount of Li_2CO_3 addition." *Materials Chemistry and Physics* **90**(2-3): 386-390.
- Yoon, S.-J., H.-J. Kim, et al. (1993). "Dielectric and piezoelectric properties of $x\text{Pb}(\text{Y}_{2/3}\text{W}_{1/3})\text{O}_3-(1-x)\text{Pb}(\text{Zr}_{0.52}\text{Ti}_{0.48})\text{O}_3$ ceramics." *Ferroelectrics* **145**(1): 1.
- Young, R. A. (1995). *The Rietveld Method*, Oxford Univ Pr.
- Zhang, Q. M., W. Y. Pan, et al. (1988). "Domain wall excitations and their contributions to the weak-signal response of doped lead zirconate titanate ceramics." *Journal of Applied Physics* **64**(11): 6445-6451.

-
- Zhang, Z. and R. Raj (1995). "Influence of Grain Size on Ferroelastic Toughening and Piezoelectric Behavior of Lead Zirconate Titanate." *Journal of the American Ceramic Society* **78**(12): 3363-3368.
- Zhilun, G., L. Longtu, et al. (1989). "Low-Temperature Sintering of Lead-Based Piezoelectric Ceramics." *Journal of the American Ceramic Society* **72**(3): 486-491.
- Zhu, Z. G., G. R. Li, et al. (2005). "Microstructure, domain morphology and piezoelectric properties of Si-doped $\text{Pb}(\text{Mn}_{1/3}\text{Sb}_{2/3})\text{O}_3\text{-Pb}(\text{Zr,Ti})\text{O}_3$ systems." *Materials Science and Engineering B* **119**(1): 46-50.
- Zimmer, J., F. Raether, et al. (1998). A system for rate controlled sintering by kinetic field approach, CIMTEC, World Ceramics Congress & Forum on New Materials. Florenz, Italy.

List of Figures

- Figure 1.1 The perovskite structure ABO_3 , shown here for $PbTiO_3$ which has a cubic structure in the paraelectric phase and tetragonal structure in the ferroelectric phase (Nelmes and Kuhs 1985) 3
- Figure 1.2 Illustration of (a) 180° and (b) 90° ferroelectric domains and domain-wall regions in a tetragonal perovskite ferroelectric. The schematic change of polarization across the domain wall is shown for a 180° wall in (a). Tetragonal distortion in (b) is exaggerated. (Damjanovic 1998)..... 4
- Figure 1.3 A polycrystalline ferroelectric with random orientation of grains before, during and after poling. Many domain walls are present in the poled material; however, the net remnant polarization is nonzero. (Xu 1991). 4
- Figure 1.4 Schematic of Polarization-Electric (P-E) field hysteresis loop. Circles with arrows represent the polarization state of the materials at the indicated fields. The symbols are explained in the text. (Damjanovic 1998) 5
- Figure 1.5 Phase diagram of lead zirconate titanate $Pb(Zr_xTi_{1-x})O_3$ (Jaffe, Cook et al. 1971)..... 7
- Figure 1.6 Shrinkage and densification rate curves of stoichiometric PZT and the sample with 3mol% PbO excess (Hammer and Hoffmann 1998)..... 11
- Figure 1.7 (a) Planar coupling factor k_p , mechanical quality factor Q_m and (b) dielectric constant ϵ_r , dielectric loss $\tan\delta$ (1kHz) of $(Pb_{0.95}Sr_{0.05})[(Ni_{1/2}W_{1/2})_{0.02}(Mn_{1/3}Sb_{2/3})_{0.06}(Zr_xTi_y)_{0.92}]O_3$ ceramics with different Zr/Ti ratio 13
- Figure 1.8 Effect of Nb_2O_3 (Kulcsar 1959) and Fe_2O_3 (Weston, Webster et al. 1969) addition on the electrical properties of lead zirconate-lead titanate ceramics..... 15
- Figure 1.9 Crystalline deficiencies in PZT ceramics (Uchino 2000) 16
- Figure 1.10 DC resistivity of PZT doped with Nb^{5+} and Sc^{3+} as function of temperature (Dih and Fulrath 1978) 17
- Figure 2.1 Back scattering electron images of reactants after wet mixing (a) and dry mixing (b) for 24 hours (PbO , ZrO_2 and TiO_2 are light grey, dark grey and black, respectively.) 24
- Figure 2.2 SEM images of green compacts from the PZT powder with (a) and without (b) freeze drying process..... 25
- Figure 2.3 Schematic of closed crucible with two sapphire windows in opposite sides either in free sintering (a) or loading dilatometry (b)..... 26
- Figure 2.4 Back scattering image of contaminated silica window 27
- Figure 2.5 Images recorded by TOMMI using two different window materials, silica (a), sapphire (b)..... 27
- Figure 3.1 Refined pattern with observed, calculated and difference profiles in the 2-theta range $10-100^\circ$ for HM $Pb(Zr_{0.53}Ti_{0.47})O_3$ using tetragonal and rhombohedral coexistence model. Bars represent the peak positions. 29
- Figure 3.2 Shrinkage of a PZT sample made from highly pure materials (HM) as function of temperature (The way to derive temperatures for the onset of shrinkage (T_{onset}) and 50 % of total shrinkage (T_{50}) is indicated in the diagram.) 31

Figure 3.3 Scaled width L/L_0 of PZT prepared from highly pure materials sintered at different heating rates	32
Figure 3.4 Kinetic field of PZT prepared from highly pure raw materials.....	32
Figure 4.1 DTA study of IM and HM mixtures.....	34
Figure 4.2 XRD patterns of IM and HM mixtures after calcination at 850°C for 2 hours.....	34
Figure 4.3 Scaled width L/L_0 (a) and densification rate dL/dt (b) of PZT samples made from different raw materials at a heating rate of 10 K/min (HM-highly pure materials, IM-industrially used materials)	35
Figure 4.4 SEM images of pure PZT samples quenched at a linear shrinkage of 10% made from industrially used raw materials (a) and highly pure raw materials (b). (Arrows indicate secondary phase).....	35
Figure 4.5 Axial and radial strain of PZT samples with or without uniaxial load of 0.4 MPa at a heating rate of 10 K/min made from industrially used raw materials (a) and highly pure raw materials (b).....	36
Figure 4.6 Comparison of hysteresis loops obtained from HM PZT and IM PZT.....	37
Figure 4.7 XRD patterns of PZT with different levels of lead nonstoichiometry.....	39
Figure 4.8 Evolution of the unit cell distortion of tetragonal phase, c/a ratio with lead nonstoichiometry.....	39
Figure 4.9 Sintering temperatures (a) and densification rates (b) of PZT samples with different levels of lead nonstoichiometry (-1.0, -0.5, 0, 0.5, 1.5, 3%; heating rate 10K/min)	40
Figure 4.10 Comparison of shrinkage rate of PZT sample with 3.0 mol% PbO excess during free sintering and sintering with 0.01MPa load (heating rate 2K/min)	42
Figure 4.11 TEM study on the PZT sample with 1.5% excess PbO quenched at a fractional density of 82%.....	43
Figure 4.12 Densities of PZT samples with different amount of lead oxide excess (-0.5, 0, 0.5, 1.5, 3) sintered at 1280°C for 2 h with a heating rate of 5K/min.....	44
Figure 4.13 SEM images of PZT samples containing 3.0%PbO (a) and 1.5% PbO (b) sintered at 1280°C for 2 h with a heating rate of 5K/min	44
Figure 4.14 (a) Mechanical quality factor Q_m (b) Planar coupling factor k_p (c) Piezoelectric coefficient d_{33} (d) Dielectric loss (e) Dielectric constant ϵ_r of PZT with different level of lead nonstoichiometry.....	46
Figure 4.15 P-E loops of PZT ceramics with different levels of lead nonstoichiometry	47
Figure 5.1 Temperatures for the onset of shrinkage (T_{onset}) and 50 % of total shrinkage (T_{50}) of PZT samples made from highly pure (HM) and industrially used (IM) raw materials and mixtures with one oxide component being replaced by the IM material.....	50
Figure 5.2 DTA (a) and TG (b) study of a mixture from highly pure oxide powders (HM) and mixtures where TiO_2 or ZrO_2 were replaced by industrially used oxides respectively	51
Figure 5.3 Temperatures for the onset of shrinkage T_{onset} and 50 % of total shrinkage (T_{50}) of PZT samples doped with different groups of impurities.....	53
Figure 5.4 SEM picture of fracture surface of sample doped with Hf and Si (one grain is partly covered with secondary phase).....	54
Figure 5.5 Temperatures for the onset of shrinkage T_{onset} and 50 % of total shrinkage (T_{50}) of pure (HM) PZT samples without impurities and stoichiometric (s) and nonstoichiometric (non) samples doped with all impurities.....	55

Figure 5.6 SEM images of polished surfaces of the pure HM sample (a) and samples from HM material doped with different impurities: Hf/Si (b), Na/Ba/Ca (c), Fe/Al/Y (d), all impurities nonstoichiometric (e), all impurities stoichiometric (f)	56
Figure 5.7 Chord length and density dependence on the doping level of impurities in PZT ceramics	59
Figure 5.8 SEM images of fracture surfaces of PZT samples doped with 0.5mol% Na (a), Y (b) and Si(c), respectively.....	60
Figure 5.9 XPS spectra of Na KLL Auger line of 0.21mol % and 0.7mol% Na doped PZT ceramics	61
Figure 5.10 XPS spectra of Y 3p lines of 0.13 mol% and 1.0mol% Y doped PZT ceramics.....	61
Figure 5.11 TEM image of 0.5 mol% SiO ₂ modified PZT quenched at shrinkage of 10% (the black dots are where the EDX analysis has been performed).....	61
Figure 5.12 SEM image of sintered sample with 0.5 mol% SiO ₂	62
Figure 5.13 T _{onset} and T ₅₀ temperatures of sintering PZT ceramics with compositional variations (a: doped with Si; b: doped with Na; c: doped with Y)	62
Figure 5.14 Densification rate of samples doped with different impurities.....	64
Figure 5.15 (a)Mechanical quality factor Q_m (b) Planar coupling factor k_p (c) Piezoelectric coefficient d_{33} (d)Dielectric loss (e) Dielectric constant ϵ_r of PZT doped with 0, 0.21, 0.5, 0.7, 1.0 mol% Na	65
Figure 5.16 (a)Mechanical quality factor Q_m (b) Planar coupling factor k_p (c) Piezoelectric coefficient d_{33} (d)Dielectric loss (e) Dielectric constant ϵ_r of PZT doped with 0, 0.13, 0.5, 0.7, 1.0 mol% Y	66
Figure 5.17 (a)Mechanical quality factor Q_m (b) Planar coupling factor k_p (c) Piezoelectric coefficient d_{33} (d)Dielectric loss (e) Dielectric constant ϵ_r of PZT doped with 0, 0.18, 0.5, 0.7, 1.0 mol% Si	67
Figure 5.18 Hysteresis loops for PZT ceramics doped with different concentration of Na (a), Y (b) and Si(c)	70
Figure 6.1 Shrinkage curves (a) and the kinetic field (b) of PZT with 1.5 wt% PbO excess sintered at different heating rates.....	74
Figure 6.2 Shrinkage curves and shrinkage rate of PZT samples with different compositions at a heating rate of 5K/min	75
Figure 6.3 Apparent activation energies calculated from shrinkage curves using the kinetic field method (All four plots on the same scale)	76
Figure 6.4 Kinetic field diagram reproduced by fitting the iso-density lines.....	77
Figure 6.5 Microstructure evolution of pure PZT ceramics at different fractional densities (a-78%; b- 83%; c- 90%; d- 95%).....	79
Figure 6.6 The scaled variance as function of fractional density of PZT samples with different compositions	80

List of Tables

Table 1.1 Comparison of reaction sequences in formation of PZT	8
Table 1.2 Grain size effect on the PZT ceramics (as the grain size decreases).....	14
Table 2.1 List of materials used in the present study (wt%).....	22
Table 2.2 Main impurities for industrially used (IM) and highly pure (HM) PbO, ZrO ₂ and TiO ₂ raw materials (wt %).....	23
Table 2.3 X-ray diffraction results of samples from different mixing methods calcined at different temperatures for 2h (lead zirconate titanate, PZT; lead zirconate, PZ; lead titanate, PT) .	23
Table 2.4 Chemical analysis of mixtures used for calcinations and PZT powder for sintering after ball milling process (wt %).....	24
Table 2.5 Mean particle size (D ₅₀) of PZT powder with different compositions after calcination and ball-milling	24
Table 3.1 Structure parameters of Pb(Zr _{0.53} Ti _{0.47})O ₃ for tetragonal (F _T) and rhombohedral (F _{R(LT)}) phase coexistence model	28
Table 4.1 Dielectric and piezoelectric properties of pure PZT samples prepared from different raw materials	37
Table 5.1 Particle size (d ₅₀) of the individual powders after ball milling.....	52
Table 5.2 Ionic radii of the various constituents in the doped PZT ceramics.....	53
Table 5.3 Mean chord length, dielectric and piezoelectric properties of sintered IM and HM samples and samples made of HM powder doped with different impurities: Hf/Si, Na/Ba/Ca, Fe/Al/Y, all impurities nonstoichiometric(non), all impurities stoichiometric (S)	58
Table 6.1 The sintering temperatures T _{onset} and T ₅₀ of PZT with 1.5wt%PbO at different heating rates	74
Table 6.2 Fitted activation energies for diffusion E _D and grain growth E _G during sintering of PZT samples with different compositions.....	78

List of symbols

a, b, c	Lattice parameters
A	Electrode area
C	Capacitance
d	Piezoelectric constant
d_{33}	Piezoelectric constant in the longitudinal Mode
d_{50}	Mean particle size
D	Dielectric displacement
D_0	Diffusion coefficient
E	Electric field
E_c	Coercive electric field
E_a	Apparent activation energy for sintering
E_D	Activation energy for densification during sintering
E_G	Activation energy for grain growth during sintering
f_p	Parallel resonance frequency
f_s	Series resonance frequency
G	Mean grain diameter
I_a	Average intercept size
k_G	Proportionality constant
k_p	Planar coupling factor
K	Boltzmann constant
l_s	Predefined edge length of quadratic sections for image analysis
L	Width of sintering sample
L_0	Width of green sample before sintering
n	Exponent depending on the mechanism of desiccation
m	Grain growth exponent
p	Pore fraction in ceramics used for image analysis
P	Polarization
P_s	Spontaneous polarization
P_R	Remnant polarization
P_{sat}	Saturated polarization
Q_m	Mechanical quality factor
R	Gas constant

S	Strain
t	Time of sintering
$\tan\delta$	Dielectric loss (10^{-3})
t_D	Thickness of the discs
T	Absolute temperature,
T_c	Curie temperature
T_{onset}	Temperature of onset of sintering
T_{50}	Temperature of reaching 50% of total shrinkage during sintering
Z_s	impedance at resonance;
X	Stress
ε	Sintering strain
ε_0	Permittivity of free space
ε_r	Relative dielectric constant
ρ	Density of ceramic
σ_{ran}	Variance of pore fraction
σ	Variance of pore fraction with 2-D randomly distributed pores
γ	Solid gas interface energy,
χ^2	Chi value of fitting

Acknowledgments

I would like to express my sincere appreciation to my advisor, Dr. Friedrich Raether, for his patient guidance and constant support throughout my PhD study at Fraunhofer Institute ISC. His insightful suggestions and strong background on sintering theory certainly advanced the quality of my thesis. My gratitude also goes to Prof. J. Brey, Prof. G. Müller and Prof. G. SEXTL for attending my committee meetings (especially those held at rural downs during the snowy days) and for advices and discussions about the design and progress of my work. Dr. Raether and Prof. Müller are greatly appreciated for reading and correcting my dissertation.

I am also grateful for the help on my work and introductions to the devices from my colleagues in ISC (Kathrin Zecho, Veronika Gössl, Kathrin Bracken, Maria Iuga, Anke Dutschke, Hans Schömig, Pay Schulze Horn, Manfred Römer, Lutful Arefin, Andreas Klimera, Jens Baber, Peter Lösckke and Peter Michel). I would like to thank Ms. Karin Fischer, Dr. David Dolejš, and Dr. Stefan Keyssner for their organization work for the trips and lectures.

The following people are appreciated for their help with the measurements: Dr. Werner Hopp and Mr. Rudi Flegler with the chemical analysis, Mr. Alexey Sidorenko with XPS measurement, Dr. Chun Wang with the TEM analysis, Dr. Brunner with the ferroelectric properties, Richard Olsowski with DTA-TG measurements, Dr. Uta Helbig for the discussion on the Rietveld refinement, Claudia Voigt and Dr. Schreiner from CeramTec with the measurements of dielectric and piezoelectric properties.

The financial support from Elitenetzwerk Bayern (ENB) is gratefully acknowledged.

Last but not least, I would like to thank my parents, my sisters and brother, sister and brother in laws, and my friends for their continuous support. On the occasion of 10th anniversary of my graduation from high school, I want to thank all the teachers from pre-school till high school for their tutoring and guidance.

Curriculum Vitae

Personal Information

Surname, Given name	Huang, Xianliang (黄贤良)
Date of Birth	10.09.1982
Place of Birth	AnQing, China
Nationality	Chinese
Marital status	Single
Language skills	Chinese (Native language), English (fluent), German (Level A2)

Primary Education

09.1988-07.1993 CheHe Elementary school, AnQing, China

Secondary Education

09.1993-07.1996 MeiDeng Junior high school, AnQing, China
09.1996-07.1999 ChengJi Senior high school, AnQing, China

Higher Education

09.1999-07.2003 Bachelor, Materials Science, University of Science and Technology
Beijing, China
09.2003-03.2006 Master, Materials Science, University of Science and Technology
Beijing, China
04.2006-03.2009 PhD student in International Graduate School under the
Elitenetzwerk Bayern "Structure, Reactivity and Properties of Oxide
Materials" at Bayreuth University, Germany

Professional Occupation

Since 01. 04. 2006 Scientific researcher at Fraunhofer Institut ISC, Würzburg, Germany
Topic: Sintering kinetics and properties of highly pure lead zirconate
titanate ceramics
09.2004-03.2006 Master Thesis, Topic: Synthesis of doped strontium titanate as anode
materials for solid oxide fuel cells (SOFC)
10.2002-07.2003 Bachelor Thesis, Topic: Studies on improvement of thermal insulation
properties of silica aerogel

Publications:

[1] [Xianliang Huang](#), Friedrich Raether, Role of impurities in the sintering behavior and properties of lead zirconate titanate ceramics, *Journal of American ceramics society*, 92(2009)2011-16

- [2] Xianliang Huang, Friedrich Raether, Systematic study of impurities, Na, Si and Y on the electrical properties of lead zirconate titanate ceramics (shortly ready for submission)
- [3] Xianliang Huang, Friedrich Raether, Sintering kinetics of lead zirconate titanate ceramics containing impurities and lead oxide, in preparation (shortly ready for submission)
- [4] Xianliang Huang, Hailei Zhao, Weihua Qiu, Weijiang Wu, Xue Li, Performance of planar solid oxide fuel cells with doped strontium titanate as anode materials, *Energy Conversion and Management*, 48(2007)1678-1682.
Featured by *Fuel Cells Bulletin*, Volume 2007, Issue 7, July 2007, Pages 12-16.
- [5] Xianliang Huang, Hailei Zhao, Wei Shen, Weihua Qiu, Weijiang Wu, Effect of fabrication parameters on the electrical conductivity of $Y_xSr_{1-x}TiO_3$ for anode materials, *Journal of Physics and Chemistry of Solids*, 67(2006)2609-2613.
- [6] Xianliang Huang, Hailei Zhao, Weijiang Wu, Weihua Qiu, Recent progress of anode materials for solid oxide fuel cells (in Chinese), *Journal of the Chinese ceramic society*, 33(2005)1407-1413
- [7] Hailei Zhao, Xianliang Huang, Xue Li, Weihua Qiu, Electrical conductivities of $La_xSr_{1-x}TiO_3$ as anode materials for SOFC (in Chinese), *Chinese Journal of Materials Research*, 21 (2007)255-260.
- [8] Chaoli Yin, Hailei Zhao, Hong Guo, Xianliang Huang, Weihua Qiu, Effect of the synthesis method of SnSb anode materials on their electrochemical properties, *Journal of University of Science and Technology Beijing, Mineral, Metallurgy, Material*, 14 (2007) 345-349.
- [9] Xue Li, Hailei Zhao, Wei Shen, Feng Gao, Xianliang Huang, Yue Li and Zhiming Zhu, Synthesis and properties of Y-doped $SrTiO_3$ as an anode material for SOFCs, *Journal of Power Sources*, 166 (2007) 47-52.

Conferences:

- [1] Xianliang Huang, Friedrich Raether, 17th International Symposium on Applications of Ferroelectrics Joint Meeting with the Electronics Division of the American Ceramic Society, Santa Fe, USA 2008
- [2] Xianliang Huang, Friedrich Raether, In situ Measurements on Sintering Kinetics of PZT Ceramics, Proceedings of 10th International Conference and Exhibition of the European Ceramic Society, Berlin, Germany 2007.
- [3] Xianliang Huang, Hailei Zhao, Weijiang Wu, Weihua Qiu, Chaoli Yin. Synthesis and Electrical properties of undoped and La-doped $SrTiO_3$ as anode materials for SOFC. Proceedings of the 5th Asian Conference on Electrochemistry, Shanghai, China, May 09-12, 2005, 2P31.